Advanced Drug Delivery Reviews xxx (xxxx) xxx

Contents lists available at ScienceDirect

Advanced Drug Delivery Reviews

journal homepage: www.elsevier.com/locate/addr

Design strategies for shape-controlled magnetic iron oxide nanoparticles

Alejandro G. Roca [a,b,*], Lucía Gutiérrez [a,c,*], Helena Gavilán [a], Maria Eugênia Fortes Brollo [a], Sabino Veintemillas-Verdaguer [a], María del Puerto Morales [a]

[a] Dept. Energía, Medio Ambiente y Salud, Instituto de Ciencia de Materiales de Madrid, CSIC, Cantoblanco, E-28049 Madrid, Spain
[b] Catalan Institute of Nanoscience and Nanotechnology (ICN2), CSIC and BIST, Campus UAB, Bellaterra, E-08193 Barcelona, Spain
[c] Dept. Química Analítica, Instituto de Nanociencia de Aragón, Universidad de Zaragoza and CIBER-BBN, E-50018 Zaragoza, Spain

ARTICLE INFO

Article history:
Received 11 May 2018
Received in revised form 20 November 2018
Accepted 11 December 2018
Available online xxxx

Keywords:
Magnetic nanoparticles
Anisometric nanoparticles
Shape anisotropy
Nanocubes
Rods
Disks
Nanoflowers
Hollow nanoparticles
Nanotoxicity
Biomedical applications

ABSTRACT

Ferrimagnetic iron oxide nanoparticles (magnetite or maghemite) have been the subject of an intense research, not only for fundamental research but also for their potentiality in a widespread number of practical applications. Most of these studies were focused on nanoparticles with spherical morphology but recently there is an emerging interest on anisometric nanoparticles. This review is focused on the synthesis routes for the production of uniform anisometric magnetite/maghemite nanoparticles with different morphologies like cubes, rods, disks, flowers and many others, such as hollow spheres, worms, stars or tetrapods. We critically analyzed those procedures, detected the key parameters governing the production of these nanoparticles with particular emphasis in the role of the ligands in the final nanoparticle morphology. The main structural and magnetic features as well as the nanotoxicity as a function of the nanoparticle morphology are also described. Finally, the impact of each morphology on the different biomedical applications (hyperthermia, magnetic resonance imaging and drug delivery) are analysed in detail.

We would like to dedicate this work to Professor Carlos J. Serna, Instituto de Ciencia de Materiales de Madrid, ICMM/CSIC, for his outstanding contribution in the field of monodispersed colloids and iron oxide nanoparticles. We would like to express our gratitude for all these years of support and inspiration on the occasion of his retirement.

Contents

* Corresponding authors at: Dept. Energía, Medio Ambiente y Salud, Instituto de Ciencia de Materiales de Madrid, CSIC, Cantoblanco, E-28049 Madrid, Spain.
E-mail addresses: alejandrogroca@gmail.com, alejandro.gomez@icn2.cat (A.G. Roca), lu@unizar.es (L. Gutiérrez), helena.gavilan@iit.it (H. Gavilán), brollo@icmm.csic.es (M.E. Fortes Brollo), sabino@icmm.csic.es (S. Veintemillas-Verdaguer), puerto@icmm.csic.es (M.P. Morales).

https://doi.org/10.1016/j.addr.2018.12.008
0169-409X/

1. Introduction

In the last decades, nanocrystals have gained attention due to their unique properties at the nanoscale and have been used in different technological applications such as energy storage, catalysis, photonics, electronics or biomedicine.[1–10] The improvement of their performance has required innovative and continuous upgrades of the chemical processes to yield "monodispersed" colloids consisting on uniform nanoparticles in both size and shape (e.g. size and shape distribution less than 10%).[11–16] In these systems, the overall physicochemical properties reflect the properties of each constituent, leading to size/shape-dependent performance materials. Interestingly, internal structure [17,18] and mesoscopic ordering (3D aggregates or 2D superlattices) [19–21] are also important parameters that control the materials properties. The control of these parameters is linked to the synthesis route used for their preparation or the post-synthesis treatments and, most of all, to the ligands used.

Studies dedicated to the formation mechanism of iron oxide nanocrystals have invoked the classical nucleation and growth theories, including LaMer and Dinegar theory for burst nucleation and diffusional growth, and Ostwald ripening theory for second phase coarsening or their combination.[22] These mechanisms take place in some of the most common synthesis routes of iron oxides, i.e. co-precipitation and high temperature decomposition of organic precursors. Co-precipitation[23] takes place in aqueous media where iron ions form a hexahydrated complex, which depending on the oxidation state and pH can undergo a hydroxylation reaction to form the iron oxide nanoparticles. On the other hand, thermal decomposition takes place in non-aqueous environment and usually occurs through a reaction between carboxylate groups (coming from the iron source) and the iron, forming oxo bridges between irons that evolve to the iron oxide nanoparticles.[24] Apart from the up-above mention mechanisms of classical nucleation and growth, colloidal anisometric particles of various well-defined shapes synthesized in aqueous routes were shown to be composed of smaller, primary nanocrystallites, indicative of aggregation during the formation of the nanoparticles.[25] These cases were explained by a two-step mechanism, in which nucleation and growth steps happen simultaneously, so the growth is controlled by aggregative processes of small primary nanocrystals and not by molecular diffusion. [26] Lastly, oriented attachment mechanism was also described for co-precipitation and thermal decomposition, suffering spontaneous self-organization of adjacent particles, so that they share a common crystallographic orientation, [25,27,28] followed by the joining of these particles at a planar interface.[29]

Recently, different efforts have been made in developing new routes for the synthesis of anisometric nanocrystals (i.e. nanocrystals which differ from spherical shape) like nanocubes, nanorods, nanowires, nanodisks, and nanoflowers among others.[30–36] These materials possess direction-dependent properties, high surface-to-volume ratio and also particular crystal facets at the surface that can confer different reactivity than their spherical equivalent.[37] The final morphology is determined during the growth stage in the synthesis procedure, where thermodynamic and kinetic aspects control the reaction.[11,38–41] In general, the shaped-controlled synthesis of iron oxide relied on the preferential adsorption of capping molecules to specific facets[30,42–44] or the existence of a small magnetic or dielectric moment among the subunits that governs the aggregation processes.[45–47] Only in few cases such mechanisms were evidenced by complete experimental mechanistic work, mainly due to the difficulty in characterising the nanoparticle formation from the first stages.[48] The current scenario is that the most-developed recipes are not robust enough for synthesizing high-quality nanoparticles due to the poor understanding of the mechanisms of nucleation and growth during nanoparticle formation. The synthetic route represents the trickiest step in the design of a nanomaterial for a specific application, as it will determine the particle size/shape, the size distribution, the surface chemistry of the particles and consequently their unique properties.

It is clear that under reduced dimensionality, shape is an important matter. For example, in the case of Au nanoparticles, when Au turns anisometric (rod-shape, nanocages, nanoshell, etc.) a second plasmon resonance band arises at the near-infrared range which can be very advantageous for their application in biomedicine and sensing.[49–51] Changing rod aspect ratio affects the longitudinal plasmon resonance frequency, which can be tuned systematically. Furthermore, ultrathin gold nanowires present mechanical flexibility and high conductivity. [52] Platinum nanocrystals, with high-performance in catalysis, have been obtained with peculiar morphologies (cubic dendrites or planar tripods) that provide high surface to volume ratio and controlled crystallographic facets.[53,54] For example, the hydrogenation of benzene is strongly affected by the Pt nanoparticle shape. Both cyclohexane and cyclohexene molecules were obtained using cubo-octahedral Pt nanocrystals, whereas only cyclohexane was selectively formed on cubic nanocrystals.[55] Anisometric magnetic nanoparticles of Fe, Co, FeCo and CoNi with high aspect ratio and enhanced magnetic properties have been obtained for permanent magnet applications. [31] However, the stability, as well as the dipolar interactions, limits the application of these materials.[56]

Among the iron oxide nanoparticles, the ferrimagnetic ones, magnetite and maghemite, (called for short "magnetic nanoparticles") are of particular interest because of their potential in fields such as magnetic recording, separation and recycling, and in the biomedical area, in magnetic resonance imaging (MRI), targeted drug delivery, hyperthermia

Please cite this article as: A.G. Roca, L. Gutiérrez, H. Gavilán, et al., Design strategies for shape-controlled magnetic iron oxide nanoparticles, Adv. Drug Deliv. Rev., https://doi.org/10.1016/j.addr.2018.12.008

treatment of solid tumours, gene therapy and tissue regeneration. [44,57–62] For the above uses, most of the synthesis studies have been concentrated on spherical magnetite nanoparticles since they are, in general, easily obtained according to reproducible experimental procedures.[63,64] However, introducing shape anisotropy in magnetite nanoparticles can change substantially their magnetic properties. [44,65,66] Shape anisotropy can be up to two orders of magnitude larger than crystal anisotropy leading to an increase in the coercive field[67–69] and strongly affecting the behaviour of the particles under an alternating magnetic field. Thus, nanodisks and nanorods of magnetite have been shown to induce mechanical damage of cancer cells,[70–72] while cubes, nanorings and nanoflowers seems to be ideal heat mediators for hyperthermia.[35,73–75]

In this review, we present an overview and recent progress on the preparation of well-controlled magnetite/maghemite nanoparticles with non-spherical shapes and the mechanisms proposed to control their formation. We have focused on the magnetite nanoparticle growth, either in one-step or through a templated-assisted reduction process from other iron hydroxides/oxides such as goethite, lepidocrocite and hematite nanocrystals, where the anisometric morphology of the precursors is preserved after the reduction process. We describe the effect of key parameters on the final magnetite morphology, including: (i) control of the precursor's formation and growth, (ii) effect of the precursor crystalline phase and (iii) crystal orientation and facets exposed on the final magnetic nanoparticles as a function of the shape. Those parameters are classified as physical parameters (those that concern the number of steps and temperature and heating rate in each step) and chemical parameters (nature and concentration of reagents and solvents). We dedicate a section to ligands, as it is one of the key parameters that control the reaction and can be manipulated to reach the desired morphology. Ligands can be very diverse in nature and they are able to favour a thermodynamic and or kinetic regime by binding specifically to a particular face altering its stability or its relative growth rate. Structural and magnetic properties for each morphology are also reviewed and related to the synthetic route. Special emphasis has been paid to the effect of the shape on cell uptake, biodistribution and degradation in biological environments. Finally, the advantages of using magnetic anisometric nanoparticles for biomedical applications such as magnetic hyperthermia, magnetic resonance imaging, drug delivery and others are also described. A flow chart summarising the content of this review is presented in Fig. 1.

2. Synthesis of anisometric magnetic nanoparticles

Magnetite has a cubic inverse spinel structure and its space group is Fd3m with a cell parameter of 8.394 Å.[76] The unit cell contains 32 O^{2-} ions forming a cubic closed-packed system. Fe(II) ions are disposed in the octahedral sites and Fe(III) ions are located in both octahedral and tetrahedral sites (Fig. 2). Maghemite (γ-Fe_2O_3) is formed during the oxidation of magnetite or by dehydration of lepidocrocite. [77] The direct synthesis of maghemite is not possible probably due to the presence of vacancies in octahedral positions (Fig. 2).[78] Maghemite (γ-Fe_2O_3) has an inverse spinel structure like magnetite with a cell parameter slightly smaller (a=8.351-8.33 Å), containing vacancies located in the octahedral positions and Fe(III) ions in both octahedral and tetrahedral positions. The stoichiometry of maghemite can be described with the formula $Fe_{Td}(Fe_{5/3}\square_{1/3})_{Oh}O_4$ (Td= tetrahedral sites; Oh= octahedral sites). Depending on the extent and nature of vacancies ordering, three different crystal symmetries for maghemite can be described. In the first one, the vacancies are randomly distributed in the octahedral positions (Fd3m space group). In the second one the vacancies are partially ordered ($P4_32_12$ and $P4_12_12$). In the last one, the vacancies are perfectly ordered forming a tetragonal superstructure along the c-axis where the value of c is around three times the value of a ($P4_32_12$ space group).[79–81]

There are two different approaches for the direct synthesis of magnetite, i) starting from iron(II) or iron(III) inorganic salts such as nitrates, sulphates or chlorides, [83,84] or ii) starting from organic precursors such as iron oleates,[85] acetates,[86] acetylacetonates[87] or pentacarbonyl.[88] In most cases, a mild reducer or oxidizer is added to the reaction to get the final Fe_3O_4 stoichiometry. In other cases, indirect methods involve the initial synthesis and reduction of different iron oxides (hematite)[79] or oxohydroxides (goethite, akaganeite or lepidocrocite)[62] which act as shape-template setting the final dimensions and shape of the nanostructure. If akaganeite or goethite are used as shape-templates, they are thermally transformed to magnetite through hematite. The well-known reduction of hematite to magnetite through a topotactic reaction is performed in dry conditions, i.e. static or dynamic atmosphere of H_2/Ar at temperatures not lower than 360 °C.[89] The reduction can also be performed in wet conditions either in organic or aqueous media. In organic media, heating hematite or iron oxohydroxide nanoparticles in trioctylamine in the presence of oleic acid at around 350 °C leads to magnetite.[90,91] In aqueous media the reduction to magnetite is achieved by using hydrazine at alkaline pH range between 9.5 and 11.5 [92] through a dissolution-recrystallization mechanism starting either from hematite or from an oxihydroxide.[93,94] The dissolution takes place in alkaline environments and consists on the reduction of Fe^{3+} in the crystal structure releasing Fe^{2+} ions, which in turn react with their surface groups, nucleating magnetite. This mechanism can be catalysed by the presence of external Fe^{2+} [95] and is usually associated to a change in the shape of the nanoparticle.[96] Recently, it has been reported that dissolution-recrystallization mechanism can be slowed down by the use of molecules with acetate groups in a polyol media, which also provide a reductive medium necessary for the transformation of β-FeOOH to magnetite. It is notable the role of acetate groups, which have high affinity for Fe^{3+} ions, slowing the dissolution of the nanoparticles, allowing the direct transformation to magnetite and, most importantly, preserving the nanoparticle's shape.[97]

In the case of maghemite, it can be obtained through oxidation of magnetite at 240 °C in air. However, when the size reduces to nano, oxidation temperature can be reduced down to 50 °C and even at room temperature for long periods of time (1 year for sizes below 10 nm). [98] Finally, maghemite can also be obtained through dehydration of lepidocrocite (Fig. 3).

It is important to mention that any colloidal synthesis route involves two main stages: nucleation and growth/agglomeration. In the case of the synthesis of monodisperse nanoparticles, both stages must be separated in temperature and time, otherwise broad size distributions and diverse particle morphology are obtained. For the case of anisometric nanoparticles, growth stage is the critical step responsible for the final morphology that in all cases results from the induction of different

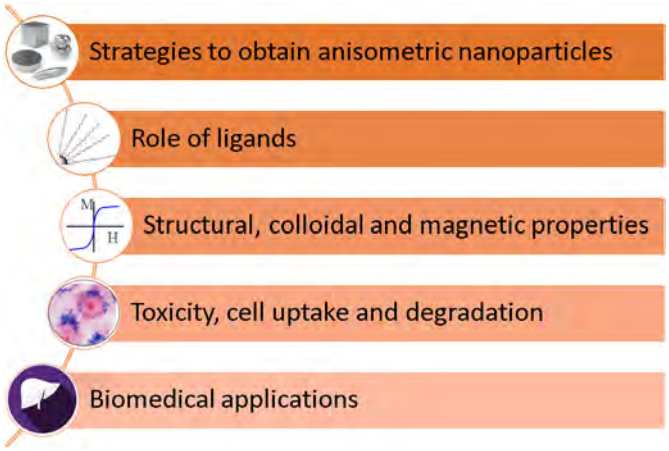

Fig. 1. Flow chart describing the content of this review.

Please cite this article as: A.G. Roca, L. Gutiérrez, H. Gavilán, et al., Design strategies for shape-controlled magnetic iron oxide nanoparticles, Adv. Drug Deliv. Rev., https://doi.org/10.1016/j.addr.2018.12.008

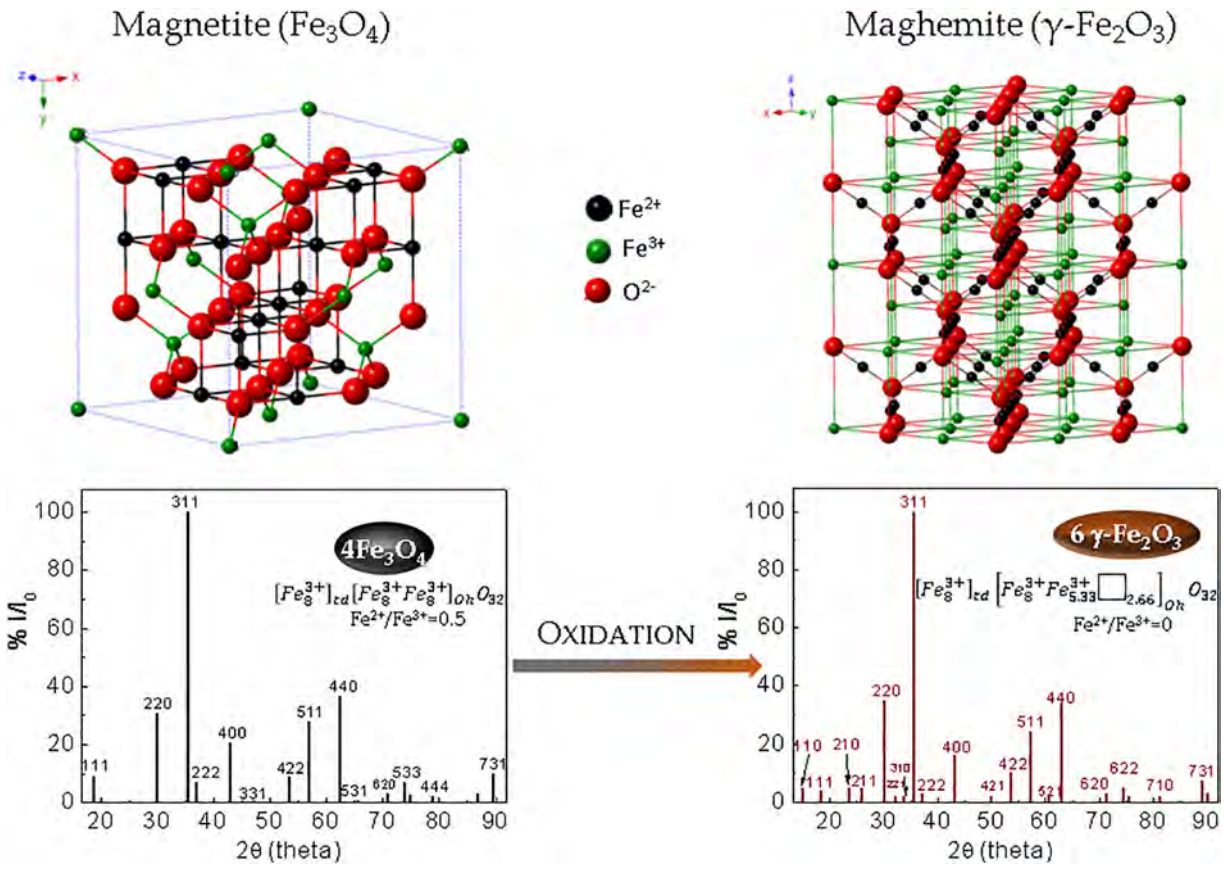

Fig. 2. Crystal structure and X-ray diffraction pattern (using Cu Kα radiation) of magnetite and maghemite phases. Adapted with permission from [82]. © 2015 National Institute for Materials Science.

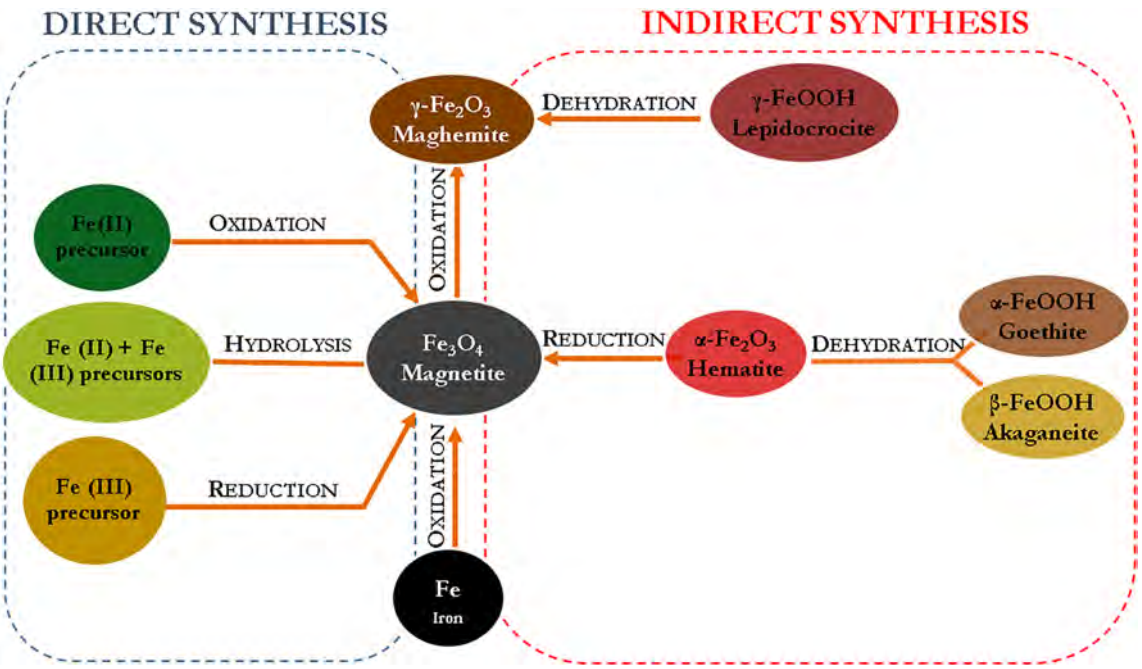

Fig. 3. Synthesis scheme and phase transformation to prepare Fe_3O_4 and γ-Fe_2O_3 nanoparticles.

Please cite this article as: A.G. Roca, L. Gutiérrez, H. Gavilán, et al., Design strategies for shape-controlled magnetic iron oxide nanoparticles, Adv. Drug Deliv. Rev., https://doi.org/10.1016/j.addr.2018.12.008

growth rates on low index planes such as {111}, {110} and {100} with low surface energy.

2.1. Cubic-shaped nanoparticles

Magnetite is most often found as cubes or octahedrons, and less frequently as rhombododecahedrons. All of these forms and their combinations, i.e. 0-D cubic-shaped nanocrystals, are compatible with the symmetry of the spinel structure (cubic) and its synthesis in liquid can be carried out by different routes depending on the nature of the solvent and the iron precursors (Fig. 4).

In water, the precipitation of an iron(II) salt in alkaline media in the presence of a mild oxidant such as potassium nitrate (KNO_3) at 90 °C renders magnetite nanocubes but only under certain conditions.[99] The most critical parameter is the [Fe(II)]:2[OH^-] ratio, so 33 nm nanocubes are achieved when [Fe(II)]:2[OH^-] ratio is 0.77. Interestingly, when [Fe(II)]:2[OH^-] gets closer to 1, size becomes larger (76 and 169 nm for [Fe(II)]:2[OH^-] ratios of 0.97 and 0.997 respectively) and shape evolves to octahedral morphology. The kinetics of the reaction is affected by the pH and how far/close it is from the isoelectric point of magnetite (pH~7). [100,101] In excess of OH^-, i.e. the pH is above Fe_3O_4 isoelectric point, cubic particles are grown by slow diffusion of $Fe(OH)_2$ species to the primary particles (negatively charged). However, if the excess of OH^- is negligible, the growth takes place mainly by aggregation and the kinetic is much faster. Primary particles are not repelling each other since they are not sufficiently charged and the aggregation is followed by subsequent recrystallization leading to octahedral particles with larger sizes from few nanometers up to microns. Interestingly, the addition of ethanol induces the cubic morphology as well, and reduces the final size of the particles because it modifies the hydrolysis of ferrous and ferri oxo-aqueous species decreasing the critical diameter at which nuclei can be formed, and finally slows down the growth hampering the diffusion process.

The decomposition of iron organic precursors in high boiling-point organic solvents in the presence of surfactants can lead to cubic magnetite nanoparticles with in a wide size range and narrow size distribution (Fig. 5). The particle size can be tailored by changing both, the precursor concentration and reflux time. For example, 79 nm Fe_3O_4 nanocubes were grown by heating iron(III) acetylacetonate in benzyl ether in the presence of oleic acid.[102] Then, by doubling the precursor concentration and increasing the reflux from 30 min to 1, 1.5 and 2 hours it is possible to achieve larger particles of 110, 150 and 160 nm respectively. The cubic shape was induced by the high amount of active species in solution being the growth kinetically controlled. In addition, surfactant/precursor molar ratio and the type of surfactant are other crucial parameters to control the final nanoparticle size. For example, by decreasing the oleic acid/precursor ratio from 5/1 to 2/1 the mean size of the magnetite nanocubes increases from 16 to 104 nm.[104] Oleic acid has a critical effect because it has the capacity of delaying the nucleation towards higher temperatures leading to smaller nuclei, but also modulating the particle growth kinetics. If oleic acid is exchanged by decanoic acid, smaller particles are grown (size range of 5-30 nm with decanoic and 16-100 nm with oleic acid [105]) and can be tuned by changing the surfactant/iron ratio. Decanoic acid is much shorter than oleic acid and also linear, so probably the coordination with Fe_3O_4 facets is more efficient leading to a drastic decrease in the mean size. The same effect was

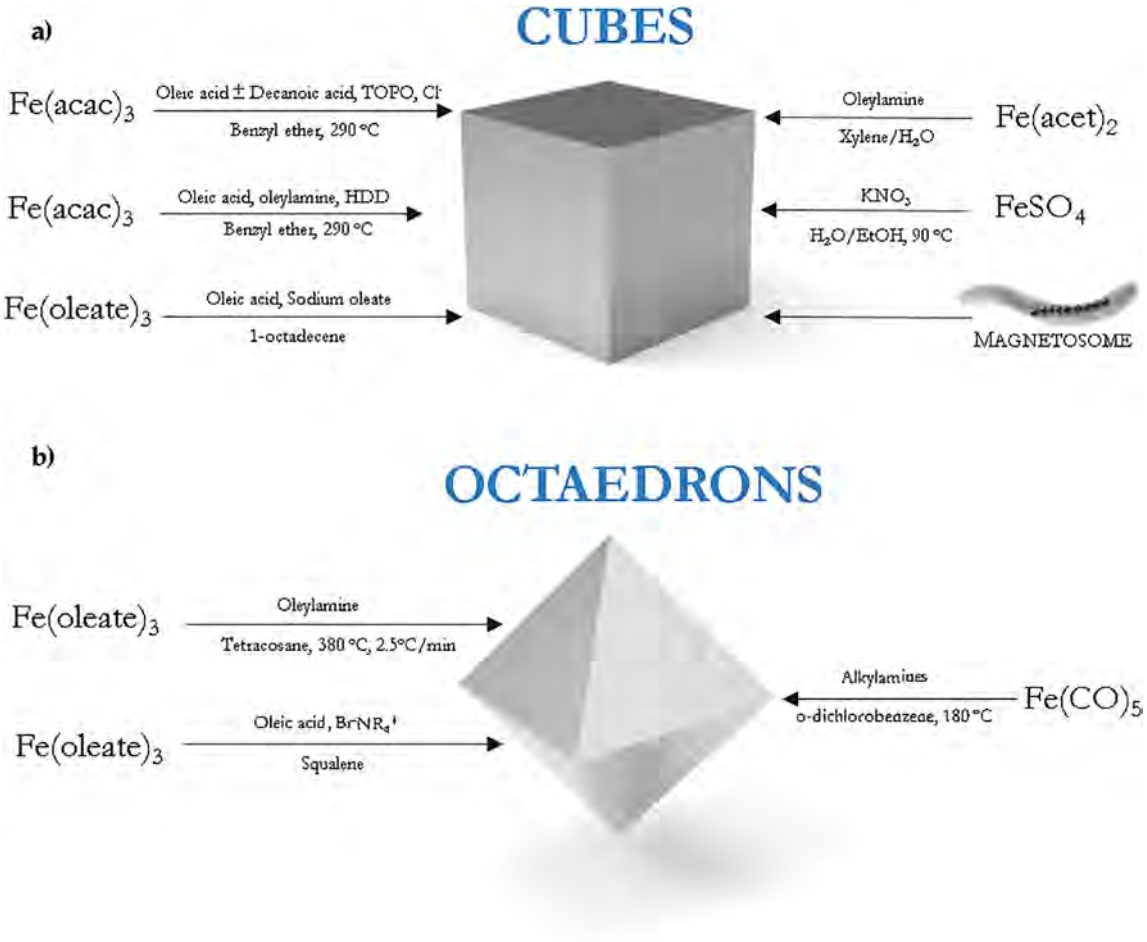

Fig. 4. Scheme of the synthetic routes for the growth of (a) Fe_3O_4 nanocubes and (b) Fe_3O_4 nanoctahedrons. (Acac = Acetylacetonate, Acet = Acetate, EtOH = Ethanol, HDD = 1, 2-hexadecanediol, TOPO=Trioctylphosphine oxide, $Br^-NR_4^+$ = Tetraalkylammonium bromide). Synthesis routes adapted from [99,102–111].

Please cite this article as: A.G. Roca, L. Gutiérrez, H. Gavilán, et al., Design strategies for shape-controlled magnetic iron oxide nanoparticles, Adv. Drug Deliv. Rev., https://doi.org/10.1016/j.addr.2018.12.008

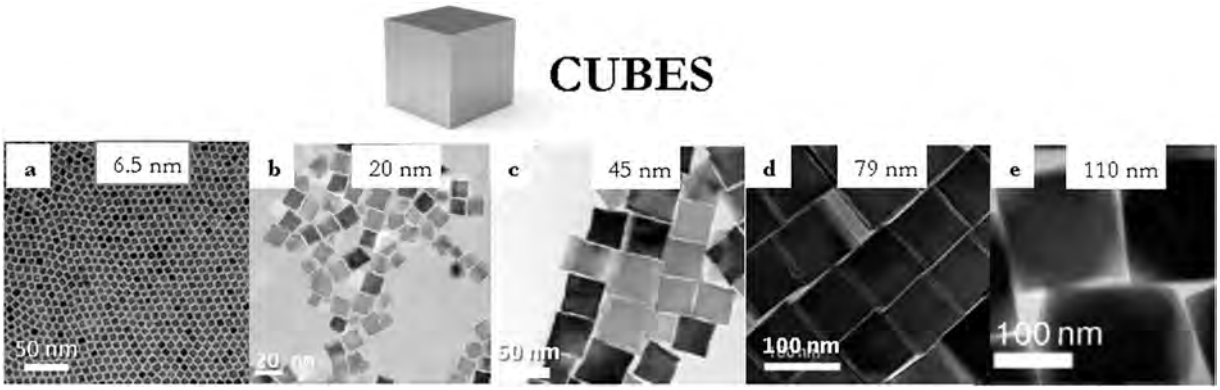

Fig. 5. TEM images of magnetite nanocubes synthesized by thermal decomposition with different mean sizes, a) 6.5 nm (Reproduced from [106] with the permission of AIP Publishing.; b) 20 nm, adapted with permission from [105] Copyright (2010) American Chemical Society; c) 45 nm, adapted with permission from [112] Copyright (2011) American Chemical Society; d) 79 nm, adapted with permission from [102] Copyright (2009) American Chemical Society; e) 110 nm. adapted with permission from [102] Copyright (2009) American Chemical Society.

observed with 4-biphenylcarboxylic acid, which leads to a sharp decrease in the mean particle size from 79 to 22 nm when used as impurity with oleic acid in the decomposition of iron(III) acetylacetonate.[102]

Heating rate is other critical parameter to control the final nanoparticle size. In the case of high temperature decomposition of organic precursors, the iron source and surfactant dissolved in the solvent are subjected to a thermal treatment achieving temperatures well above 200 °C. In this route, the heating rate critically defines the number of formed nuclei, and hence the size of the final nanoparticles. Therefore the heating profile applied should be controlled with an external thermo-controller. For example, a huge enlargement from 13 to 180 nm can be achieved when the heating rate slows down from 5.2 to 0.8 $°C \cdot min^{-1}$ in the decomposition of iron(III) acetylacetonate and decanoic acid in benzyl ether. The heating rate dominates the nucleation process of the nanocubes so when heating rate decreases the nucleation rate decreases too, less nuclei are formed and they are able to grow more.[106] Interestingly, in the same synthesis but using a surfactant mixture of oleic acid, oleylamine and 1,2-hexadecanediol, when the heating rate decreases from 35 to $5°C \cdot min^{-1}$, the size of the cubes increases from 5 to 30 nm.[106]

The nature of the surfactants has also been demonstrated to determine, at least in part, the final morphology of magnetite nanoparticles synthesised in organic media. For example, the addition of sodium or potassium oleate leads to cubic nanocrystals between 9 and 23 nm. [107] However, if the surfactant is replaced by oleic acid or dibutylammonium oleate, spherical nanoparticles were grown. In this case cubic shape is induced by the selective adhesion of the sodium and potassium oleate on the {100} facets reducing its growth rate. [113] However, it should be noted that depending on the amount of oleate and the synthetic conditions during and post-synthesis, non-stoichiometric wüstite (FeO) can be formed.[114,115] Trioctylphosphine oxide (TOPO), chloride ions[116] and β-amyrin[117] are other ligands which selectively bind to {100} facets inducing cubic shape.

Changing the precursor, it is possible to obtain magnetite octahedrons by thermal decomposition. Thus, the decomposition of iron(III) oleate in tetracosane in the presence of oleylamine leads to 21 nm Fe_3O_4 octahedral nanocrystals induced by the selective binding of oleylamine to {111} facets.[118] Furthermore, the use of quaternary ammonium bromide salts (which generate trioctylammonium bromide at high temperatures)[119,120] in conjunction with oleic acid in the decomposition of iron(III) oleate using squalene as solvent also leads to 50 nm Fe_3O_4 octahedrons. Interestingly, the increase of the alkylamine/Fe ratio from 2:1 to 10:1 using $Fe(CO)_5$ in o-dichlorobenzene leads to the formation of 50 nm hexagonal-shaped Fe_3O_4 nanocrystals because once the octahedral {111} facets saturated of alkylamine molecules reduce their growth there is chance for the dodecahedron form {110} to appear, the combination of both forms project as a hexagon in the TEM micrographs.[121] Finally, heating a solution of iron(II) chloride in oleylamine up to 200 °C at a rate of 10 $°C \cdot min^{-1}$ renders 8 nm Fe_3O_4 octahedrons.[122] A synthetic strategy lying between the aqueous and organic media consist on the hydrolysis of iron(II) acetate in the presence of oleylamine dissolved in xylene. Heating the reaction mixture followed by fast injection of water triggers the hydrolysis of the Fe-oleylamine complex leading to 9 nm nanocubes.[109]

Recently, 47 nm rhombohedral Fe_3O_4 nanocrystals were synthesized using a three-step process, which comprises the generation of hematite nanoparticles, further encapsulation in silica and final reduction to magnetite. The first step is critical for the growth of rhombohedral scaffolding and it was achieved by solvothermal synthesis by heating at 180 °C for 12 hours iron(III) chloride in a mixture of ethanol/water 5:1 using sodium acetate as base.[90]

Finally, biological synthesis of iron oxide nanocrystals, cubes and octahedron between 30 and 100 nm in size, can be generated by bacterial magnetosomes following a natural pathway and constitutes one of the most fascinating processes of iron biomineralization.[103,110,111] These magnetosomes (often ferrimagnetic) are grown enveloped in membranes and form chains, which allows the cells to align with external magnetic fields.

2.2. Elongated nanoparticles

By "elongated nanoparticles" we cover all the 1-D nanostructures described in the literature with different names such as nanowires, spindle, ellipsoids, needles, nanobelts, nanorice, rods or nanowhiskers (Fig. 6). The different names are attributed to their different axial ratio (length/width) and final morphology at the particle edges (sharp or rounded).

Traditionally, synthetic strategies for the growth of elongated magnetic iron oxide nanostructures were based on aqueous media using other iron oxides or oxohydroxides as templates (Fig. 7 and 8). Interestingly, in the last years, one-step organic-based approaches have come up succeeding in the direct synthesis of elongated Fe_3O_4 nanoparticles that differ in the intermediate and the strategy to tailor length and axial ratio. Final properties will depend mainly on the geometry of the particles but also on the synthetic route used as it determines the internal structure (crystallinity, porosity and long axis direction).

Starting at the end of the 80´s and particularly during the 90´s, the main strategy for the synthesis of elongated magnetic nanoparticles for magnetic recording media was using goethite as shape template, followed by its transformation to hematite and further reduction to magnetite.

Templating with goethite (α-FeOOH) as an intermediate, larger axial ratios up to 10 can be accomplished although the further thermal

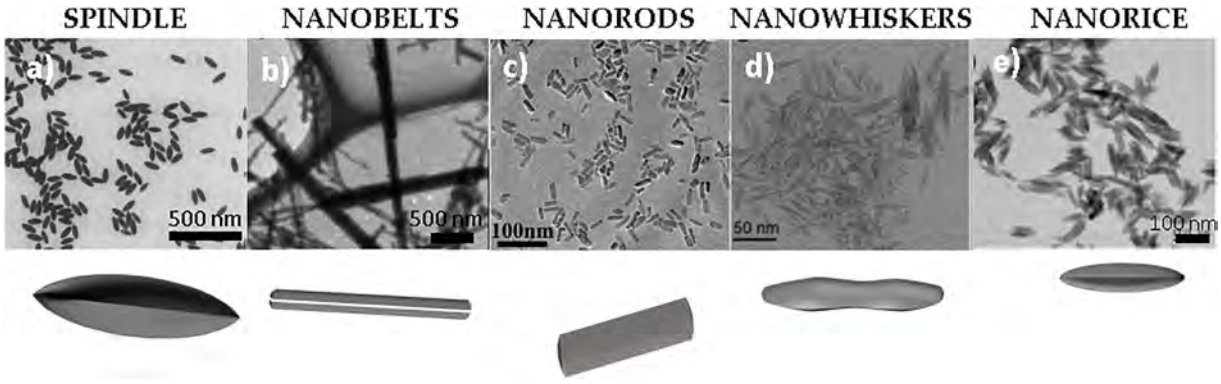

Fig. 6. Different types of elongated nanostructures reported in the bibliography. a) spindles, adapted/reprinted with permission from [123] © 1984, by Elsevier; b) nanobelts, adapted/reprinted with permission from [124], copyright (2011) American Chemical Society; c) nanorods, adapted/reprinted with permission from [91]), copyright © 2016, by Wiley; d) nanowhiskers, adapted/reprinted with permission from [125], copyright (2011) American Chemical Society; e) nanorice, adapted/reprinted with permission from [126], copyright © 2008, by Wiley.

reduction produces a high porous structure associated to dehydroxilation. Uniform goethite particles with lengths ranging between 80 and 250 nm and diameters between 25 and 65 (axial ratios~3-4) can be obtained by hydrolysis and oxidation of iron(II) sulphate in water in the presence of carbonate ions at 40 °C. The concentration of iron(II) sulphate and carbonate, air flow rate and reaction time are critical parameters to tailor the final nanoparticle dimensions. [126] Larger α-FeOOH particles can be grown by increasing the pressure and substituting sodium carbonate (Na_2CO_3) by sodium acetate (NaAc). The reaction takes place by hydrothermal synthesis at 100 °C for 8 hours and leads to goethite rods of 170-300 nm in length and 15-25 nm in diameter (axial ratio around 10).[127]

Akaganeite (β-FeOOH) is the other iron oxohydroxide phase that serves as template for final synthesis of magnetite 1-D nanorods. In general, the hydrolysis of iron(III) chloride above 0.02M at 60-100 °C in water for several hours renders monoclinic β-FeOOH anisometric nanoparticles, whose length depends on the synthesis temperature, hydrolysis time, concentration of iron(III) chloride, internal pressure (hydrothermal synthesis) and the presence of several additives acting as pH modifiers to control the reaction kinetics or as shape/growth modulators. For example, β-FeOOH nanoparticles of 500 x 50 nm can be synthesized in water with an HCl concentration of 0.012 M at 100 °C for 24 hours.[92] Smaller rods of 200 x 22 nm were grown at 60 °C without HCl and with a shorter the reaction time (5 h) rods of 72 x 10 nm were produced.[133] Reduction was carried out in liquid after protecting the akaganeite particles with silica by heating at 245 °C in 2-hydroxiethyl ether. If the initial concentration of iron(III) chloride is around the nucleation limit for akaganeite (0.02 M), rods with 63 x 14 nm can be achieved.[134] Smaller rods (50 x 10 nm) were synthesized by hydrothermal treatment using short heating times (6 h).[91] Other strategy leading to a drastical reduction in size was the synthesis of akaganeite nanoparticles in the presence of polyethyleneimine (PEI) (from 291 x 42 nm to 32 x 5 nm (M_W PEI= 2500 g/mol)), because PEI is adsorbed on the lateral plane (200) of the nanorods, changing also the shape from rod to spindle with the edges more rounded (Fig. 8). [135,136] Moreover, the presence of polyvinylpryrrolidone (PVP) at 100 °C for 12 h lead to hollow elongated particles of 300-200 x 30-50 nm after reduction.[128]

Finally, the use of a ternary water-in-oil/water system has been used to grow β-FeOOH nanoparticles. In this approach the iron(III) chloride solution is placed at the bottom and a water-in-oil microemulsion formed with cyclohexane and Igepal CO-520.[129] The aqueous phase of the microemulsion contains NH_4OH and when the system is destabilized by action of the temperature a phase separation begins.

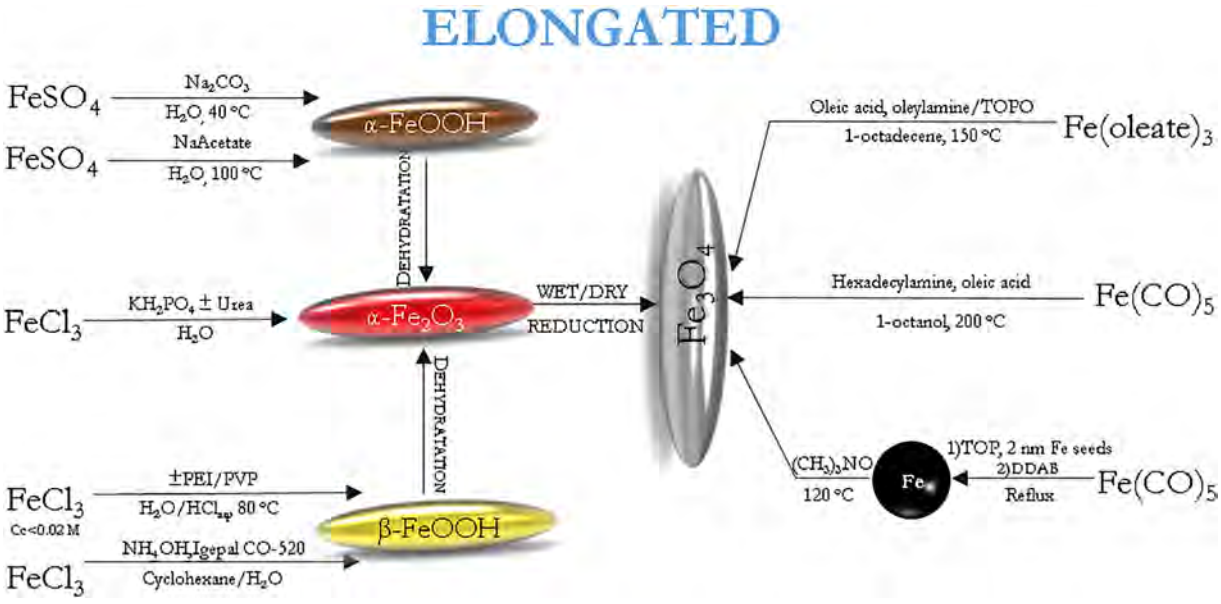

Fig. 7. Scheme of the synthetic routes to produce elongated Fe_3O_4 nanostructures. (PEI = Polyethyleneimine, PVP = Polyvinylpyrrolidone, TOP = Trioctylphosphine, DDAB = dodecyl dimethylammonium bromide). Synthesis routes extracted from references [46, 125–132].

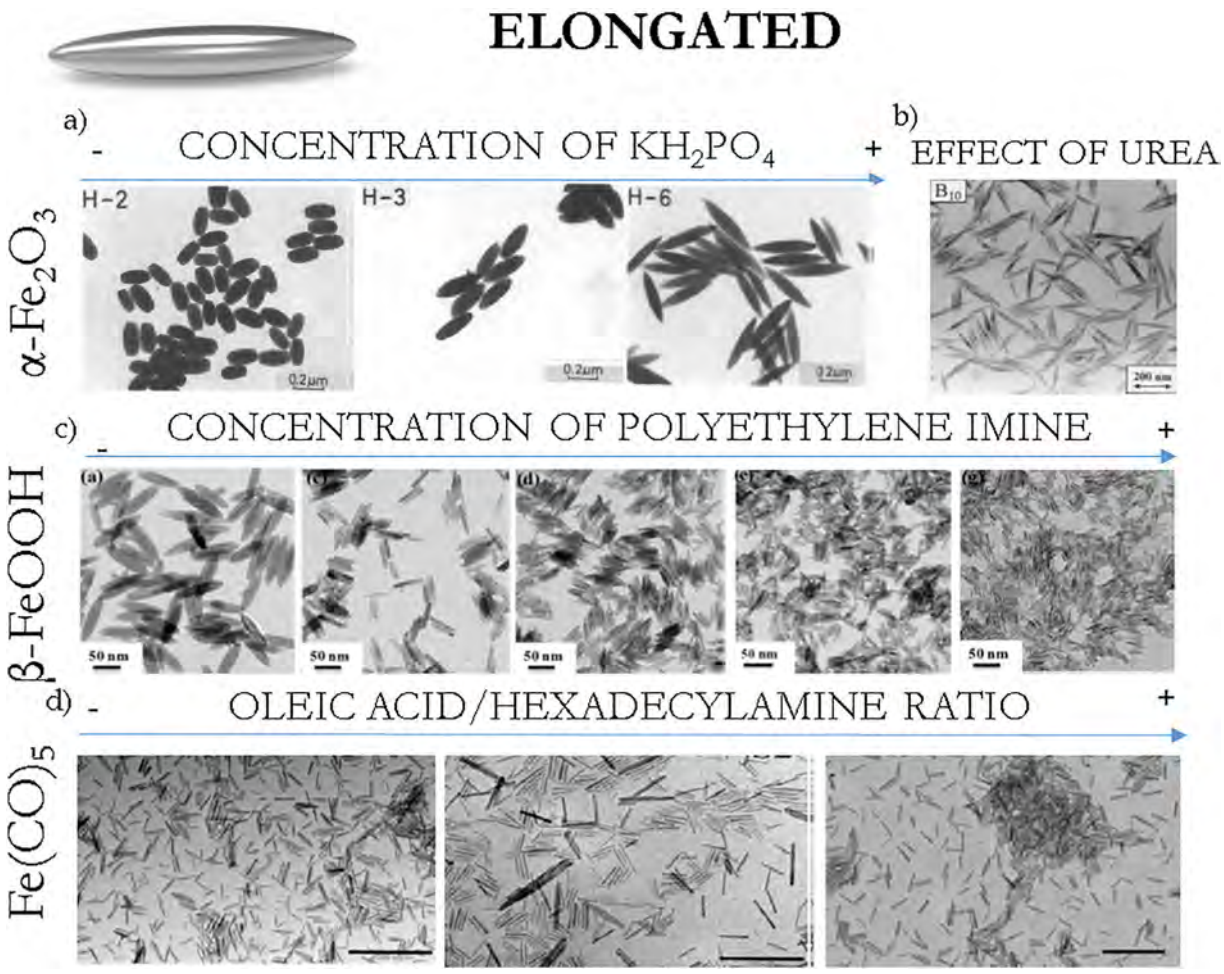

Fig. 8. TEM images of Fe_3O_4 elongated nanoparticles with different sizes modulated by tailoring different reaction parameters. a) Concentration of KH_2PO_4. Adapted/reprinted with permission from [46], © 2010, by Cambrindge University Press; b) Effect of urea; adapted/reprinted with permission from [130] © 1999, by Elsevier; c) Concentration of polyethylenene imine; adapted/reprinted from [135], ©2015, by The Royal Society of Chemistry; d) Oleic acid/hexadecylamine ratio. adapted/reprinted with permission from [132], copyright (2016) American Chemical Society.

By gravity action, NH_4OH migrates to the bottom of the tube leading to the hydrolysis of the iron(III) chloride. Temperature reaction and concentration of iron(III) chloride and NH_4OH are the critical parameters to tailor the final dimensions. β-FeOOH rods of 45 x 8 nm were achieved when the concentration of $FeCl_3$ was 0.1 M and the volume of NH_4OH was 320 μL at 100 °C, while the longest rods (450 x 120 nm) where grown using 1 M [$FeCl_3$] and 128 μL NH_4OH at 50 °C. The nucleation is less intense at acidic pHs, (i.e. increasing the concentration of iron(III) chloride or decreasing the concentration of NH_4OH) and at lower temperatures, leading to larger particles.

Other strategy for the synthesis of elongated magnetite nanoparticles is based on the synthesis of hematite (α-Fe_2O_3) elongated particles as shape template. Hematite can be directly synthesized by forced hydrolysis of iron(III) salt (i.e. chloride and perchlorate) at 100 °C during several days in the presence of phosphate ions, which are the responsible for conferring the anisometric growth along the c-axis and setting the axial ratio, leading to particles from 100 to 500 nm in length and axial ratios between 1 and 5 (Fig. 8).[46,79]. In general, the particle size can be tailored with the concentration of the ferric salt, pH, solvent and ions present in the solution.[94,137] Furthermore, hot-injection of iron(III) chloride salt at 100 °C leads to hematite nanostructures with axial ratios around 3.[138] The main disadvantages of the direct synthesis of hematite is the long reaction time (several days) and the poor yield. Additives such as urea overcome these disadvantages reducing the synthesis time and increasing the yield (because of the hydroxyl anions release that promotes β-FeOOH precipitation) resulting in structures with an aspect ratio close to 10. [130,139] [130]

Direct synthetic methods to grow 1D Fe_3O_4 nanostructures based in organic media and surfactants have experienced a great upsurge in the last years. These routes for the growth of elongated particles start with the formation of nuclei with octahedral shape. The exposition of {111} facets permits the anisometric growth along the [111] direction.[131] Another option is the growth along the [100] direction by elongation of the octahedral edges. For example, seeded-growth of a mixture of iron(0) pentacarbonyl with trioctylphosphine (TOP) to a suspension containing 2 nm Fe particles capped with TOPO at high temperatures, followed by a reflux with dodecyl dimethylammonium bromide (DDAB) leads to Fe nanorods of 11 × 2 nm.[131] By increasing the concentration of DDAB it is possible to reach magnetite nanoparticles 27 nm in length without changing the diameter. The formation of the rod shape can be understood by the unidirectional coalescence of the spherical nanoparticles induced by the strong attachment of the DDAB molecules to the central part of the particle.

The synthesis of iron oxide nanowhiskers (20 x 2 nm) can be done by selective decomposition of iron(III) oleate in 1-octadecene in the presence of a surfactant mixture composed by oleic acid, oleylamine and TOPO.[125] In this synthesis route, the temperature (150 °C) is too low to produce the decomposition of iron(III) oleic complex which is reported to take place at temperatures above 250 °C.[107] Consequently, an alternative mechanism suggests that these nanowhiskers

were produced by hydrolysis of iron(III) oleate complex. In this sense, a further step forward in the synthesis was the exchange of the iron(III) oleate by iron(0) pentacarbonyl with a more controllable decomposition and reactivity. The addition of iron(0) pentacarbonyl to a mixture of hexadecylamine, oleic acid and 1-octanol in a solvothermal synthesis heated at 200 °C for 6 hours renders rods of 63 x 6.5 nm in size (axial ratio~10). Length and axial ratio can be increased up to 140 x 12 nm (axial ratio ~12) by increasing the amount of hexadecylamine from 0.2 to 0.6 g probably due to the amount of water generated during the hydrolysis (Fig. 8). In summary, the proposed mechanism of this reaction is as follows. First, oleic acid is involved into two different reactions, i) formation of Fe(0)-oleic complex and ii) formation of an amide via reaction with hexadecylamine which renders water molecules. Then, part of the Fe(0)-oleic complex generates Fe nuclei, which rapidly oxidizes to FeO and the rest is hydrolysed by the water molecules generated before leading to Fe_3O_4. Due to the slow water releasing rate, the cluster concentration is below the nucleation threshold so there is a heteronucleation of the initial Fe_3O_4 nanorods on the surface of the FeO nuclei. Finally, another important parameter to control the final dimension and aspect ratio is the autoinduced pressure inside the reactor that can be tailored by changing the filling percentage of the reaction vessel. When the reaction volume decreases from the 80 to 53%, the particle length decreases from 163 to 56 nm and the axial ratio from 12 to 6 .[132]

2.3. Disk-shaped nanoparticles

The synthesis of Fe_3O_4 nanodisks/nanoflakes/nanoplates has been reported through a two-step methodology consisting on the formation of α-Fe_2O_3 by the solvothermal route and further reduction to Fe_3O_4 (Fig. 9). The formation of hematite nanodisks can be achieved by the hydrolysis of iron(III) chloride in a mixture of water/ethanol in the presence of sodium acetate. This reaction is carried out at 180 °C for 12 hours growing nanodisks with 226 x 26 nm size (aspect ratio, i.e. thickness/diameter ~ 0.11).[140] Diameter and thickness of the hematite nanoparticles can be controlled by the amount of water in the solvent and sodium acetate.[141] Thus, nucleation is delayed in absence of water forming spherical particles at first instance, which rapidly transform to iron oxide structures with circle-pancake shape instead of hexagonal plates after several days. Water acts as an accelerating agent, which leads to an increase of the thickness and a decrease of the diameter. Diameter and thickness of nanodisks changes from 400 x 8 nm to 40 x 40 nm respectively when the volume of water added increases from 0.3 to 2.5 mL. The decrease of the alcohol polarity also leads to a decrease in the aspect ratio. Finally, sodium acetate regulates the growth of the nanodisks because it strongly coordinates to surface atoms on (001) planes of hematite. If sodium acetate is not present or is just in a minimum amount in the reaction, small particles are synthesized. However, for a certain range, it coordinates to (0001) facets

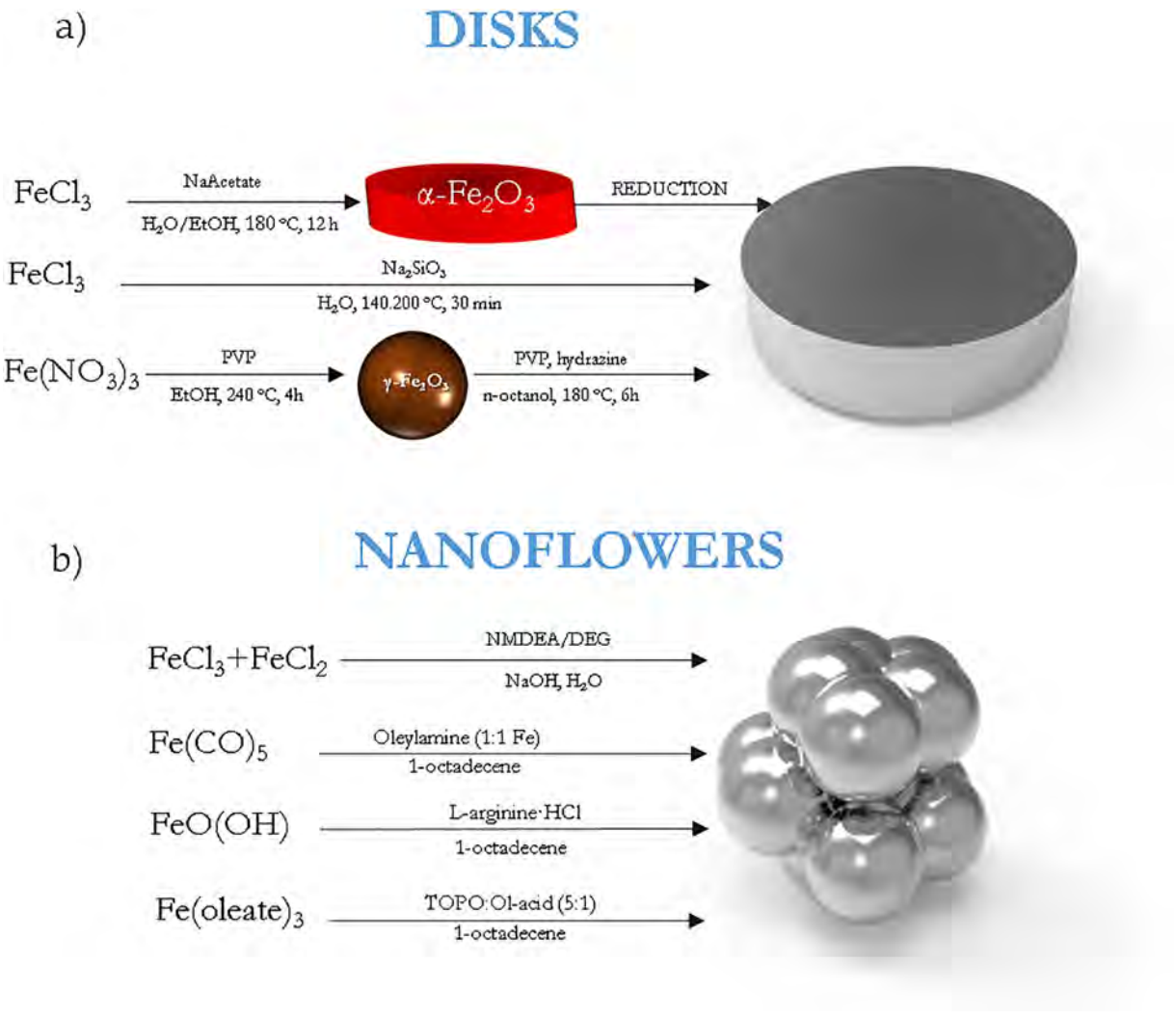

Fig. 9. Synthesis routes to obtain magnetite nanodisks/plates and nanoflowers. (PVP = Polyvinyl pyrrolidone, NMDEA = N-methyldiethanolamine, DEG = Diethyelene glycol). Synthesis routes from references [140, 142–147].

Please cite this article as: A.G. Roca, L. Gutiérrez, H. Gavilán, et al., Design strategies for shape-controlled magnetic iron oxide nanoparticles, Adv. Drug Deliv. Rev., https://doi.org/10.1016/j.addr.2018.12.008

leading to a decrease in the nanoparticle aspect ratio. Based on the same strategy, magnetite nanodisks were synthesized by using Na_2SiO_3 instead of sodium acetate, and heating in a microwave digestion system for 30 minutes at temperatures higher than 140 °C, achieving nanodisks of 100 x 60 nm.[142]. Smaller nanoplates of 35 nm in lateral size with a thickness of 10-13 nm were synthesized in two steps (Fig. 9). The first step consists on the reaction of iron(III) chloride with PVP in ethanol at 240 °C under solvothermal conditions to lead to maghemite nanoparticles. In a second step, using n-octanol as solvent, the addition of more PVP and hydrazine and heating up to 180°C for 6 hours completes the transformation to magnetite .[143]. Nanoplate size can be controlled through the first reaction by tailoring the temperature and the reaction time.

2.4. Flower-like nanoparticles

Magnetite nanoparticles are able to aggregate in a hierarchical way and form 3D structures with flower-like morphology. [148] Apart from the core size, another important parameter is the final aggregate size of the particles and most importantly the degree of fusion between cores.[149] Both sizes are controlled and tailored essentially by selecting the synthetic route and the reagents involved in the reaction. There are two clear strategies to synthesize the 3D flower-like Fe_3O_4 nanostructures that can be differentiated in the final size: the polyol route and thermal decomposition (Fig. 9b and 10).

The polyol method used in the growth of flower-like nanostructures consists in the alkaline hydrolysis of iron salts (usually chlorides) at high temperatures (usually 210 or 220°C) and slow rates.[150] Interestingly, the inclusion of N-methyldiethanolamine (NMDEA) in the solvent mixture with ethylene glycol (EG) or alone makes possible the formation of flower-like Fe_3O_4 nanoparticles, otherwise spherical single core Fe_3O_4 particles are grown.[151] The generation of primary units of 4-6 nm quickly agglomerates to 11-16 nm cores that aggregate up to 55 nm particles depending on the amount of NaOH and the time at 220 °C. [35,144] Starting from an iron(II) salts in polyol media, in the presence of different polymers such as PVP, or citrate and using an autoclave for long time heating at high temperature, larger flower-like particles between 50 and 250 nm in size composed of 5-15 nm cores are obtained. PVP and NaAc can be used to increase the stability of the as-synthesized colloid, achieving flower-like nanoparticles with tuneable size and shape.[152–156] Besides, this type of flower-like nanoparticles can be obtained with a carbon shell structure using ferrocene as a single reactant. [157,158] Interestingly, by forcing the magnetic interaction of the cores using a polymeric matrix, flower-like nanoparticles of regular size can be achieved.[73,159]

Fe_3O_4 nanoflowers can be also synthesized by thermal decomposition in organic media. For example, the decomposition of iron(0)

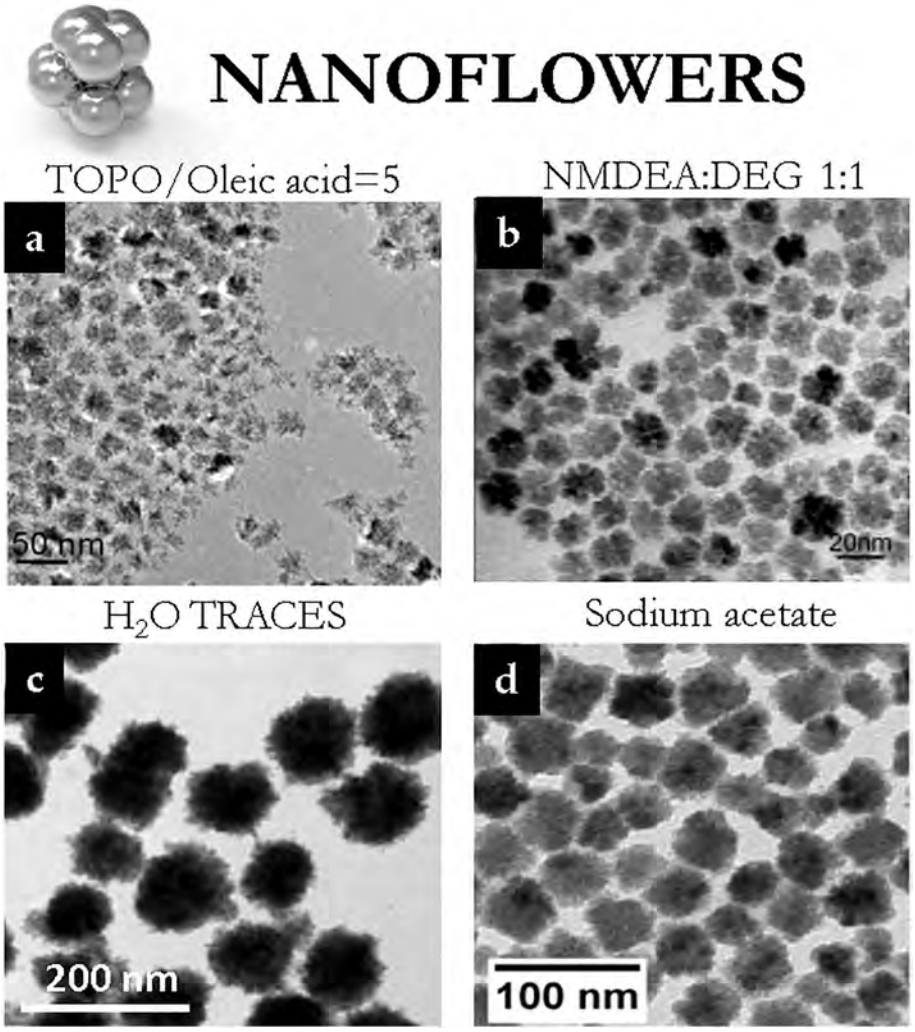

Fig. 10. TEM images of diverse nanoflower-like Fe_3O_4 nanoparticles synthesized under different conditions; a) Thermal decomposition; b-d) Polyol method. Sources: a) adapted/reprinted with permission from [145], © 2012, by The Royal Society of Chemistry; b) adapted/reprinted with permission from [160], copyright (2017) American Chemical Society; c) adapted/reprinted with permission from[149], © 2017, by Wiley; d) adapted/reprinted with permission from[151], copyright (2004) American Chemical Society.

Please cite this article as: A.G. Roca, L. Gutiérrez, H. Gavilán, et al., Design strategies for shape-controlled magnetic iron oxide nanoparticles, Adv. Drug Deliv. Rev., https://doi.org/10.1016/j.addr.2018.12.008

pentacarbonyl in 1-octadecene in the presence of oleylamine with a equimolar ratio of Fe and oleylamine leads to 17 nm aggregates composed by small crystals of around 5 nm.[146] The low concentration of oleylamine that cannot prevent the agglomeration of the particles points as the reason for the formation of these Fe_3O_4 nanoflowers. Also, the use of L-arginine monohydrochloride in the decomposition of FeO(OH) in 1-octadecene leads to 40 nm flower-like aggregates. Ostwald ripening seems to be responsible for the formation of the aggregates and chloride ions from L-arginine seem crucial for reaching the flower-like structure. [147] Moreover, the decomposition of iron(III) oleate in a surfactant mixture of TOPO and oleic acid (5:1 in molar ratio) renders aggregates of Fe_3O_4 with a size around 20 nm composed of small 5 nm nanocrystals. In this scenario, TOPO induces a burst nucleation at 290 °C (synthesis temperature) leading to a huge number of nuclei that no further grow so, in order to minimize surface energy, the nuclei tend to aggregate. [145] Also calixarene molecules have been shown to stabilize intermediate reaction stages, leading to flower-like structures before magnetite particles are transformed to octahedrons. [161] Comparing the synthetic approaches to obtain flower-like nanoparticles, organic medium containing surfactant stabilizers (thermal decomposition of organic precursors) allows to control nucleation events for the formation of the nanocrystals and thus the size, and the use of surfactants allows monodispersity. However, it yields hydrophobic particles stabilized by the surfactants that need further treatments to make them hydrophilic. On the other hand, polyol-mediated process allows the dissolution of compounds, including surfactants, of very different nature and polarity allowing the tuning both the core and particle size of the flower in a larger range (thus, it is more versatile than thermal decomposition of organic precursors). In addition, synthesis in poly-alcohols provide a versatile surface chemistry of the nanoflowers, from hydrophobic to hydrophilic surface, depending on the reagents used in the synthesis.

2.5. Other shapes

In this section those morphologies which cannot be fully identified with the aforementioned ones are covered (Fig. 11, 12 and 13). The most studied nanoparticles from this group are the hollow ones. The synthesis of **hollow nanoparticles** emerged at the beginning of this century for their possible applications in catalysis, lithium-ion batteries and drug delivery. There are different approaches to achieve the hollowed morphology, including hollow nanorings, nanotubes and also rods, but all of them are based on the carving of a sacrificial template by different mechanisms (Fig. 11).

The most common hollow nanostructures are **hollow spheres** (Fig. 11). Etching can be carried out using Fe_3O_4 nanoparticles as template. Heating magnetite nanoparticles in technical TOPO at 300 °C for 2 h leads to hollow nanoparticles. It seems that the responsible for this carving effect is the presence of alkyl phosphonic acid as impurity which coordinates to the Fe ions at the particle surface, dissolves the ions by forming an iron-phosphonate complex and generates a pseudo-Kirkendall process where there is an inward diffusion of phosphorous and oxygen and outward diffusion of Fe ions.[162] Fe_3O_4 nanoparticles in a range of 11-24 nm have been successfully etched leading to equivalent size structures with a minimum shell thickness of 3 nm, while particles smaller than 10 nm are dissolved.

Using core/shell Fe/Fe_3O_4 nanoparticles as sacrificial template, it is also possible to fabricate hollow Fe_3O_4 nanoparticles inducing a Kirkendall reaction by flowing oxygen into the reaction at high temperatures (Fig. 11). There are different ways to mix the colloidal Fe/Fe_3O_4 suspension with oxygen, i.e. flowing Ar enriched with O_2 (20%, 20 mL/min)[163], decomposing trimethylamine N-oxide $(CH_3)_3NO$ at 210 °C [164] or at the expense of oxygen captured inside a sputtering deposition chamber.[165] It has been observed that the existence of a passivated layer of Fe_3O_4 is necessary to start the oxidation due to the unbalanced interfacial diffusion of oxygen and Fe atoms.[88] Hollowing mechanism begins once the Fe/Fe_3O_4 nanoparticles are in contact with O_2 because it triggers the outward diffusion of Fe ions to the outer shell and oxygen ions inward. Fe ions diffuse faster so Fe_3O_4 collects at the metal oxide interface leaving vacancies behind that coalesces into a single central cavity. With this approach, hollow Fe_3O_4 nanoparticles from 4 to 20 nm with a shell thickness between 3 and 4 nm have been synthesised controlling the extension of the oxidation process by controlling temperature and time.

Another approach using the same template Fe/Fe_3O_4 is to induce a corrosion by the in situ generation of a sodium molten salt derived from the presence of sodium oleate.[172] In particular, the decomposition of iron(II) stearate in the presence of oleic acid with the addition of 1% of sodium oleate at 380 °C generates 21 nm **hollow magnetite**

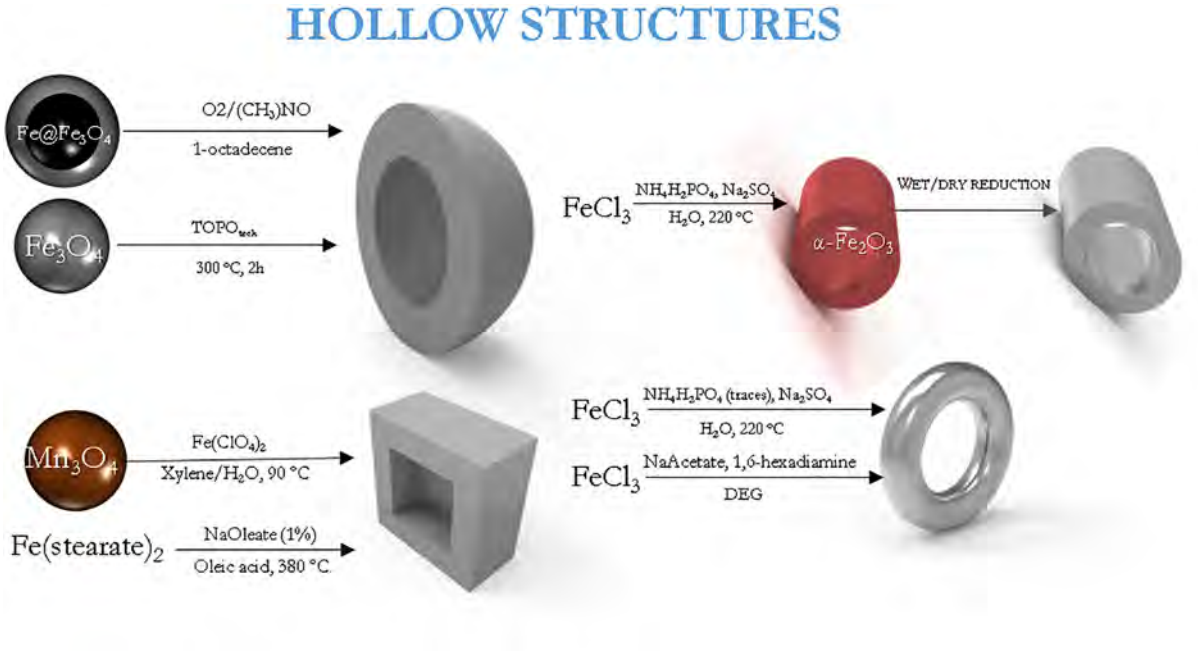

Fig. 11. Scheme of the synthesis routes for the growth of hollow Fe_3O_4 nanostructures (nanospheres, nanoframes, nanotubes and nanorings). Synthesis routes from references [162–164, 166–171].

Please cite this article as: A.G. Roca, L. Gutiérrez, H. Gavilán, et al., Design strategies for shape-controlled magnetic iron oxide nanoparticles, Adv. Drug Deliv. Rev., https://doi.org/10.1016/j.addr.2018.12.008

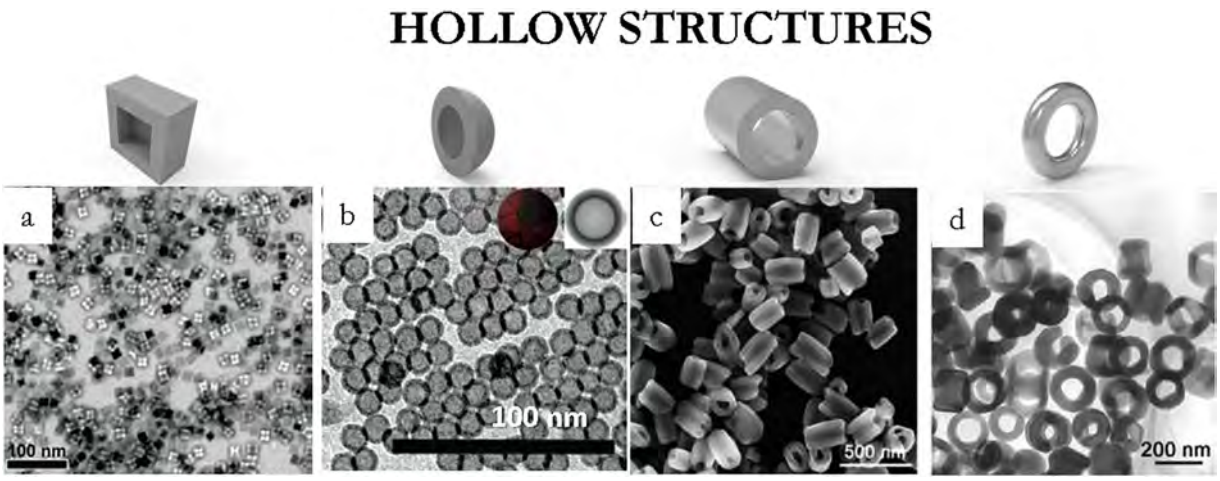

Fig. 12. Transmission electron (a,b,d) and scanning electron microscopy (c) (TEM/SEM) images of diverse hollow nanostructures and their ideal representations; a) Nanocubes: Adapted/reprinted with permission from [172]. Copyright (2007) American Chemical Society; b) Nanospheres; Adapted/reprinted with permission from [163]. Copyright (2007) American Chemical Society; c) Nanotubes; Adapted/reprinted with permission from [170]. Copyright (2008) American Chemical Society; d) Nanorings. Adapted/reprinted with permission from [170]. Copyright (2008) American Chemical Society.

nanocubes. At high temperatures, sodium oleate decomposes and Na reacts with O_2 and H_2O forming Na_2O and NaOH,[166,167] which are responsible for the continuous etching of Fe nanoparticles. It is noteworthy that only Fe {110} faces undergo prominent etching maybe due to absorption or underpotential deposition of Na species on this face. Changing the amount of oleic acid and the heating rate seems to be crucial to grow hollow Fe_3O_4 with different sizes (15-50 nm) and shapes (**hollow stars**).

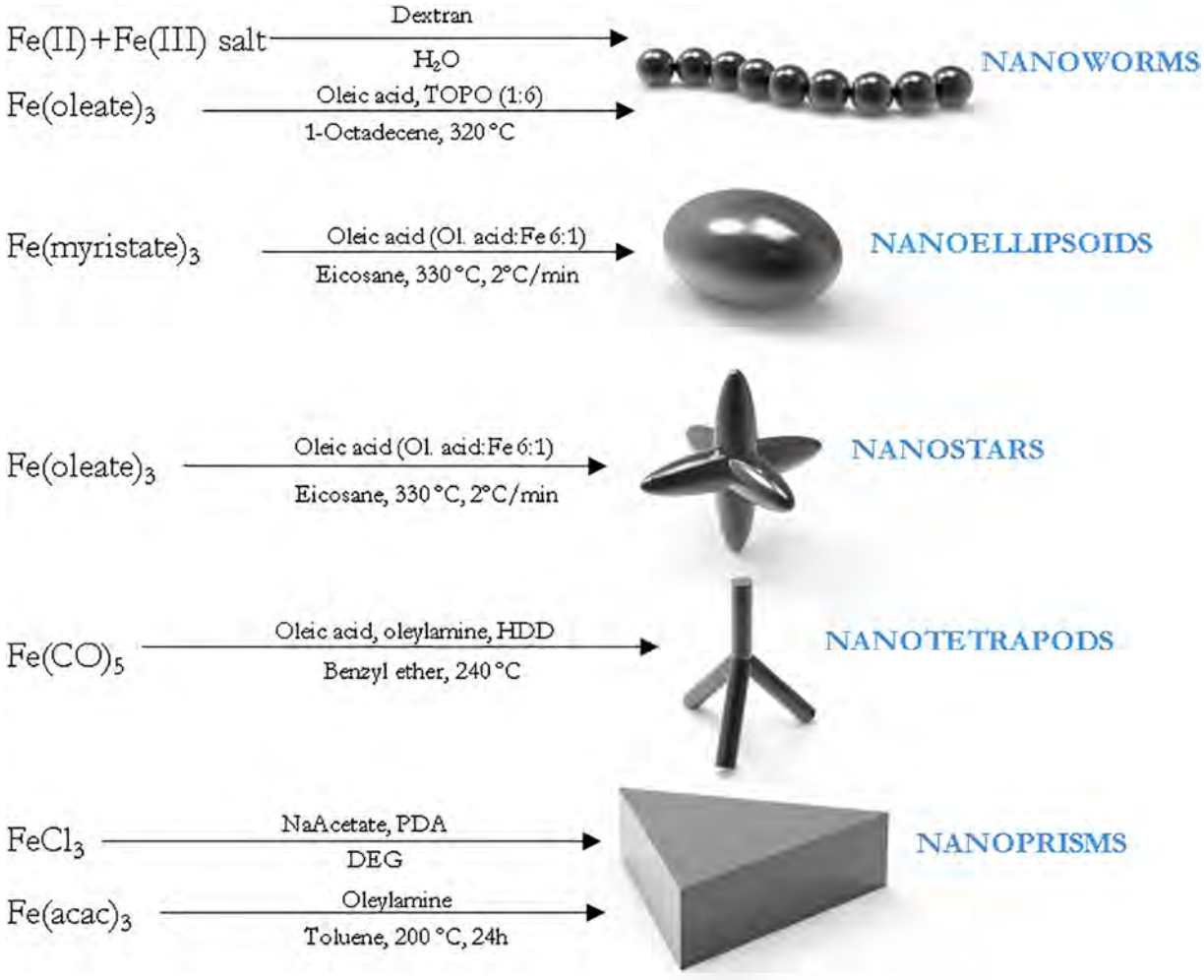

Fig. 13. Scheme of the synthesis routes for the generation of magnetite nanoworms, nanoellipsoids, nanostars, tetrapods and nanoprisms. Synthesis routes from references[176–181]

Please cite this article as: A.G. Roca, L. Gutiérrez, H. Gavilán, et al., Design strategies for shape-controlled magnetic iron oxide nanoparticles, Adv. Drug Deliv. Rev., https://doi.org/10.1016/j.addr.2018.12.008

Sacrificial templates can be made of metal oxides different from the previously described iron ones, leading to hollow bi-phasic metal oxide nanoparticles as intermediate (Fig. 11). For example, 21 nm Mn_3O_4 nanoparticles can be used as seeds for the deposition of γ-Fe_2O_3 (Fig. 11). The mixture of Mn_3O_4 in xylene with a solution of iron(II) perchlorate at 90 °C triggers a galvanic reaction[168] through the xylene-water interface where iron(II) cations oxidize to iron(III) and manganese(III) species reduces to manganese(II) which are etched leading to opposite diffusion of electrons (inward) and manganese(II) (outward) through the pin holes created at the interface. At the end of the reaction, all the Mn_3O_4 is dissolved and 23 nm γ-Fe_2O_3 remains. Moreover, a more simple version of this approach using MnO/Mn_3O_4 core/shell nanoparticles as templates and trimethylamine N-oxide instead of water in an all-organic environment also leads to hollow γ-Fe_2O_3 nanoparticles at the end of the galvanic reaction.[173]

It is worth mentioning that hollowing process can be achieved with the electron beam of the electron microscope. Poor crystalline Fe/Fe_3O_4 particles derived from the decomposition of iron(0) pentacarbonyl in a mixture of TOPO and hexadecylamine leads to hollow particles once exposed to the electron beam for 2 minutes. It seems that the beam creates a quasi-melting state were Fe atoms diffuse and voids coalesce creating a single void to minimize the surface area.[174] Thus, a poor crystalline structure with lots of defects is the origin of this carving effect. Moreover, an excess of oleylamine in Fe/Fe_3O_4 nanoparticles also creates hollow particles.[175] In this case, an increase from 14.5 to 17 nm is achieved in the final particles with near 4 nm of thickness.

Fe_3O_4nanorings and nanotubes can be produced using hematite (α-Fe_2O_3) as sacrificial template. The hydrolysis of iron(III) chloride in water with the presence of $NH_4H_2PO_4$ and Na_2SO_4 carried out under hydrothermal conditions at 220 °C for several hours leads to α-Fe_2O_3 nanotubes with a height up to 250 nm and diameters up to 170 nm.[169,170] In a second step, α-Fe_2O_3 nanotubes can be transformed to Fe_3O_4 by annealing at 360 °C under a mixture of H_2 and Ar flow. The mechanism of the nanotube formation can be understood as a coordination-assisted dissolution process. In the first stage of the reaction phosphate groups induce an anisotropic growth along the [001] axis because of the selective binding to {100} and {110} faces. In the case of sulphate groups, their affinity to Fe is much weaker than phosphates so do not play a key role at this step. However, at some point in the reaction, a dissolution of α-Fe_2O_3 tips towards the interior happens to be until hollow tubes are formed. In this stage, sulphate ions play a key role assisting the dissolution process. The proposed explanation for the selective dissolution is that hematite tips have a high surface energy and are easily attacked by the protons in acidic solution (pH 1.8 is reached due to the chloride ions from the Fe precursor). By changing the ratio between phosphate and sulphate ions it is possible to tailor the aspect ratio of the hematite rods and also the final nanotubes, reaching a nanoring structure when the concentration of phosphate ions is low. Interestingly, Fe_3O_4 nanorings between 15 and 50 nm can be also obtained in one step through the hydrolysis of iron(III) chloride in ethyleneglycol in the presence of sodium acetate and 1,6-hexadiamine under solvothermal conditions at 200 °C.[171]

Apart from hollow morphologies, there are several shapes that have been grown occasionally under extreme synthetic conditions (Fig. 13). For example, **Fe_3O_4nanoworms** can be synthesized by coprecipitation of high–concentrated solutions of iron(II) and iron (III) salts in water in the presence of dextran (Mw~20 kDa). These worms can reach a length of 50 nm as a result of the string of 5 nm spheres. When higher molecular weight dextran was used, multibranched structures with a size of 100 nm were grown.[176] An alternative to grow Fe_3O_4 nanoworms [177] using thermal decomposition approach can be accomplished decomposing iron(III) oleate in 1-octadecene with a mixture of oleic acid and TOPO (molar ratio~ 1:6) at 320 °C for 5 hours. The final nanoworms could reach a final length of 200 nm from the aggregation of spherical particles. This aggregation was possible because of the presence of weakly-bound TOPO on the iron oxide surfaces.

Fe_3O_4nanostars with 50 nm branches can be accomplished through the decomposition of iron(III) oleate in eicosane in the presence of oleic acid with a slow heating rate (2 °C·min^{-1}) and a final reflux temperature of 350 °C.[178] The key point for achieving a star-shape morphology relies on the oleic acid:Fe ratio of 6, which is extremely high, i.e. around the upper limit to get nanoparticles. Authors justify this shape due to an uneven growth of nanoparticles around the nuclei because of the large concentration of oleic acid adsorbed in the nanoparticle surface. Interestingly, **Fe_3O_4ellipsoids** can be grown following the same synthetic route but using iron(III) myristate instead of iron(III) oleate, which was attributed to the slower decomposition of myristates in comparison to other iron carboxylates.

Multribranched **Fe_3O_4tetrapods** with sizes between 3 and 30 nm in length and a fixed branch diameter around 3-3.5 nm can be grown by slowly heating iron(0) pentacarbonyl in 1-octadecene in the presence of a ligand mixture composed by oleic acid, oleylamine and 1,2 hexadecanediol (in a molar ratio 3:3:5) at temperatures below 240 °C.[179] The length can be modulated with the amount of iron(0) pentacarbonyl and the number of branches can be modulated with the amount of oleic acid.

Fe_3O_4nanoprisms can be synthesized through the hydrolysis of iron (III) chloride in the presence of sodium acetate, 1,3-propanediamine (PDA) and ethyleneglycol (EG).[180] EG/PDA ratio are the key parameters to determine the final size and morphology. Fe_3O_4 nanoprisms with edges between 50 and 70 nm and thickness with 15-20 nm can be synthesized using a mixture EG/PDA=20 mL/2 mL. However, an EG/PDA mixture of 35 mL/5 mL leads to Fe_3O_4 octahedrons. Another synthetic route using organic solvent lies on the decomposition of iron(III) acetylacetonate in toluene with the presence of oleylamine at 200 °C for 24 hours.[182] The oleylamine controls the anisotropic growth of the nanocrystals to the final nanoprism shape and the molar ratio between the oleylamine and the Fe precursor (15:1) leads to 22 nm nanoprisms in lateral size with 10 nm in thickness.

2.6. Shape-controlled magnetic nanoparticles of other transition metals

This review is centred in the synthetic strategies for shape-controlled magnetic iron oxide nanoparticles, since they have largely demonstrated to have good magnetic features and low toxicity in bioenvironments.[183] However, the progress on nanotechnology has allowed the development of nano-tools with broader composition and outstanding magnetic features that amply surpass those from iron oxide nanoparticles (i.e. in terms of saturation magnetization, coercive field, etc.). This improvement is associated not only with the shape of the nanoparticle, but also in this case due to the presence of other elements, such us other transition metals (Co, Mn, Zn, Cu, Ni) in the crystal structure that will suitably modify the spin structure of the nanomaterial. [184] Recently, the up-above mentioned routes for the fine shape-controlled synthesis of cubic/polyhedral, elongated, flower-like, hollowed nanometric structures, etc., were further developed in order to include other elements apart of Fe while preserving the shape. Table 1 summarizes the developed synthetic routes for each system of nanoparticles (with specific shape and size) and the precursors used in order to introduce the transition metal elements, along with other compounds involved in the synthetic reactions. Thus, it is possible to use organic metal precursor such as acetyacetonate or oleates, including Fe^{3+} and other divalent transition metals: Fe^{2+}, Mn^{2+}, Zn^{2+}, Cu^{2+}, Ca^{2+}, Mg^{2+}. Such M^{2+}/Fe^{3+}–organic precursors can be decomposed at high temperature allowing the formation of the corresponding mixed ferrites.[185] For example, the composition of magnetic nanocubes synthesized via thermal decomposition of organic precursors can be stoichiometric adjusted with Co by simply introducing $Co(Acac)_{2/}Fe(Acac)_3$ ratio.[186] Lastly, the shape-controlled synthesis of hollow spheres was achieved via galvanic replacing on 24 nm MnO/Mn_3O_4

Please cite this article as: A.G. Roca, L. Gutiérrez, H. Gavilán, et al., Design strategies for shape-controlled magnetic iron oxide nanoparticles, Adv. Drug Deliv. Rev., https://doi.org/10.1016/j.addr.2018.12.008

Table 1
Colloidal synthetic strategies for other shape-controlled magnetic composites.

Route	Composition	Shape	Dimensions (nm)	Metal Precursors	Reagents involved	Reference
Thermal decomposition	$Co_xFe_{3-x}O_4$	Nanocubes	15-27	$Fe(Acac)_3$/ $Co(Acac)_2$	Decanoic acid	[186]
Thermal decomposition	$M_xFe_{3-x}O_4$ (M^{2+} =Fe^{2+}, Mn^{2+}, Zn^{2+}, Cu^{2+}, Ca^{2+}, Mg^{2+})	Nanocubes	10-20	M^{2+}/Fe^{3+}–Oleate	TOPO, OA	[185]
Thermal decomposition/ Galvanic replacement	MnO_x/FeO_x	Hollow nanospheres	24 (7-10 inner voids)	$Mn(Oleate)_2/Fe(Acac)_3$	OA, Oleylamine	[173]
Polyol	$MnFe_2O4$	Flower-like	50	$FeCl_3/MnCl_2$	PAA	[187]
Polyol	$ZnxFe_{3-x}O_4$	Nanorings	13-20 x 100-150 x 70-110	$Zn(Acac)_2$/ $FeCl_3$	EG / H_2O / $(NH_2)_2CO$	[188]

nanoparticles. The voids in the structures were successfully achieved upon the addition of $Fe(Acac)_3$, and water or $(CH_3)_3NO$, which both allow concomitant $Mn^{3+} \rightarrow Mn^{2+}$ reduction to form hollow Mn_3O_4/Fe_3O_4 structures and thus, the deposition of Fe^{2+}.[173]

Polyol mediated synthesis has recently demonstrated to likewise allow the formation of various transition metals ferrites, as it is the case of 50 nm Mn ferrite flower-like nanoparticles,[187] through the use of stoichiometric feed ratio of $FeCl_3$ and $MnCl_2$ leaf-like nanoplatelets. Interestingly, 13-20 nm $Zn_xFe_{3-x}O_4$ leaf-like nanorings (in thickness) could be synthesized by the combination of the polyol and calcination methods.[188] This a an indirect method that yields alkoxide leaf-like nanoplatelets starting from metal sources of different nature: $Zn(Acac)_2$ and $FeCl_3$, achieving interestingly homogenous solid solutions of iron and zinc. After polyol synthesis, a calcination process provokes the formation Zn ferrite nuclei and inner holes, achieving the final nanorings. This was attributed to the degradation of the organic component of the nanoplatelets with formation of CO_2, CO, and H_2O. The evolution of such gases would generate in-situ pores in the nanoplatelets (the bigger pores were thought to grow via swallowing the smaller ones). Simultaneously, to minimize the interfacial energy, the as-formed Zn ferrite nuclei diffuse outwards and aggregate along the edge of the nanoplatelets leading to the final nanorings.

It must be highlighted that the use of Mn^{2+}, Zn^{2+}, Cu^{2+}, Ca^{2+}, Mg^{2+} for biomedical application brings another concern into the picture, which is the toxicity and the need to avoid metal leaching from the nanoconjugates.[60] Thus, different coating strategies should be studied in these cases in order to protect the inorganic core of the magnetic nanoparticles from the surrounding media, and to increase their stability in biological environments. Lastly, cytotoxicity studies in these nanosystems are mandatory.

3. Ligands

The synthesis of monodisperse size and shape-controlled particles requires the separation in time of nucleation and growth stages as previously mentioned and has been addressed in numerous works (Fig. 14).[11,12,22,28,30,53,189–196] Ligands (often called capping agents/molecules/stabilizers/adsorbates) are used for this purpose because of their determinant role in all the stages of the synthesis process. Ligands compile the group of small molecules, surfactants or polymers with functional groups that coordinate to metal cations through covalent bonds donating electrons to the electron-poor metal atoms or by any other chemisorptions process. Some examples of ligands are surfactants such as carboxylic acids (oleic acid, decanoic acid), amines (oleylamine, dodecylamine, quaternary ammonium salts) and phosphines (TOP, TOPO) or polymers (dextran, PVP).

Prior nucleation, ligands are responsible for solubilizing the cations forming metal complexes or metal hydroxides often referred as "monomers", "reactive species" or "solute" in the bibliography, stabilizing the oxidation state of the cation and preventing undesired side reactions. Some examples regarding the formation of these monomers are i) the reaction of unstable precursors such as iron(0) pentacarbonyl in the presence of ligands such as oleic acid, which forms intermediate Fe-oleic acid complexes, soluble in organic media that delays nucleation [27], ii) redox reactions among the precursors that will determine the final product,[198] iii) hydrolysis of iron salts leading to polyhydroxycations involved in the formation of akaganeite, goethite or hematite [199] and iv) alkolysis in organic polar media such as the formation of Fe-alkoxide in glycol that gives rise to the formation of 3D nanoflowers.[151] The concentration of these monomers increases by the sudden or progressive change of a physicochemical parameter (mainly temperature or pH) leading to nucleation when its

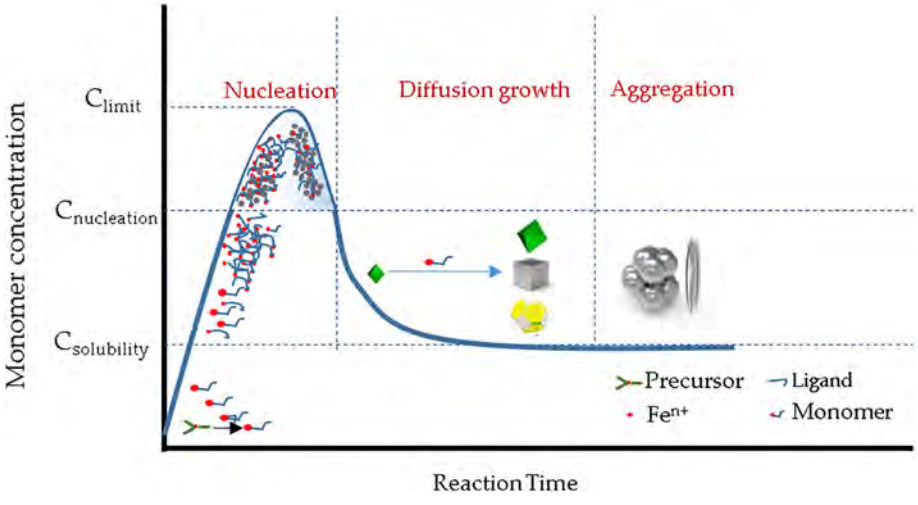

Fig. 14. Formation mechanism of some anisometric nanoparticles in solution. Adapted with permission from [197]. Copyright (1950) American Chemical Society.

concentration overcomes the supersaturation limit. At that moment, the monomer concentration is depleted. (Fig. 14).

Once the nuclei are formed, ligands still have a key role in regulating the growth of the particles their shape evolution, and stabilizing the particles in solution. The absence of ligands leads to an uncontrolled growth driven by the need to diminish the total surface energy as fast as possible, resulting in large and irregular particles. Ligands dynamically adsorb on certain faces by interaction with the particle surface cations decreasing their surface energy. The growth rate along this direction is reduced or inhibited so other growth directions are favoured. The fact that certain ligands only bind to certain faces depends on the characteristics of the faces (e.g. outermost atoms, distance among them and charge) (Fig. 15) and obviously the surfactant functional groups that adsorb or coordinates onto them (functional group, electron-donor or coordination type).[191]

It should be taken into account that under thermodynamic control the growth rate of the different faces is exponentially proportional to its surface energy (Wulff construction model).[200] In the case of magnetite nanocrystals, the primary nuclei have octahedral morphology as (111) are the faces with lower surface energy (Fig. 14 and 15). In general cubic symmetry strongly favours isotropic shapes whereas anisometric shapes are favoured for nuclei presenting monoclinic, orthorhombic or hexagonal crystal structures.[167] It is known that for close packing based cubic crystals, the {100} faces are more energetic than {110} and {111} so its growth rate is faster. Then, the key factor to modulate the crystal shape is the ratio of growth rates between [100], [110] and [111] directions, so for example faster growth of [111] and [110] direction over [100] leads to the final exposure of the slowest {100} faces, i.e. cubic shape nanoparticles (Fig. 14).[113] Conversely, faster growth of [100] and [110] directions over [111] leads to octahedral particles.

In general, for non-cubic structures, the faces with the highest energy are those with smaller reticular interplanar distance,[201–203] which are perpendicular to the longest axis so, thus, growth occurs along this direction. As an example, CdSe growth is highly anisotropic with a high monomer concentration (kinetic control), however, if the growth rate slows down spherical particles can be achieved.[204] One strategy for this purpose is the use of specific ligands, which selectively binds to specific facets modifying their surface energies or the growth kinetics. The effect of the nature and concentration of the ligands on the morphology of magnetite nanoparticles are summarized in Tables 2-3.

Apart of the ligand, temperature and monomer concentration are also important parameters to control the shape of the nanoparticles (Fig. 16).[205,206]. Low monomer concentration and high temperatures favours thermodynamic regimes that lead to isotropic structures. However, high flux of monomers and low temperatures are associated with kinetically controlled regimes that favour the growth of anisometric nanostructures.

3.1. Tips for cubic-shaped nanoparticles

There are two main strategies to grow **cubic magnetic nanoparticles**. The first one deals with the fixed experimental conditions and the second one with the use of ligands with specific affinity to (100) faces. Regarding the former one: i) for thermal decomposition routes: extremely **low heating rates** (0.8 °C·min^{-1}), [207] considerably **high concentrations of Fe precursor**, above 0.3 M,[102] or considerably **low surfactant/precursor ratio** (~2),[104] have reported the successful synthesis of iron oxide nanocubes. ii) for aqueous route (oxidative precipitation): **high heating rates** (20-35 °C·min^{-1}),[106] **high surfactant/Fe ratios** (around 5 or 6),[104] **short refluxing times** (10-20 minutes) or **low Fe precursor concentrations** (0.044 M), have allowed obtaining cubic shape. With regard to the second strategy to achieve cubic shape, the use of **sodium oleate,** [107] **decanoic acid,**[105] **TOPO**[108] **or chloride ions** [116] has reported to lower the surface energy of the growing nuclei and promote their growth along [111] direction. Lastly, it is remarkable that an excess of sodium oleate has accounted for the formation of FeO (wüstite), an antiferromagnetic iron oxide phase, as it will be detailed in Section 4.1.[17,115] The choice of FeO nanocubes as starting material is a smart strategy, due to their magnetically noninteracting nature that allows their controlled anisotropic arrangement, its transformation to Fe_3O_4 and formation of magnetic nano-systems with improved heating efficiency for magnetic hyperthermia.[208]

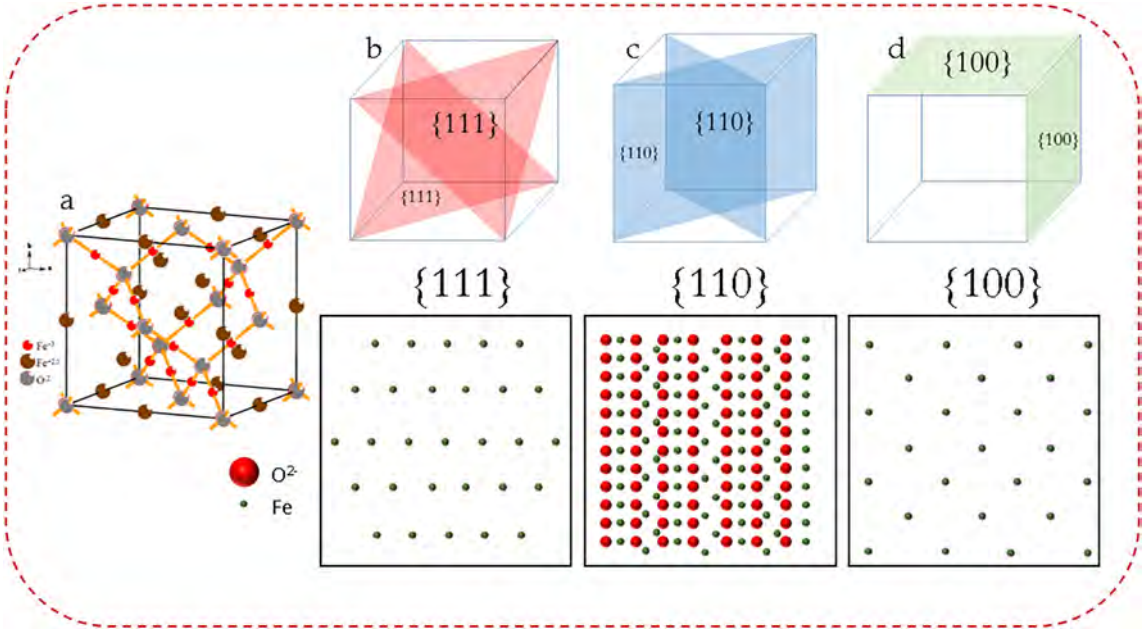

Fig. 15. a) Crystal structure of magnetite. Atomic configuration of low-index faces for cubic crystal systems, b) {111}, c){110} and d){100}. Adapted with permission from [116]. ©2010, by The Royal Society of Chemistry.

Please cite this article as: A.G. Roca, L. Gutiérrez, H. Gavilán, et al., Design strategies for shape-controlled magnetic iron oxide nanoparticles, Adv. Drug Deliv. Rev., https://doi.org/10.1016/j.addr.2018.12.008

Table 2
Role of different ligands as a function of the reaction conditions to reach the target morphology.

Shape	Iron precursor	Solvent polarity	Ligand	Comments
Spherical	$Fe(CO)_5$/ $Fe(oleate)_3$	Organic apolar media	Oleic acid	Under thermodynamic regime.[85,88]
	$Fe(acac)_3$		Oleic acid/oleylamine	In coordinated solvents [87]
	$Fe(acac)_3$		Oleylamine	In excess in the reaction [209]
Cubic	$Fe(oleate)_3$	Organic apolar media	Na(K)-Oleate	Binds selectively to (100) faces[107]
	$Fe(oleate)_3$		Chloride, bromide	Stabilizes (100) faces[116]
	$Fe(acac)_3$		Oleic acid	High supply of monomers (kinetic regime)[102]
	$Fe(acac)_3$		Decanoic acid	Preference binding to (100) faces. Used as growth inhibitor [105]
	$Fe(acac)_3$		4-biphenylcarboxylic acid	Preference binding to (100) faces. Used as growth inhibitor [102]
	$Fe(acac)_3$		TOPO	As impurity, it selectively binds to (100) faces [108]
Octahedra	$Fe(oleate)_3$	Organic apolar media	Quaternary ammonium salts	Generation of TOA cations which selective binding to (111) faces [119]
	$Fe(acac)_3$		Oleylamine	In nearly equimolar ratios to precursor, binds selectively to (111)faces [118]
	$Fe(acac)_3$		Oleic acid/oleylamine 1:1 mixture	In excess leads to truncated octahedral [210]
Elongated	$FeCl_3$	Aqueous	Sodium (potassium) dihydrogen phosphate	C-axis growths due to selective binding on (110) & (100) faces [46,123]
	$Fe(ClO_4)_3$		Urea	Source of OH^- ions. Favours c-axis growth (α-Fe_2O_3) [130]
	$FeSO_4$		Sodium carbonate	C-axis growths due to selective binding on goethite (001) faces [126]
	$FeSO_4$		Polyethyleneimine	Specific adhesion on lateral planes, inhibits growth [135,136]
	$FeSO_4$		Sodium acetate (NaAc)	Allows growth on [001] direction [127]
	$Fe(CO)_5$	Organic apolar media	Hexadecylamine/oleic acid	Generates water through condensation and hydrolyses Iron(0)-oleic complex.[211]
	$Fe(oleate)_3$		TOPO	Weak binding to nanoparticles, easy to remove [125]
	$Fe(CO)_5$		DDAB	Strong binding to central region leading to coalescence & growth of Fe edge particles [131]
	$Fe(oleate)_3$		Oleic acid	Induces elongated nanostructures when heating at 150 °C [125]
Disk	$FeCl_3$	Aqueous	Sodium acetate (NaAc) Ethanol	C-axis growths due to specific adsorption on (0001) hematite faces [141]
Flower	$Fe(CO)_5$	Organic apolar media	Oleylamine	At low concentrations cannot prevent agglomeration due to incomplete capping [146]
	FeO(OH)		L-arginine monohydrochloride	Chloride ions are critical for the formation of flowers [147]
	$Fe(oleate)_3$		TOPO	At high concentrations induces a burst nucleation at 290 °C and aggregates [145]

3.2. Tips for elongated nanoparticles

For **elongated magnetic nanoparticles,** the growth mechanism depends on the solvent and/or the precursors involved. In aqueous media, the growth of elongated particles takes place by the aggregation of primary particles using an iron oxide or oxohydroxide intermediate that acts as shape-template. When **hematite (α-Fe_2O_3)** was used as shape template, particle size can be controlled with the **nature** and **concentration of the iron(III) salt**, the **concentration of phosphate ions** [46,79] that promotes elongated growth through c-axis achieving ellipsoidal shapes, the **addition of urea**[130] and the **ageing time,** promotes the formation of smaller or larger α-Fe_2O_3 nanoparticles respectively. For example nanoparticles of around 600 nm in length with 80 nm in diameter with aspect ratios up to 10 can be achieved by using high

Table 3
Role of different ligands reach hollow, star, tetrapods, prime and worm nanoparticles.

Shape	Iron precursor	Solvent polarity	Ligand	Comments
Hollow	$Fe(CO)_5$	Organic apolar media	Trimethylamine N-oxide	Generates O_2 from decomposition at high T and induce hollow structures by Kirkendall effect[164]
	$Fe(oleate)_2$		Sodium oleate	Corrosion by Molten salts derived from decomposition at high temperature [172]
	$Fe(oleate)_3$		TOPO	Coordinates to outer Fe cations, dissolves them and induces an outward flow of Fe and an inward flow of O and P [162]
	$FeCl_3$	Aqueous media	Ammonium dihydrogen phosphate	Induces anisotropic growth of hematite along [001]. Selective binding to (100), (110) and (012) faces of α-Fe_2O_3 [169]
	$FeCl_3$		Sodium sulphate	Coordinates and dissolves the edges of the α-Fe_2O_3. Leads to smaller nanotubes [170]
Star	$Fe(acac)_3$	Organic apolar media	Oleic acid	At high ligand:precursor ratio.[162]
Tetrapod	$Fe(CO)_5$	Organic apolar media	Oleic acid-oleylamine-hexadecanediol	At T<240 °C acts as templating for anisotropic growth [179]
Prism	$Fe(acac)_3$	Organic apolar media	Dodecylamine (DDA)	At low DDA concentrations, binds selectively to (111) faces.[121]
	$FeCl_3$		Sodium acetate (NaAc)	Binds to (001) faces inhibiting the growth [141]
	$FeCl_3$	Organic polar media	1,3-propanediamine (PDA)	Induces octahedral shapes by stabilization of the (111) EG[180]
			Ethylenglycol	Induces flat shapes together with NaAc under hydrothermal conditions.[180]
Worm	$Fe(oleate)_3$	Organic apolar media	TOPO	Excess of TOPO leads to aggregation of small spheres due to weak binding of TOPO at 320 °C[177]

Please cite this article as: A.G. Roca, L. Gutiérrez, H. Gavilán, et al., Design strategies for shape-controlled magnetic iron oxide nanoparticles, Adv. Drug Deliv. Rev., https://doi.org/10.1016/j.addr.2018.12.008

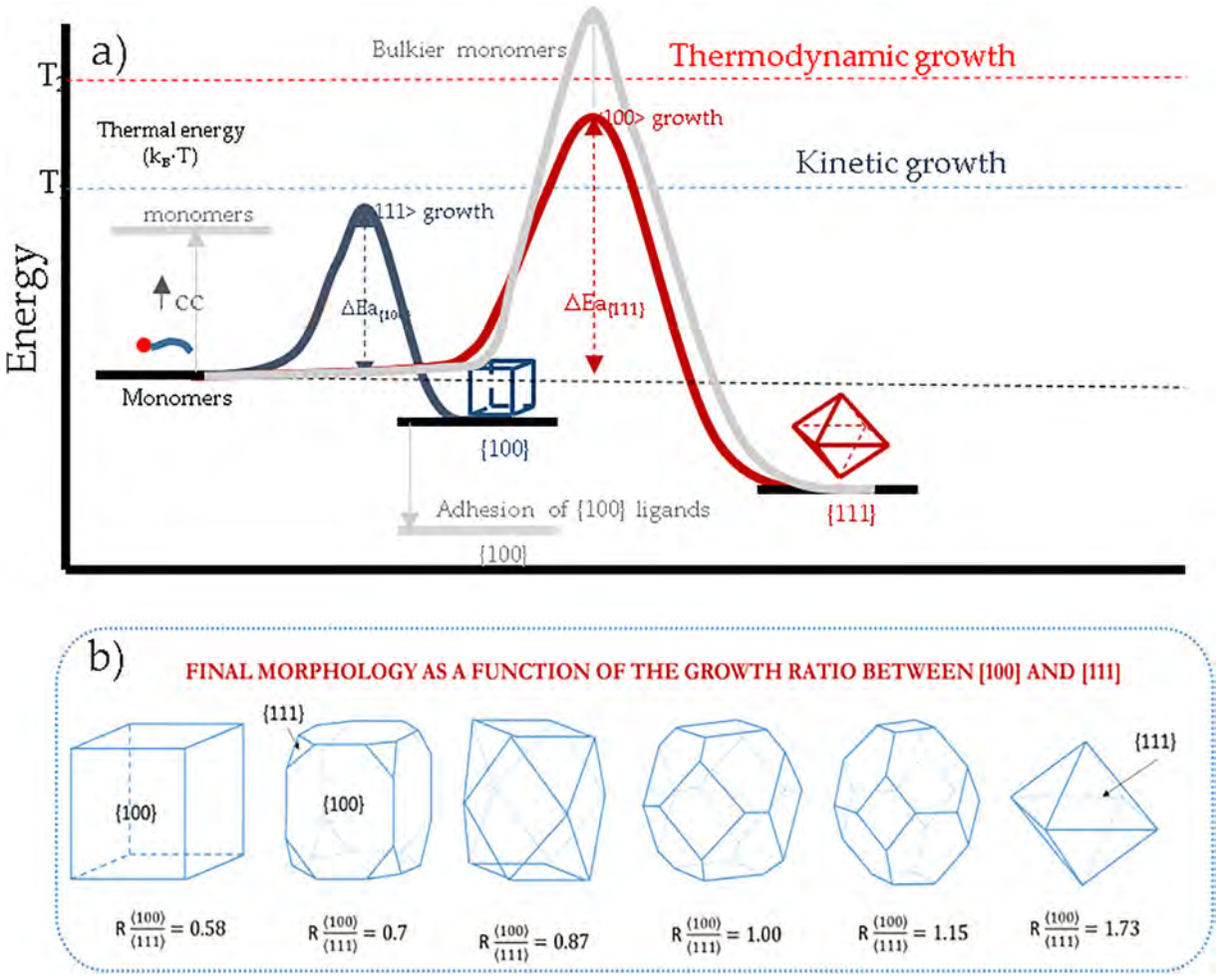

Fig. 16. a) Growth regime of nanoparticles with cubic symmetry and final morphology as a function of the different reaction parameters; b) Final morphology of the nanoparticles as a function of R (ratio between the growth rate along the [100] and the [111] direction). Adapted with permission from [116]. ©2010, by The Royal Society of Chemistry.

concentrations of KH_2PO_4 and large ageing times. The addition of urea leads to the formation of around 300 x 60 nm particles. Smaller hematite particles could be produced by using **low amounts of phosphate ions** and **short ageing times** reaching sizes down to 95 nm with aspect ratios of 2.

When using **goethite (α-FeOOH)** as shape template particles lengths between 60-300 nm and aspect ratios between 6 and 10. The **Fe(II) salt concentration** and the **carbonate or sodium hydroxide concentration**[126] are critical for tailoring the final goethite size. In the case of **akaganeite (β-FeOOH) nanoparticles**, the **concentration of iron(III) chloride** should be higher than **0.1 M** [133]. Large elongated particles up to 500 nm in length and 50 nm in diameter can be synthesized at **high temperatures (100 °C)** with an **ageing time of 24 hours**. [127] Strategies to decrease the nanoparticles size include **lowering the concentration of Fe(III) chloride to 0.1 M**, [134] the **inclusion of polyethylene imine** in the reaction,[135,136] **the reduction of ageing times** (few hours) and the increase of the pH by adding NH_4OH [129]. These strategies allow lower the dimensions to 30 nm in length and 4 nm in width.

In organic media, using iron(III) oleate or iron(0) pentacarbonyl, the mechanism seems to be much more complex. Briefly, the growth proceed by the classical diffusion mechanism of iron oleic complex molecules to iron oxide nuclei previously formed. Largest particles can be achieved by **increasing the reaction time at 200 °C** (if the total decomposition of the iron oleic complex is avoided), the **amount of hexadecylamine** or the volume of the reaction up to 80 % inside the reactor (solvothermal approach). Under these conditions, sizes up to 140 nm x 12 nm can be achieved. On the other side, lowering the filling percentage of the reaction vessel down to 50%**, lowering the amount of hexadecylamine** and the temperature of reaction lead to nanowhiskers of 20 x 2 nm.

3.3. Tips for disk-shaped nanoparticles

The growth of Fe_3O_4 disk shape nanoparticles occurs through reduction of previously synthesized α-Fe_2O_3 nanoparticles having the target morphology, which is obtained by hydrolysis of iron(III) chloride in a mixture of water/ethanol with the presence of sodium acetate. The growth of hematite takes place by diffusion of amorphous ferric hydroxide onto hematite initial nuclei. The amount of **water, the polarity of the alcohol and the presence of sodium acetate** seem to be critical to control the diameter and thickness of the nanodisks, which can grow up to 400 x 8 nm. Low aspect ratios (thickness/diameter) are **favoured using low water/ethanol ratios and large amounts of sodium acetate**.[140] Large aspect ratios are favoured by the opposite conditions (high water/ethanol ratios and minimum amounts of sodium acetate) and using alcohol with high polarity. These conditions allow reaching structures of 40 nm x 40 nm in size.

3.4. Tips for flower-like nanoparticles

Flower-like nanoparticles produced by the **polyol method**, grow in ethylene glycol (EG) by aggregation of primary particles in the presence of **N-methyldiethanolamine (NMDEA)**.[151] For the growth of large

aggregate size particles, it is interesting to use a solvent mixture of EG and NMDEA with a larger proportion of the last one, over stoichiometric amounts of NaOH, heating in steps instead of continuous heating and adding water at the beginning of the reaction. The size of the aggregates can be up to 55 nm formed by cores of 11 nm. However, small aggregates can be achieved with low ageing times, under stoichiometric amount of NaOH. [35,144]

Flowers synthesized in organic media through thermal decomposition lead to small aggregates ranging from 17 to 40 nm always composed of small particles of around 5 nm. The smallest aggregate size was achieved using an **equimolar amount of oleylamine** with **iron (0) pentacarbonyl** [146] while the largest clusters (40 nm) were synthesized with **iron(III) oleate** using **L-arginine monohydrochloride.** [147]

3.5. Tips for other morphologies

Conditions for the production of special morphologies are collected in table 3. **Hollow nanoparticles** always require special and, in some cases, extreme conditions to carve the particle. Some examples are the generation of **nanoframes** and **hollow spheres**. In the case of **nanoframes**, a reaction temperature of 380 °C is needed to decompose sodium oleate and the sodium acts as a Molten salt.[212] In the case of **hollow spheres**, inducing Kirkendall effect on oxidizable Fe nanoparticles (Fe/Fe_3O_4) by passing/generating O_2 *in situ* leads to an inward diffusion of oxygen and outward diffusion of the iron cations generating the target hollow particles. [163,213]

Nanostars are formed at high oleic acid:Fe ratios, just below the limit of nucleation because if oleic acid is present in a big excess, it solubilizes the monomers and inhibits the nucleation of the particles.[178] **Nanoworms** are formed by oriented attachment of small primary particles where the growth by diffusion was not possible because of the strong binding of certain ligands such as TOPO[177] or the effect of bulky ligands like dextran,[176] who drives the oriented attachment to form the nanoworm.

4. Properties

4.1. Structural properties

4.1.1. Nanocrystal structure

The nanocrystal structure is determined by the synthesis route chosen and the growth mechanism. There are different techniques that allow the examination of the nanocrystal structure. One is the scanning and transmission electron microscopy (SEM, TEM), including dark field imaging, high resolution TEM (HRTEM) and related fast Fourier transformation (FFT). They provide local valuable information for the evaluation of the crystallinity, crystal morphology, symmetry and the orientation of crystallographic axes in anisometric nanoparticles. In addition, X-ray diffraction (XRD) provides an overall characterisation of the crystal structure of the sample and statistical measurements. Other interesting techniques such as Infrared and Raman spectroscopy for analysing surface bonds, and Mossbauer spectroscopy, especially interesting for Fe compounds, for determining the iron state, will not be discussed in this review.

Nanocubes are formed by the faster growth of the particles along the [111] direction over the [100] leading to surfaces composed of {100} faces in the case of perfect crystals (Fig. 16). This can be corroborated by the observation of (400) lattice fringes lying parallel to the edge of the cube by HRTEM.[214] Moreover, it is also common to identify the (220) and (111) planes, which are disposed in diagonal within the nanocube.[107,108,116,215] Interestingly, when forming a superlattice, the (220) and (440) XRD peaks show an enhanced intensity with respect to the bulk ones and the (311) decreases because each nanocube has a preferred crystal orientation with {110} planes parallel to the silicon substrate.[106]

Particular attention deserves the structure of Fe_3O_4 nanocrystals synthesized from Fe(III) oleate in eicosane under the presence of oleic acid and sodium oleate [17,115]. In this particular case and due to the reducing atmosphere, magnetite is grown from wüstite through topotaxial growth over shared planes ($(200)_{WÜSTITE}$ //$(400)_{MAGNETITE}$ and $(220)_{WÜSTITE}$ //$(440)_{MAGNETITE}$) of both iron oxide phases. [18,216] Magnetite grows in small subdomains with a high number of defects and antiphase boundaries. This high amount of dislocations created a high number of crystalline boundaries leading to the formation of a mosaic texture, which explains the limited structural coherence in the XRD patterns in comparison to those of pure magnetite structure synthesized by thermal decomposition. [217]

In the case of Fe_3O_4 nanocubes synthesized by a biogenic route trying to imitate the magnetosomes, their morphology can be described as pseudo-cubic, with {100} faces but also {110} from dodecahedron and {111} from octahedron (Fig. 17).[218] It has been observed that the protein Mms6, located in the magnetosome membrane, modifies the crystal morphology from octahedral to cuboctahedral through stabilization of the (100) facets because the negatively-charged C-terminal domain strongly binds to iron and controls magnetite formation. [219–221]

Contrary to nanocubes**, octahedral particles** are formed from the faster growth on [100] direction leading to nanoparticles enclosed on eight {111} faces, which are the most stable for face-cantered cubic systems. Typical family planes observed by HRTEM are (111), (11) and (220).[118] The octahedrons can be slightly truncated exposing {110} faces and when forming self-assembled monolayers, they are supported by contacting two vertices of two adjacent nanoparticles in the first row. During thermal decomposition of iron(0) pentacarbonyl, the addition of capping ligands such as dodecylamine (DDA) can tune the morphology of the crystals to diamond-like nanocrystals. In this case the nanocrystals grow along the [110] zone axis with separation angles of 70° and 90° between the planes, which is a dodecahedron truncated along the [111] and [100] directions.[121] Triangular nanocrystals are also achieved, showing (220) planes along the [111] zone axis, which points that it is a tetrahedron with highly truncated {111} faces.

Solvothermal process reported to directly synthesize **magnetite nanorods** using iron(0) pentacarbonyl ($Fe(CO)_5$), oleic acid, and hexadecylamine exhibiting (222) and (311) planes by HRTEM of Fe_3O_4. The growth takes place along [110] axis (Fig. 17).[135] However, indirect methodologies lead to elongated structures with different growth directions (Fig. 17). The reported lattice spacing for magnetite rods coming from hematite reveals that the long axis is the [001] axis. [141] Interestingly, akaganeite (β-FeOOH) rods reduced to magnetite via wet reduction in trioctylamine exhibit an interplanar spacing of 0.20 nm along the long axis which reveals that the growth direction is the [311].[91] However, when akaganeite nanorods were reduced in the presence of hydrazine under microwave irradiation the growth direction of the long axis is parallel to the [001] direction.[222] Finally, magnetite elongated nanoparticles with spindle shape reduced from goethite, show that the (311) planes forms an angle of 30° with the longest axis.[110] [90] A typical feature observed for elongated nanoparticles obtained by shape-templating from other oxides is the porosity that arises from the dehydration during the annealing at high temperatures to reach the target magnetic iron oxide. This porosity is important as it increases the surface area of the crystals and the pores act as nucleation points for the magnetization reversal.[90]

In the case of **disks** and **nanoplatelets**, the final magnetite crystal properties depend on the hematite that acts as template for the final Fe_3O_4 disks/nanoplatelets. The study of hematite nanoplatelets by HRTEM and related FFT patterns reveals that the basal plane is the (001) (Fig. 17).[141] Magnetite disks, obtained after a hydrogen-wet method, confirm the single crystal nature of their precursor, which has been shown independent from the reduction method (dry/wet) [90]. Moreover, the formation of pores randomly distributed has been observed in the magnetite structure for both types of reductions,

Please cite this article as: A.G. Roca, L. Gutiérrez, H. Gavilán, et al., Design strategies for shape-controlled magnetic iron oxide nanoparticles, Adv. Drug Deliv. Rev., https://doi.org/10.1016/j.addr.2018.12.008

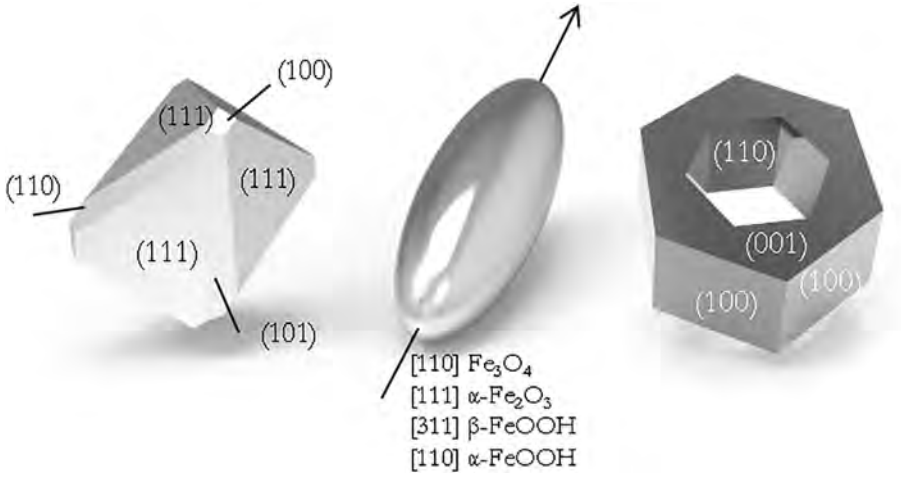

Fig. 17. From left to right. Magnetite with hexa-octahedral crystal habit elongated along one of the [111] direction from magnetotactic bacterium. Orientation of longest dimension of the elongated nanoparticles as a function of the precursors and crystal structure of hexagonal nanorings.

which is associated to the formation of tunnels by the removal of oxygen. Magnetite is formed in the surrounding areas parallel to the tunnel generation.[223] The nanodisks obtained by this route possess (220) lateral planes and (111) planes in the basal surface.[224] It is noteworthy that the alignment of the nanodisks produces modification in the relative intensities of the X-ray diffraction pattern, in comparison with the standard Fe_3O_4, showing enhanced intensities for (111) and (222) peaks, whereas the intensities of (220), (400) and (440) were reduced.[140] Fe_3O_4/γ-Fe_2O_3 nanoplatelets obtained by solvothermal method and a post-reduction step in hydrazine, renders basal planes corresponding to (111) surfaces of a spinel-structured iron oxide hindering the growth along the [111] direction. [225] Besides, the flattening of the nanoplatelets was assigned to the (220) and (311) planes of γ-Fe_2O_3.[53] The authors claimed that in the Fe-terminated (111) surfaces of the nanoparticles, the absorption of PVP can take place due to its strongest polarity as it exposes alternated octahedral coordinated Fe^{3+} and O^{2-} layers so Fe^{3+} ions can interact with other functional groups. The adhesion of PVP to the {111} faces reduces the growth rate along the [111] direction.

Hollow iron oxide spheres obtained by Kirkendall effect of initial Fe/Fe oxide core/shell particles are polycrystalline with no preferential orientation of the individuals. [213] However, hollow nanoframes obtained by "molten salt corrosion" are oriented crystal aggregates and dissolution proceed in a certain direction, causing prominent etching only in {110} faces.[172] However, a different behaviour arises from the use of sacrificial templates of iron oxides. In the case of hematite nanorings synthesized by Ostwald ripening and subsequent oriented dissolution, there is a preferential dissolution of the tip of the (100) plane (highest concentration of exposed Fe^{3+} ions) and then on (001) planes among the normal low index planes (Fig. 17).[226] Usually, certain ions are used in order to form binuclear, bidentate complexes with iron, adhering on (110) and (100) surfaces and preventing the iron atoms to detach from the surfaces.

Fe_3O_4nanorings obtained after dry reduction in a furnace are single-crystal and present two crystallographic orientations ([111] and [112]) from respective lattice spacing of 0.48 and 0.29 nm in their basal plane. After the phase transformation, [001] α-Fe_2O_3 crystallographic direction transforms to [111] and [112] Fe_3O_4 direction, being the latter one observed directly by electron microscopy for the first time (Fig. 17).[170] Absorption spectroscopy on HRTEM revealed also that the Fe atoms are homogeneously distributed without change of valence. For the case of hollow rods, obtained from the direct transformation of hematite, a perfect single crystal structure is obtained. The reported lattice spacing for hematite rods is 0.253 nm, which corresponds to the (110) planes. The selected area diffraction pattern and HRTEM analyses have revealed that nanorods grow along the [001] direction. After the phase transformation, [001] and [110] crystal directions of α-Fe_2O_3 leads to [111] and [311] in magnetite. Lastly, hollow structures obtained through galvanic replacement reactions in metal oxide nanocrystals showed that, in the case of Mn_3O_4 square prisms, whose top and side surfaces were enclosed by (001) and (100) facets, respectively, where transformed to **γ-Fe_2O_3nanocages** with a hollow interior and holes and crystalline structure with highly ordered continuous lattice fringes in their shell.

N**anoflowers structure** critically depends on the synthesis process used that determines for example the degree of contact between cores within a particle. In fact, if the continuity of the crystal orientation is ensured along the particle, magnetic ordering across the interfaces is favoured.[149] For one-step surfactant assisted hydrothermal process, the reported HRTEM analysis reveals that each particle behaves as a single crystal with spinel structure and similar crystalline orientation. [227,228] However, high temperature organic precursor decomposition with a second injection of TOPO and hexane produces nanoflowers composed of many small (5 nm) iron oxide nanocrystals, causing a ring dot pattern of the HRTEM Fast Fourier Transformation (FFT) typical of polycrystals.[145] Polyol process in the presence of NMDEA allows obtaining nanoflowers composed of large cores (approximately 11 nm). This was clearly indicated by the FFT of monocrystalline nanoflowers, showing misalignments from 1 to 3° between the cores and defect holes, possibly containing traces of solvents used for the synthesis. Nevertheless, the authors claimed that 30% of the nanoflowers are still polycrystalline.[35] Lastly, self-assembled 3D flowerlike iron oxide nanostructures formed by the assembly of microspheres, caused a ring dot pattern of the FFT.[229]

4.1.2. Nanocrystal stability and dispersability

Most of the applications of magnetic nanoparticles, especially for *in vivo* biomedical applications, involves the use of magnetic nanoparticles in solution forming long-term stable colloids.[82] In fact, one of the limiting issues precluding the use of these nanoparticles in clinic is the difficulty of forming stable colloids for nanoparticle sizes close or above the superparamagnetic regime[48] and the fact that its magnetic behaviour depends on the colloidal properties. Therefore, the size of the magnetic nanoparticles in solution overtime should be systematically studied. In the particular case of the up-above mentioned shape-controlled iron oxide magnetic nanoparticles, just in few systems, the colloidal properties are studied, and if so, most cases just report data in aqueous media. In Table 4, the hydrodynamic sizes found for iron oxide shape-controlled nanoparticles synthesized through different routes and stabilized in aqueous media via diverse ligands/coatings are summarized.

Please cite this article as: A.G. Roca, L. Gutiérrez, H. Gavilán, et al., Design strategies for shape-controlled magnetic iron oxide nanoparticles, Adv. Drug Deliv. Rev., https://doi.org/10.1016/j.addr.2018.12.008

Table 4
Hydrodynamic sizes found for iron oxide shape-controlled nanoparticles synthesized through different routes and stabilized in aqueous media via diverse ligands/coatings. (DMSA: Dimercaptosuccinic acid, PMAO: poly-(maleic anhydride alt-1-octadecene)).

Shape	TEM Size (nm)	Synthesis route	Ligand/Coating	Hydrodynamic Size (nm)	Ref.
Cubic	12	Thermal decomposition	PMAO	17	[230]
	19			37	
	25			40	
	38			61	
Octahedra	50	Thermal decomposition	DMSA	255	[145]
Rod	30	Hydrothermal	Polyethyleneimine	71	[116]
	40			76	
	50			86	
	60			95	
	70			105	
Disk	225x26 nm	Solvothermal Wet-reduction	CTAB	180	[126]
Flower	19	Polyol	Citrate	27	[130]
	24			37	
	28			38	
	41	Oxidative Precipitation	Dextran	192	[141]
	47	Polyol	Dextran	51	
	110		Citrate	158	
	172	Post synthesis - Emulsion Solvent Evaporation	Polystyrene	250	
	40	Thermal decomposition	DMSA	95	[145]
Bead	108	Post synthesis - Polymer coating	PMAO	159	[138]
	239	Polymer coating	PMAO	378	
	370			552	

The hydrodynamic size is usually bigger than the size analysed by TEM, accounting for the presence of the coating and the hydration layer on the nanoparticle surface. However in some cases, i.e. 50 nm octahedra, [145] we can find huge differences due to the formation of aggregates. Depending on the size, shape and composition of the iron oxide cores and due to the aggregation, nanoparticles may show a ferrimagnetic nature at room temperature,[231] as it is the case of the highlighted system, having a certain coercivity. In these cases, special emphasis in the study of the colloidal properties of the magnetic nanoparticles with ligands that provide enough electrostatic/steric hindrance is recommended.

Dimercaptosuccinic acid (DMSA, ligand attached to the surface of iron oxide after ligand exchange with oleic acid) is a small molecule that probably does not provide enough repulsive forces for 50 nm magnetite with such magnetic features. Nevertheless, DMSA could render stability to 40 nm flower-like nanoparticles (due to their smaller coercive field in comparison with the octahedra) and it has demonstrated to be effective for iron oxide nanoparticles with smaller size providing NCs with negative surface charges at physiological pH and allowing a wide range of pharmaceutical applications, especially for targeted drug delivery, biomedical imaging, biosensing, hyperthermia, or nano-thermometry, improving either the efficiency of the therapy, or the detection limit of the technique.[232] On the other hand, poly-(maleic anhydride alt-1-octadecene) are polymers more suitable for magnetic nanoparticles above 30 nm. It must be highlighted the importance of the amphiphilic polymers, whose alkyl intercalate with the chains of the surfactants bound at the nanoparticle hydrophobic shells, at the surface, i.e. to oleic acid, and the anhydride rings hydrolyze and ensure colloidal stability by means of negative electrostatic repulsions.[233] As observed in Table 4, this polymer allows the stabilization of nanocubes with sizes up to 38 nm (therefore already above the superparamagnetic regime) [230] and nanobeads with a broad range of sizes (108-370 nm). [138]

The colloidal properties of nanorods were studied by means of the hydrodynamic size (although Dynamic Light Scattering is a technique that can be used to determine the size distribution profile of spherical nanoparticles). The nanorods were coated with polyethyleneimine (PEI), a polymer with a repeating unit composed of the amine group and two carbon aliphatic CH_2CH_2 spacer, and therefore providing positive surface charge to the nanorods. This polymer is able to stabilize nanorods with longest axis up to 70 nm. [116]

Citrate groups have also demonstrated to provide electrostatic forces strong enough to allow the stabilization of flower-like nanoparticles with a broad range of sizes (19-110 nm), [130][141] despite the small size of citric acid molecule. From the practical use of the flower-like nanoparticles in biomedicine, it was also reported their coating (mean TEM size 47 nm) with dextran. [141] This polysaccharide polymer binds the nanoflower through the OH functionality contained in each sugar unit on the polymer. An important issue with these coatings is that heat treatment can cause the polymer to dissociate from the iron oxide, which could have implications on the long-term colloidal stability as well as the resistance of the iron oxide nanoflowers against the slightly acidic lysosomal compartment. Researchers have been able to work around this problem via crosslinking the polysaccharide chains through crosslinkers such as epichlorohydrin.[234] Other strategy to stabilize flower-like nanoparticles is to embed them in polystyrene beads of 172 nm. [141] From the biomedical application of magnetic nanoparticle's point of view, polystyrene has advantages, as it has reported to provide colloidal stability, but also to follow pathways to pass epithelial monolayers by opening the tight junctions, thus offering a new possibility for drug delivery across the blood–brain barrier.[235]

Lastly, hexadecyltrimethylammonium bromide (CTAB) has allowed the stabilization of 225x26 nm nanodisks in aqueous media. Although this surfactant is able to form micelles in aqueous solutions and stabilize nanoparticles of big size, it is not a biocompatible coating agent and therefore, for biomedical applications it is not suitable.

In conclusion, we have highlighted the importance of colloidal stability of magnetic nanoparticles and brought up some of the ligands/polymers used to stabilize them in water, having different sizes and shapes. There is plenty of room to improve its dispersibility considering the important differences of anisometric nanoparticles in terms of surface area. This is an issue of the utmost importance, as both the cell uptake and transport across intestinal cells revealed remarkable differences as a function of the shape.[236] Deepening in this issue could have great impact, for instance, on the delivery of drugs with inherent poor oral bioavailability.

4.2. Magnetic properties

In general, Fe_3O_4**nanocubes** synthesized in organic media by thermal decomposition exhibit saturation magnetisation values (M_S) at

room temperature close to the bulk ones M_S= 92 emu·g^{-1} for sizes larger than 13 nm, being Ms_{bulk}= 96 emu/g) (Fig. 18, Table 5).[207] It has been observed that nanocubes saturate at much lower field (0.2 T) than spheres (1 T).[107] In the zero field cool/ field cool curves (ZFC/FC), it is also observed an important difference in the blocking temperature (T_B), being larger for spheres (235 K) than for nanocubes (190 K) and corroborated by Mössbauer spectroscopy. Surface anisotropy, enhanced for spheres, seems to be responsible for the different magnetic behaviour.[114] Apart of the shape, size is the other important factor governing the magnetic behaviour of these cubes. Thus, 100 nm nanocubes exhibit coercivities around 110 and 600 Oe at room temperature and 5 K respectively.[104,214] Contrary to expected, coercivity (H_C) increases for sizes larger than the monodomain. This is due to the formation of chain superstructures where the coercivity is proportional to the length of the chain and inverse to the separation between cube faces.[237,238] Moreover, Verwey transition (see below) is observed in the ZFC/FC curves for 16 nm Fe_3O_4 nanocubes prepared by thermal decomposition in organic media [104] but no for nanocubes of similar size (20 nm) synthesized in water using precipitation in alkaline media, in spite of being both of them pure magnetite as demonstrated by Mossbauer spectroscopy.[99] However, magnetic properties in terms of M_S and H_C do not differ significantly for these two samples (Table 5).

The magnetic properties of **elongated Fe_3O_4** or **γ-Fe_2O_3nanoparticles** present special features respect to their spherical counterparts mainly due to the enhancement of the effective anisotropy as the shape term appears in addition to the magnetocrystalline one. This means that only two possible directions (along the largest dimension) are possible for the magnetic moment. In theory, it leads to an increase of the blocking temperature and coercivity of the particles. However, there are other factors such as the surface disorder or the existence of crystal defects or pores, determined by the synthesis approach and/or reduction strategy that should be taken into account. Magnetic properties of these anisometric particles and spheres with equivalent volumes, either Fe_3O_4 or γ-Fe_2O_3, have been compared (Table 6). For example, for Fe_3O_4 elongated nanoparticles synthesized in organic media by solvothermal route exhibit the Verwey transition (T_V) around 120 K, even for rods with small dimensions down to 41x7 nm (volume equivalent to a spherical particle of around 14 nm).[132,241] The Verwey transition marks a structure change from cubic (above T_V) to monoclinic (below T_V) having a clear impact in their physical properties.[242] For spherical particles smaller than 30 nm is not common to observe the Verwey transition because of the surface spin canting, defects or lack of stoichiometry.[85,243] The presence of the Verwey transition is a clear sign of highly crystalline and stoichiometric magnetite.

A proof of their high crystallinity are the high M_S values (84-87 emu/g) for rods with dimensions larger than 40x7 nm,[132] which are close to the bulk one. It is also remarkable that blocking temperatures have not been found below 300 K, due to the effect of the dipolar interactions, which leads to a negligible coercivity at room temperature (0-50 Oe).[211] Interestingly, Fe_3O_4 rods (72x8 nm) grown epitaxially on $SrTiO_3$

Table 5
Magnetic properties of different iron oxide nanoparticles with cubic shape.

Author/year/reference	Length (nm)	Ms_{RT} (emu·g^{-1})	Hc_{RT} (Oe)	Hc_{5K} (Oe)
Guardia/2010 [207]	13	------	0	400
	45	------	50	200
	180	------	50	50
Yang&Ogawa/2008 [215]	6.5	39	------	190
	15	80	------	500
	30	83	100	790
Kovalenko/2007/[107]	7	29	0	------
Kim&Hyeon/2009 [102]	25	------	20	------
	50	------	75	------
	79	------	90	------
	100	------	110	------
	150	------	100	------
	170	------	113	------
Gao/2010 [108]	12	60.3	------	------
Moya/2015[104]	16	82	9	320
	50	90	82	327
	104	91	94	598
Pardo/2015[214]	27	------	------	333
	48	------	------	460
	94	------	------	609
Andres-Verges/2008[99]	30	83	50	------
	33	83	90	------
	45	87	80	------
	76	92	106	------
Vereda/2013 [239]	54	82	80	------
Nishio/2007 [240]	31	82	------	------
	40	88	------	------
	46	90	------	------
	102	92	------	------

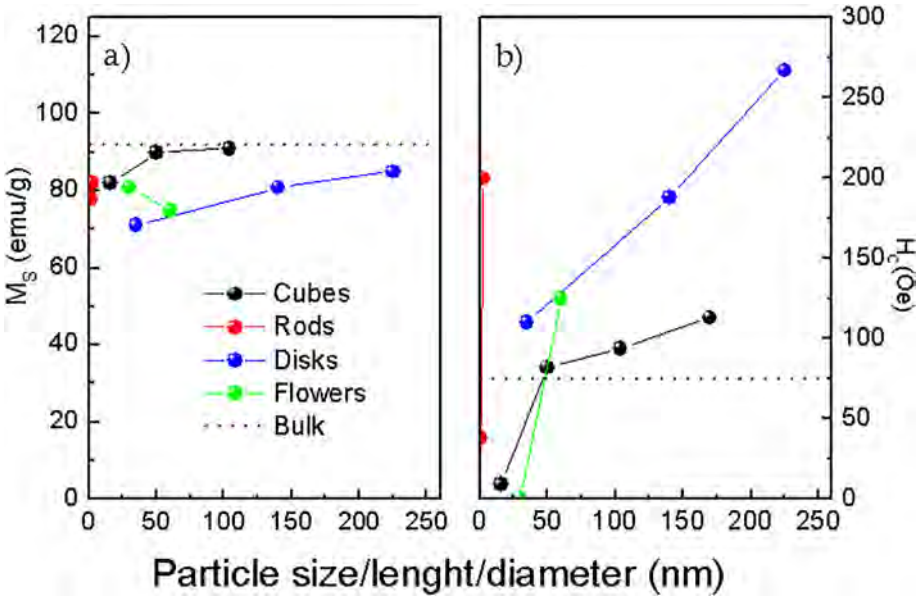

Fig. 18. Magnetic properties at room temperature of magnetite nanoparticles with different morphologies; a) Saturation magnetisation (M_S), and b) Coercive field (H_C) as a function of the particle size. Dot lines represents M_S and H_C of bulk magnetite taken from [249].

substrate exhibit biaxial magnetic anisotropy with differences of one order of magnitude between the hard and the easy axis.[241] Moreover, the T_V increased for the same rods when grew epitaxially on a substrate (120 K) than without substrate being the presence of antiphase boundaries the main responsible for the T_V shift to lower temperatures.[248] Different behaviour was observed for ultrathin nanorods (called nanowhiskers) of 20x2 nm grown by hydrolysis of iron(III) oleate in the presence of oleylamine at 150 °C. Magnetization loops at room temperature show a paramagnetic component due to the high surface-to-volume ratio (around 2) and low crystallinity.[245]

When the synthetic route chosen to get Fe_3O_4 is *via* goethite or akaganeite, the nanostructures are not as well crystallized as their equivalents grown from hematite or by solvothermal method, and present pores. In general, M_S values range from 20 to 60 emu/g due to their surface spin disorder .[91,129,135,136,222,246,247] The smallest rods where the Verwey transition can be observed are 40x6 nm (equivalent to 13 nm spherical particles).[135] Blocking temperatures of 80 and 110 K were measured for 30x4 nm and 40x6 nm, respectively[135] but for longer rods (400 x 40 nm), the ZFC and FC do not converge showing ferromagnetism at room temperature and coercivity values up to 350 Oe at room temperature due to the large diameter of the nanostructures.[136] **Magnetite nanobelts** obtained by reduction of α-FeOOH of 50 nm in diameter and several μm of length exhibit a high M_S at 300 K (81emu/g) and a coercivity of 170 Oe.[124]

Nanoplates/disks/rings with diameters between 3-15 times larger than their thickness are reported to exhibit magnetic vortex structures (Fig. 19). In this configuration, the majority of the spins align circularly in plane forming a flux closure while the ones located at the centre are aligned out of plane leading to weak interacting structures without any stray field and with coercivities and remanent magnetizations close to zero being ideal for theranostic applications. The stabilization of this vortex depends on the diameter, the thickness and also the extension of the inner cavity in the case of nanorings.[140] Once an external field is applied, the magnetic vortex state can be transformed into another state, which depends on the morphology of the nanostructure. In the case of nanorings the hysteresis loop consists in a two-step process involving onion-vortex transition and vortex-reverse onion state (Fig. 19) [140,250]. In nanodisks, the evolution is more complex. At zero field from a saturate state, there is a transition to c-state were the vortex core is located close to the edge of the particle. An increase of H leads to a shift of the vortex from the edge to the centre forming a vortex state in the particles. A further increase leads to a shift of the vortex to the opposite edge and finally the vortex disappears once the nanodisk is saturated. It is noteworthy that the vortex configuration is a stable state in nanorings rather than in nanodisks. In the case of the nanoplates/disks, in spite of their large size, the saturation magnetization is below the bulk one. Small nanoplates of 35 nm in diameter and aspect ratio 3 (equivalent diameter=27 nm) have a M_S of 71 emu/g.[143] On the contrary, large nanodisks with a diameter of 225 nm and an aspect ratio of 14, displays a M_S of 85 emu/g, much closer to the bulk one.[140] Differences in the M_S are given again by the structure of the oxide or oxohydroxide precursor and the further annealing which gives the final Fe_3O_4 phase. In all cases and spite of their magnetic configuration, plates and disks exhibit high values of H_C at room temperature. Coercivity ranges from 110 to 267 Oe for the 35 nm nanoplates and 225 nm nanodisks, following a linear trend with the size (Table 7).[90,140,143]

Superferrimagnetism is the main property ascribed to **Fe_3O_4/γ-Fe_2O_3nanoflowers,** which makes them ideal for biomedical applications, especially as hyperthermia and MRI contrast agents. Superferrimagnetism arises from the exchange interaction between

Table 6
Magnetic properties of different iron oxide nanoparticles with elongated shape. Spherical size means the diameter of a sphere with the same volume than the elongated particle.

Reference	Length (nm)	Width (nm)	Aspect ratio	Spherical Size(nm)	Ms_{rt} (emu/g)	Hc (Oe)
R. Das/2016 [132]	41	7	5.9	14.4	86	0
	65	6	10.8	15.2	84	0
	56	10	5.6	20.3	87	0
H.Sun/2012 [211]	63	6.5	9.7	15.8	20	46.5
Si/2014[244]	58	8	7.3	17.7	62.15	------
	250	64	3.9	115	62.15	------
Macher/2014[245]	20	2	10.0	5	25	0
Chandra/2017[241]	72	8	9.0	19	86	412
	72	8	9.0	19	86	412
Bomati/2008[129]	40	7	5.7	14.3	25	-------
	65	10	6.5	21.3	25	-------
	100	18	5.6	36	40	-------
	140	20	7.0	430	50	650
YJ. Chen/2009 [246]	1000	80	12.5	202	59	266
Wang/2010[247]	200	50	4.0	90	68	
Milosevic/2011 [222]	38	12	3.2	20	18	55
Mohapatra/2015 [135]	30	4	7.5	8.9	50	0
	40	6	6.7	12.9	54	0
	50	8	6.3	16.9	58	0
	60	10	6.0	20.8	63	0
	70	12	5.8	24.7	66	0
Geng/2016[91]	50	10	5.0	19	78	38
	400	40	10.0	98	--------	334
Lentijo/2017[136]	212	46	4.6	87	83	789 (10K)
	21	5.7	3.7	10	69	497
	17	5	3.4	8.6	15	511
H. Gavilan/2017[90]	183	33	5.5	66	60	0
	183	33	5.5	66	82	200

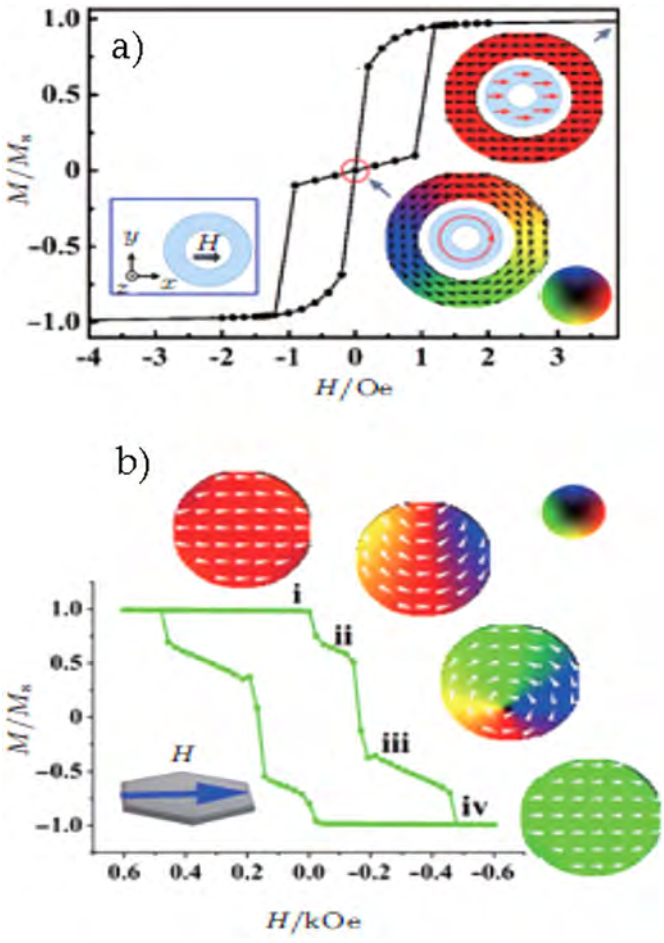

Fig. 19. Magnetic stated during switching when field is parallel to, a) nanorings, reprinted with permission from [250], ©2012, by AIP Publishing; b) nanodisks. Cartoons are schematic diagrams of the domain structures. Reprinted with permission from [140], ©2015, by Wiley.

Table 7
Magnetic properties of different iron oxide nanoparticles with disk/plate like morphology.

Author/year/eference	D (nm)	t (nm)	Aspect ratio	Spherical size (nm)	Ms_{RT} (emu/g)	Hc_{RT} (Oe)	Hc_{5K} (Oe)
Lu/2009 [143]	35	11.5	3.04	27	71	110	------
Gavilan/2017[90]	140	22	6.36	86	81	188	628
Yang/2015[140]	225	16	14.06	125	85	267	490

the cores that are in close contact within the particle. The remanent magnetization of these nanoflowers is weaker compared to single core particles with similar cluster size.[251] The other characteristic is that their saturation magnetization values are close to the bulk ones given by the use of high temperature synthesis routes that reduce the presence of spin disorders and canting. In all cases, the nanoflowers exhibit residual coercivities [252] or are superparamagnetic as a consequence of the super exchange interaction between the core within the particle and they have a very high magnetic moment per particle. Both characteristics enable the production of stable suspensions of nanoflowers compatible with high magnetic response.

Magnetic properties of **hollow iron oxide nanoparticles** depend in a great extension of the hollowing procedure. For example, Fe_3O_4 nanoparticles, with at least 10 nm in size, etched with TOPO technical grade at 300 °C, have experienced a dramatic change of their magnetic properties from superparamagnetic to paramagnetic. This change is due to the inward diffusion of P atoms on the nanoparticle leading to amorphous iron oxide. Another interesting feature is the loss of M_S from 50 to 3 emu/g.[162] For those iron oxide particles hollowed by using Kirkendall effect-based techniques using Fe nanoparticles/clusters as templates, the magnetic properties dramatically change, not only because of the phase change (from Fe to Fe_3O_4 to γ-Fe_2O_3) but also for the promotion of surface spin canting and the change to a polycrystalline nature of the particles.[165] Thus, saturation magnetization drops from 80 to 47.9 emu/g from solid 13 nm Fe/Fe_3O_4 nanoparticles to their equivalent 16 nm hollow Fe_3O_4 ones after oxidation with trimethylamine N-oxide. Moreover, these hollow structures were not able to saturate under a field of 1.5 T.[164]

An evidence of how important is the reduction method is shown by the different magnetic properties of Fe_3O_4 needles obtained from α-FeOOH nanoparticles of 183x33 nm subjected to both dry (treatment at high temperatures under hydrogen/argon gas) and wet (treatment at high temperature in organic media in the presence of oleic acid) reduction treatments. In the case of the needles obtained by wet reduction, the M_S measured at 300 and 10 K were much lower (60 and 70 emu/g respectively) than the values obtained for the needles reduced by the dry method (82 and 90 emu/g).[90] Interestingly, for the sample obtained by wet reduction the hysteresis loop presents a wasp-waisted shape with a negligible coercivity (observed at low sweeping field rate) due to the mixture of single and multidomain remanence states.[253] In the case of the needles obtained by dry reduction there are no sights of such behaviour probably due to the less pronounced defects and pores within the reduced needles.

In general, it can be concluded that magnetic properties of magnetite and maghemite nanoparticles are strongly dependent on not only the nanoparticle size and shape but also on the synthesis route and, in particular, on the reduction conditions if other iron oxides/oxihydroxides have been chosen as shape templates. Thus, in the case of elongated nanoparticles with sizes below 150 nm in length, they show coercivity values at room temperature similar to other morphologies probably due to incoherent magnetisation reversal process. On the other hand, the low coercivities and remanent magnetization values observed for nanoflowers are due to their superferrimagnetic behavior (Fig. 18). In theory, nanorings/disks exhibit lower coercivity due to their magnetic vortex structure but the reality shows that there are other factors such as the internal structure, defects and pores that also accounts for the final magnetic properties. Low coercivities are interesting to preserve the reversible magnetic behaviour and minimize the formation of aggregates after applying a magnetic field. Nanocubes exhibit higher M_S values than other morphologies, closer to the bulk value (96 emu/g), which is a key parameter to obtain high MRI relaxivities and the heating capabilities under an alternating magnetic field.[184]

The interpretation of the magnetic properties of colloidal suspensions of magnetic nanoparticles is complex, as well as their correlation to the nanoparticle structure, shape, defects etc... That is why engineering magnetic nanoparticles with special properties for a specific application in biomedicine is still challenging.

4.3. Relevant properties for nanomedicine

4.3.1. Toxicity

Magnetite and maghemite nanoparticles have been proposed for biomedical applications and their main advantage over other magnetic compounds is their low toxicity. This is a consequence of the existence in the body of metabolic pathways able to deal with iron atoms.[254] Specialized proteins such as ferritin are able to store iron released from the nanoparticles during their degradation process in a safe form that allows a recycling process of iron.[255,256] In fact, iron oxide and oxyhydroxide nanoparticles are currently being used as iron supplements. In addition, the Food and Drug Administration (FDA) of the USA has also approved iron oxides as contrast agents for magnetic resonance imaging (MRI).[257]

Generally, most of the studies evaluating the toxicity of iron oxide magnetic nanoparticles reinforce the idea of their low cytotoxicity, in spite of the difficulty comparing toxicity studies from the literature due to the lack of standardization (several iron concentrations, cell lines and assays are randomly used). The cytotoxic effects revealed for magnetite and maghemite, if any, are usually negligible or limited to extreme conditions such as very high doses (> 0.5 mg Fe/ml) or long exposure times (> 120 h).[258] However, in most cases only the decrease in cell viability is evaluated and other potential toxic effects (genetic or carcinogenic among others) are not generally studied. Likewise, no signs of additional toxicity have been found for the different anisometric nanoparticles in agreement with the observations reported for spherical ones.

In the case of 19 nm **nanocubes**, cytotoxicity using the Trypan Blue test has been tested in human adenocarcinoma cells (KB cells). Cell viability was decreased to 70 % when the cells were incubated with poly(maleic anhydride alt-1-octadecene) coated nanoparticles (1 mg/mL, 24 h).[230] The same group studied the cell viability by the Alamar Blue assay with three malignant cell lines, SKOV3 (ovarian cancer), PC3 (prostate cancer), and A431 (epidermoid cancer) using 20 nm nanocubes, indicating the low toxicity of this material.[74] The degradation of similar sized nanocubes has also been followed *in vitro* (in SKOV3 ovarian and PC3 prostatic carcinoma cells) and *in vivo* in a murine model observing the formation of ferritin and proving the activation of iron metabolism routes to deal with iron coming from the nanoparticles degradation.[259] Calcein staining and Magic Red caspase detection kits were used in a human lung carcinoma cell line (A549) and cytotoxicity has just been observed in the case of hyperthermia application using nanocubes forming multi-core structures.[260] 10 nm nanocubes have been tested for *in vitro* toxicity using a L929 mouse cell line and the Alamar Blue assay and no toxicity was found with concentrations below 0.1mg Fe/mL. [261] Toxicity studies of these nanocubes in rats have also shown high biocompatibility as the nanoparticles were efficiently removed from the body by renal excretion.[261]

Please cite this article as: A.G. Roca, L. Gutiérrez, H. Gavilán, et al., Design strategies for shape-controlled magnetic iron oxide nanoparticles, Adv. Drug Deliv. Rev., https://doi.org/10.1016/j.addr.2018.12.008

In general **elongated iron oxide particles** with high aspect ratio are expected to be more toxic than those with lower ones. Few examples can be found in the literature suggesting higher cytotoxicity effects of elongated nanoparticles in comparison with spherical ones associated with cellular damage, in a similar way as the performed by uric acid crystal deposition.[262]. In particular, **nanorods** have shown a higher degree of membrane damage than spherical ones in mouse macrophage cells.[190] However, these results have to be cautiously analysed as, in addition to the different shape, particles also presented very different size and surface area, also it was reported that cell viability decreased both for nanorods and nanospheres. It is also worth mentioning that very high doses of other elongated formulations based on iron oxyhydroxides (akaganeite) nanoparticles as part of their composition are well tolerated in animal models.[263] On the contrary, there are examples of iron oxide nanorods with high aspect ratio (an average length of 10 μm) whose cytotoxicity has been studied showing that, even though the nanorods are internalized and located in the perinuclear region, cell viability remained at 100% level within the experimental conditions (NIH/3T3 fibroblast cells using the MTT assay with iron concentrations between 10 μM ($5.5 \cdot 10^{-4}$ mg Fe/mL) and 10 mM (0.55 mg Fe/mL) after 24 h incubation time).[264] PEGylated maghemite (γ-Fe_2O_3) nanotubes and silica coated elongated nanoparticles have also revealed excellent biocompatibility properties assessed by MTT and flow cytometry (Fig. 20).[265,266]

Cytotoxicity of citrate-coated multicore **maghemite nanoflowers** has been checked in MCF-7 cells incubated during 30 min with concentrations between 0.01 mg Fe/mL and 0.28 mg Fe/mL by the Alamar Blue assay showing no significant differences with the control cells.[144] A more complete cytotoxicity assay has been performed using U87n human glioma cell lines, assessing the internalization of the nanoflowers (29 nm particle size) by confocal microscopy, TEM, fluorescence and bioluminesce imaging and flow cytometry. This study also corroborated the low toxicity of the nanoflowers.[267] **Multicore nanoflowers** of around 140 nm have been assessed in two cell lines (Hep G2 and Caco-2) by the MTT assay and have proved that cell viability is only reduced at the highest dose tested (0.64 mg Fe/mL).[268] This material has also been administered to a Xenopus Laevis animal model, where a strong dependence on the particle coating and the accumulation in the animal has been found. Although the particles were not lethal in the evaluated doses, several malformations were observed in the embryos. This work highlights the necessity of using simple animal models to assess nanoparticles toxicity that may not be found using just cell cultures.

Cytotoxicity had been assessed **for hollow nanospheres** of 13 nm and OVCAR8 and OVCAR8-ADR cells through MTT studies and no considerable toxicity was found for 72 h, with Fe concentrations up to 0.89 mg Fe/mL.[269] In addition, hollow nanospheres have been administered to a mouse model confirming the lack of toxicity signs one month after the injection.[171] In the case of tripod particles, cytotoxicity has been compared with spherical particles and it has been found to be low by the MTT assay in Hepa 1-6 and HeLa cells at different time points up to 24 h and using concentrations between 0.022 and 0.35 mg Fe/ mL.[270]

In general, it can be concluded that other parameters such as the concentration, the nature of the nanoparticles coating or the incubation time have stronger effects on the nanoparticles citotoxicity than their shape.[271] Therefore, the effect of the shape on the nanoparticles toxicity is relatively limited and maybe just slightly relevant in the case of high aspect ratio conditions. Besides, contradictory results are found in the literature regarding the influence of the shape and aspect ratio of nanomaterials on their cellular uptake.[272] Inconsistencies may be due to the general lack of standardization in the methodology assessing the toxicity, leading to comparison of data coming from different experimental setups.

4.3.2. Cell uptake and biodistribution

Geometry has an important effect on two key parameters with strong impact on the success of biomedical applications, the particles cellular uptake and their biodistribution. [58]

In general, it appears that higher aspect-ratio particles have a higher surface area that increases the cell membrane interactions and therefore the particles internalization.[265] In the case of nanoflowers, opposed results can be found in the literature. Some authors have shown that when comparing with **nanoflowers, nanocubes or nanospheres**, nanoflowers showed a weaker association with the cell membrane but, after the nanoparticle internalization the amount of internalized iron was in the same range for the different morphologies.[273] Other authors have shown that the internalization of nanoflowers (multicore particles) was higher than single-core ones.[267] The reason of these differences probably relies on the many other different parameters affecting the cell internalization such as the particles volume, surface curvature, coating, etc.

It is also generally accepted that for nanomaterials with different geometries, particles with high aspect ratio geometries show longer circulation times when compared to spherical particles. However, the number of studies comparing the biodistribution of iron oxide magnetic nanoparticles with different shapes is scarce. In the case of iron oxide nanoparticles, **nanoworms** have been shown to have an increased uptake in tumours in comparison with the single nanoparticles counterparts.[176] In contrast, when comparing the amount of **nanooctapods** to nanospheres that reach the liver of a mouse model, similar amounts of material were found. [274]

It can be concluded that, given the complexity of biological systems and the multitude of parameters, such as the particle volume, polydispersity, colloidal stability, surface coating, protein corona formation, endotoxin presence, etc. that have a fundamental role in the nanoparticles uptake and biodistribution, it is difficult to find two materials that allow the evaluation of the role of the nanoparticles geometry by isolating this

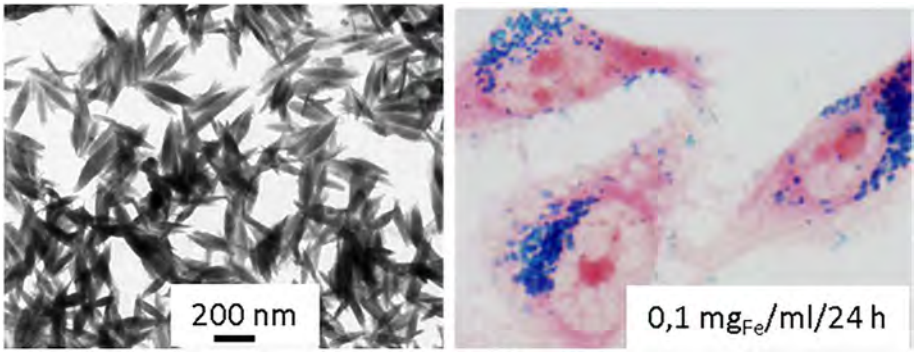

Fig. 20. Silica coating elongated magnetic nanoparticles of around 250x50 nm showing high uptake in HeLa cells and low toxicity after 24 and 48 h of incubation. Images adapted from [266].

Please cite this article as: A.G. Roca, L. Gutiérrez, H. Gavilán, et al., Design strategies for shape-controlled magnetic iron oxide nanoparticles, Adv. Drug Deliv. Rev., https://doi.org/10.1016/j.addr.2018.12.008

variable from the rest of parameters that affect the experiments. Therefore although the shape of the particles seems to have an important role in the cell uptake and biodistribution of the particles, further investigations are required to have a complete picture of the impact of shape on the interactions between the particles and the biological environment. [58]

4.3.3. Degradation in biological environments

Another important parameter to understand the possible long-term toxicity of these materials is their biodegradation. Biological environments may present very hostile conditions for the particles. Especially highly acidic media with specific proteins able to degrade the particles coatings found in lysosomes can cause the fast nanoparticles corrosion. Knowledge on the degradation process of the particles is fundamental to design particles able to be rapidly cleared from the organism, or long-lasting ones, in case they need to be used for long-term applications such as repeated MRI image acquisitions or repeated hyperthermia treatments.

The degradation of iron oxide **nanocubes** has been evaluated in simulated lysosomal environment, in cell cultures and in vivo. It was found that the degradation of the cubes is not correlated with crystalline orientation. The process fits better with a stochastic degradation, which was initiated in the areas not covered by the particles coating, rendering smaller particles with eroded shapes.[259] In addition to the important role of the coating on the degradation process, the aggregation of particles has also been found as a critical parameter affecting the degradation kinetics, in this case, protecting from the particles degradation. The degradation of **nanoflowers** has also been followed when exposed to a media that simulates the intracellular lysosomal environment. In this case, the pores of the nanoflowers structure seem to enhance the gradual corrosion of the particle.[275] In this kind of particles, the junctions between the cores are the most vulnerable sites, leading to a fast disintegration of the multi-core structure. [276]

Knowledge on the degradation kinetics of the particles is also fundamental in the frame of recent discoveries on an iron-dependent cell death mechanism termed ferroptosis.[277,278] The iron-catalyzed ROS production through the Fenton reaction may play a fundamental role for iron-induced ferroptosis. This process may have a negative impact on the particles toxicity once they start degrading but it can also be used as a positive tool in the frame of new iron-oxide-based catalytic cancer therapy.[279]

The fact that very few works have evaluated the degradation of anisometric iron oxide nanoparticles in biological environments makes it difficult to draw general conclusions on the advantages or disadvantages of specific shapes. Therefore, further studies on the degradation of iron oxide nanoparticles with different shapes are required to achieve a complete picture of the role of the particles shape on their degradation.

5. Biomedical applications

5.1. Hyperthermia

Magnetic hyperthermia using Fe_3O_4/γ-Fe_2O_3 nanoparticles has the advantage of selectively killing tumoral cells over healthy ones just by increasing the temperature up to 42-43 °C in the target area where the particles are located.[280] Briefly, the particles are able to release heat under the action of an alternating magnetic field. Usual frequencies range from 100 to 700 kHz and field amplitudes up to 500 Oe but there is a safe limit that the product of the frequency by the field should fulfil ($5.1 \cdot 10^9$ A·m^{-1}·s^{-1}), otherwise inductive heating through eddy currents are generated and heating becomes non-specific. [281,282] The specific absorption rate (SAR) is a physical magnitude related to magnetic nanoparticles heat dissipation. The most common calorimetric method to evaluate the SAR is the placement of a suspension of magnetic nanoparticles into an alternating magnetic fields (AMF), which absorbs energy from the field which is subsequently transformed into heat. If the field is strong enough, and also thermal losses are small enough, SAR values can be calculated from the following equation: $SAR = (C_{LIQ}/c_{Fe}) \times [dT/dt]_{t=0}$, from the temperature derivative over time at instant t = 0 [283] and the heat capacity of the solvent (C_{LIQ}) and the mass iron concentration (c_{Fe}) Fig. 21 shows SAR values obtained under moderate values of field and frequency (<300 Oe and <300 kHz) for magnetite nanoparticles of different shape (Data and references shown in Table 8). It is important to highlight that there are several heating mechanisms implied in the heat release.[284] The structural and colloidal properties of the particles (i.e. particle size, shape, aggregation state, interactions), the media and the AC applied field (frequency and amplitude) determine the dominant mechanism making the others of little importance.

An extensive research has been done in the use of **Fe_3O_4nanocubes** on magnetic hyperthermia. For example, the heating properties of samples with sizes ranging from 13 to 38 nm were tested under different conditions of field and frequency.[230] The best performance was achieved for 19 nm cubes reaching a SAR of 2277 W·g^{-1} (700 kHz, 300 Oe). Smaller and larger cubes did not register a significant heating (< 300 W·g^{-1}) due to the lack of contribution of hysteresis losses for 13 nm nanocubes, while for the 38 nm cubes the reason was the large anisotropy field and formation of isotropic 3D aggregates. However, when these 38 nm cubes were isolated by gallol-polyethylene glycol (GA-PEG), they exhibited a SAR of 1400 W·g^{-1} (320 kHz and field of 300 Oe).[285] Bacterial magnetosomes of 30 nm in length were also evaluated as nano heaters registering values up to 960 W·g^{-1} at 410 kHz and 125 Oe.[282] Much larger nanocubes, 60 nm in size coated by chitosan, leads to a SAR value of 2614 W·g^{-1} under an AC field of 1 MHz and 8.2 Oe due to the contribution of the hysteresis losses mechanism. [260] It should be mentioned in this case that sizes are of the order or slightly above the domain size, so magnetization reversal mechanism should be domain wall motion.

For ferromagnetic nanoparticles where hysteresis losses are the dominant mechanism, aggregation is in general an undesired effect diminishing the heating efficiency.[286] Direct studies performed on cubic nanoparticles reveal that SAR values decreases when particles are arranged forming 3D clusters which look like magnetic beads.[73] However, it has been demonstrated theoretical and experimentally that if the particles are forming chain-like structures and aligned in the direction of the field, SAR values increase at least five times in

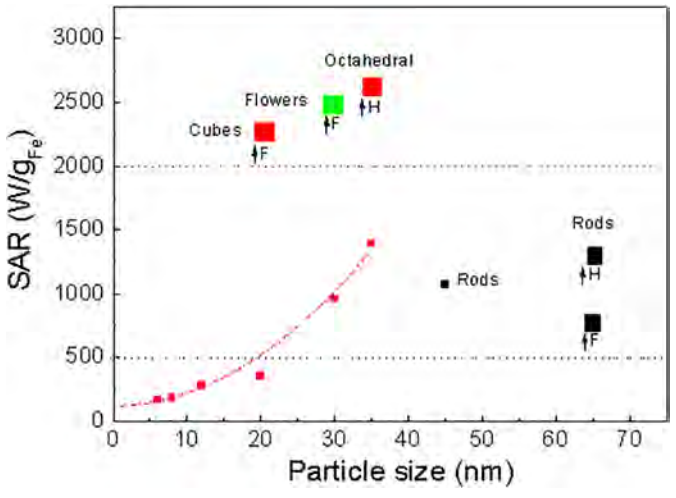

Fig. 21. Specific adsorption rate values (SAR) obtained under moderate values of field and frequency (<300 Oe and < 300 kHz) for magnetite nanoparticles of different shape (Cubes/Octaherdra) in red, elongated in black and flowers in green). Red line show the effect of the size on the SAR values for cube-like shape nanoparticles. The effect of the field conditions are shown also for cubes, rods and flowers (high frequency (F) and high field (H)). (Data and references shown in Table 8).

Table 8
Hyperthermia performance of Fe_3O_4 nanoparticles with different morphology under AC magnetic fields with different frequency and amplitude.

Morphology	Author/Year/reference	Size (nm)	Frequency (kHz)	Field (Oe)	SAR ($W \cdot g^{-1}$)
Cubes	Guardia 2014[285]	35	320	300	1391
	Hergt 2005 [282]	30	410	125	960
	Tong 2017 [295]	40	325	250	2560
	Guardia 2012 [230]	20	700	300	2277
	Bae 2012 [260]	60	1000	8	2614
	Espinosa 2016 [74]	20	900	250	4850[a]
Octahedrons	Mohapatra 2015[290]	6	247	310	163
		8	247	310	184
		12	247	310	275
	Lv 2015[291]	13	358	800	1220
		22	358	800	2483
		43	358	800	2629
		98	358	800	750
Rods	Geng 2016[91]	45x10	390	415	1072
	Das 2016[132]	65x5.7	310	800	1300
		41x7	310	800	540
Nanoplates	Ma 2013[292]	150-200 x10-20	180	12	253
	Yang 2014[140]	225x26	488	580	4400
	Nemati 2017[296]	12x3	310	800	125
Flower-like	Hugounenq 2012 [35]	50 (11 nm single core)	700	270	1790

[a] SAR calculated under the action of a 808 nm laser.

high viscosity medium.[287] The comparison of structures with different morphologies but same volume reinforces the latter assumption. It was found that 24 nm spheres dissipate less heat than 19.5 nm cubes and this was attributed to the formation of chain-like aggregate structures in the case of the cubes. However, comparing heating properties of 53 nm spheres and 43 nm cubes it was found better heating properties for the spherical ones because the cubes were forming strong and isometric aggregates.[288]

In the last years, magnetic hyperthermia has been combined with photothermal therapy bringing positive effects as it is known that Fe_3O_4 presents some absorption in the Near-infrared (NIR) range (Fig. 22a).[289] By using a NIR laser of 808 nm with a power density of 2.5 $W \cdot cm^{-2}$ combined with an alternant magnetic field (900 kHz, 250 Oe) to a suspension of non-aggregated 20 nm nanocubes, SAR values around 4850 $W \cdot g^{-1}$ are obtained. It is worth to note that the SAR value measured using only magnetic hyperthermia is around 1000 $W \cdot g^{-1}$ and, in principle, there is no coupling between the magnetic and electric field as the iron oxide is not a good magnetoplasmonic material. [74]

Octahedral Fe_3O_4particles (12 nm) presented also enhanced SAR values comparing to the spherical ones as a result of their better magnetic properties (higher M_S and susceptibility). Thus, 6-12 nm octahedrons exhibit values from 163 to 275 $W \cdot g^{-1}$ (247 kHz, 310 Oe) due to the susceptibility losses mechanism (Néel and Brown relaxation). [290] SAR values from around 40 nm octahedrons measured at 358 kHz at different fields goes from 157 $W \cdot g^{-1}$ at 200 Oe to 2483 $W \cdot g^{-1}$ at 800 Oe (Fig. 21).[291] When the particle size of the octahedrons increases to 98 nm, the measured SAR reached 2629 $W \cdot g^{-1}$.

Elongated Fe_3O_4nanoparticles have received a great attention due to their larger effective anisotropy given by their high aspect ratio. Values up to 1072 $W \cdot g^{-1}$ have been measured for rods of 45x10 nm (390 kHz, 415 Oe) synthesized by reduction of akaganeite (β-FeOOH) nanoparticles. Besides, larger rods (400x40 nm) displayed lower SAR values due to its higher switching field to reverse the magnetic moment.[91] In the case of iron oxide nanorods made by solvothermal approach (65x6 nm), their SAR value reaches 1300 $W \cdot g^{-1}$ (310 kHz, 800 Oe) showing that, if the field amplitude is large enough to reverse the magnetic moment, SAR values increases with the aspect ratio. In contrast, low aspect ratio elongated particles (41x7 nm) only reached SAR values of 540 $W \cdot g^{-1}$.[132] Interestingly, it has been reported that the elongated morphology of Fe_3O_4 rods (200x50 nm) could induce cancer cell death on HeLa cells under mechanical oscillations under exposure to a 35 kHz oscillating magnetic field.[71] This low frequency is associated to the Brownian motion of the nanorods, i.e. physical rotation or vibration leading to mechanical disruption of the cell membrane.[70]

Fe_3O_4hexagonal nanoplates with a side length of 150-200 nm and a thickness of 10-15 nm synthesized by hydrothermal method in one step display a SAR value of 245 $W \cdot g^{-1}$ (180 kHz, 12 Oe).[292] However, for nanodisks of similar sizes (225 nm in diameter and 26 nm in thickness) when the frequency and applied field increases, a boost of the SAR value up to 4400 $W \cdot g^{-1}$ (488 kHz, 580 Oe) can be observed. [140]This high performance is due to the parallel alignment of the nanodisks with the magnetic field. The dominant heating mechanism was hysteresis loss induced by a vortex domain structure originated by the circular arrangement of the spins. [225,293] This vortex domain structure has the advantage of providing a negligible remanent magnetization so agglomeration due to dipolar interactions is avoided. In conclusion, parallel orientation and vortex domain structure are the responsible for the high SAR values observed for this morphology. However, nanodisks of 12x3 nm lack of this vortex domain configuration and exhibit low SAR values (125 $W \cdot g^{-1}$) in spite of using high frequency and field (310 kHz, 800 Oe).

Like elongated nanoparticles, **nanodisks morphology** could induce cell death through magneto-mechanical effects (Fig. 22b).[294] Nanodisks of Permalloy coated with gold (1 μm in diameter and 60 nm thickness) where able to exert mechanical forces to the cell under a low alternating field of maximum 60 Hz and 90 Oe and induce cell death by apoptosis in N10 glioma cells. Cell death mechanism, either apoptotic or necrotic, can be regulated by the magnitude of the magnetic field. Alternating magnetic fields of low frequency induce a shift of the disk vortex structure, creating an oscillation and transmit a mechanical force to the cell. This strategy opens a new pathway where magnetic iron oxide nanodisks could be applied.

Superparamagnetic **flower-like particles** of 50 nm consisting in spherical aggregates of 11 nm grown by the polyol method exhibit a large SAR value of 1790 $W \cdot g^{-1}$, much larger than the SAR measured for single 11 nm particles (48 $W \cdot g^{-1}$). For this special morphology, as the aggregate size increases the SAR becomes larger but a compromise should be reached between colloidal stability and heating performance. It is clear that the improvement of the SAR values comes from the cooperative interaction of these superparamagnetic cores within the particle. [35]

In general, the morphologies that exhibit better heating performance under an alternating magnetic field are nanocubes and octahedrons. It should be noted that SAR values have been enhanced going from around 100-200 $W \cdot g^{-1}$ up to over 3000 $W \cdot g^{-1}$ improving materials and magnetic conditions. Two recent strategies have shown to amplify the heating efficiency of magnetite suspensions: Controlling specific magnetic interactions between particles (exchange and dipolar interactions) and the combination of magnetic hyperthermia with photothermal therapy. In the former case, shape-controlled iron oxide nanoflowers, firstly synthesized by Caruntu et al. can be highlighted. [150] In recent years, they have emerged as promising candidates for magnetic hyperthermia because of exchange interaction found for this particular structure, which consists of densely packed aggregates of iron oxide crystallites/cores, with an irregular shape and a slight shape anisotropy. It was recently demonstrated that the individual nanoflowers had a remanent magnetization (due to an exchange coupling between the cores), were preferentially magnetized along their longest dimension (due to shape anisotropy), but with a slight internal spin disorder/misalignment.[297] Moreover, it was showed that the intrinsic loss power of the nanoflowers was independent of the viscosity of the surrounding medium for the high-frequency applied field, unlike previous hyperthermia studies of these systems conducted at other frequency conditions. This is in agreement with the high-frequency range relaxation dynamics of the nanoflowers dominated by internal moment

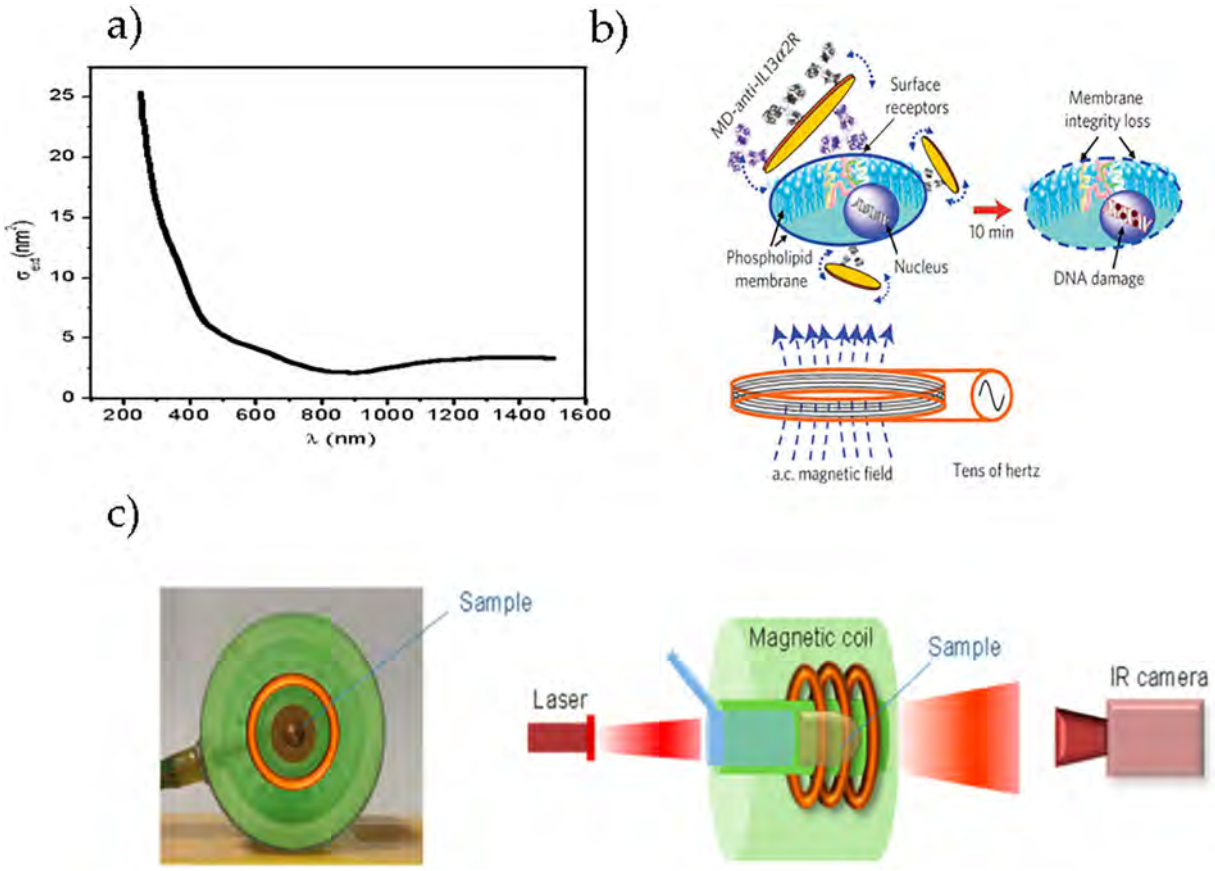

Fig. 22. a) UV-VIS-NIR spectrum of Fe_3O_4. Reprinted with permission from [289]. Copyright (2003) American Chemical Society; b) Scheme of the magnetochemical cancer-cell destruction system using disk-shaped magnetic particles possessing a spin-vortex ground state. Reprinted with permission from [294]. ©2010, by Springer Nature; c) Scheme of the experimental device for combined hyperthermia experiments, consisting of a magnetic coil in which the sample is placed so that it can be illuminated by the NIR laser (808 nm). Reprinted with permission from [74]. © (2016) American Chemical Society.

relaxation. Besides exchange coupling, improved heating efficiency has been obtained by forming chain-like structures, controlling dipolar interactions. Dipole-dipole interactions generally leads to effective decrease in coercivity, remanence, and hysteresis losses with respect to the isolated particles, which leads, among other effects, to worse magnetic hyperthermia efficacy.[287] However, it was theoretically predicted that chain-like arrangements biomimicking magnetotactic bacteria has larger area of hysteresis losses and therefore superior heating performance, increasing more than 5 times in comparison with the randomly distributed system.[298] Recently, such dipolar interactions were exploited for enhanced heating thanks to the shape-controlled synthesis of asymmetric dimer and trimers of iron oxide nanocubes. By means of a kinetic Monte Carlo computational model, the effect of magnetic dipolar interactions on the heating efficiency was unequivocally demonstrated.[208]

The second strategy to amplify the heating efficiency is the combination of magnetic hyperthermia with photothermal therapy. Here, it was demonstrated that it is important to retain the Fe_3O_4 phase on the nanocubes as its absorbance in the NIR range decreases when oxidize. Interestingly, in terms of SAR values, elongated nanoparticles have not shown high SAR values as expected due to the magnetic shape anisotropy contribution. Nevertheless, for this morphology it is interesting the possibility of promoting cell death under magneto-mechanical forces exerted to the cell membrane by application of alternating magnetic fields of low frequency (20-70 kHz), enough to promote physical rotation of the particles. The same mechanisms could be expanded to nanodisks, but in this case using smaller frequencies of tenths of Hz due to their larger volume.

5.2. Magnetic resonance imaging

It is well known that magnetic nanoparticles, either magnetite or maghemite, can act as contrast agents leading to a negative contrast as a consequence of the shortening of the transversal relaxation time (T2 contrast agent) of the nearby water protons induced by the local field from the magnetic nanoparticles. Indeed, there are different formulations for superparamagnetic iron oxide nanoparticle suspensions such as Feridex, Endorem or Resovist approved by the FDA. Unfortunately, they were removed from market due to the lack of clinical use. [299] However, their comeback is not discarded if the toxicity and side effects from gadolinium complex is confirmed.[300]. To evaluate the performance of a contrast agent, one of the parameters is the measurement of the longitudinal or transversal relaxivity (r_1 or r_2 respectively) as it measures the perturbation of the local field generated by the magnetic nanoparticles on the relaxation time of the water protons

Small nanocubes coated by DMSA with different sizes exposing (100) facets revealed that the transversal relaxivity (r_2) increases with particle size rising from 76 $mM^{-1}\cdot s^{-1}$ for 7 nm nanocubes up to 298 $mM^{-1}\cdot s^{-1}$ for 21 nm ones, revealing that the relaxation takes place in the motional averaging regime (MAR).[301] However, single Fe_3O_4 nanocubes 23 nm in size and prepared by thermal decomposition presents r_2 values up to 398 $mM^{-1}\cdot s^{-1}$, much larger than when clustered in beads of 200 nm in size, in which case they exhibit r_2 relaxivities around 161 $mM^{-1}\cdot s^{-1}$ indicating that such beads promotes the relaxation of water protons in the dephase regime (static dephase regime, SDR).[73] The reason for such decrease lies on their lower magnetic moment per bead compared to the single cubes. Larger nanocubes around

the domain size of Fe_3O_4 (58 nm) surrounded by PEG-phospholipid exhibit a r_2 of 324 $mM^{-1}\cdot s^{-1}$ (Fig. 23).[302]

Elongated magnetite nanoparticles exhibit a great performance in MRI only at high fields (3 T) (Table 9). For example, Fe_3O_4 rods of 25 and 50 nm in length (with 5 nm in diameter) coming from the decomposition of iron(III) acetylacetonate and coated by PEI have r_2 values of 670 and 905 $mM^{-1}\cdot s^{-1}$ respectively.[303] This boost enhancement arises from the high M_s and high surface to volume ratio of the nanostructures leading to an enhancement of the water molecules diffusion around the particles. In the same way, magnetite nanorods of 70x12 nm in size, coming from the reduction of β-FeOOH rods, displays a r_2 constant of 608 $mM^{-1}\cdot s^{-1}$. Smaller rods of 30x4 nm exhibit a relaxivity constant of 312 $mM^{-1}\cdot s^{-1}$.[135]

Hollow iron oxide nanoparticles of 11 nm with a void of 5 nm carved under the etching done by TOPO, shows poor performance as T2 contrast agent because the r_2 goes from 60 $mM^{-1}\cdot s^{-1}$ before etching, to 1.25 $mM^{-1}\cdot s^{-1}$ once the particles have been carved by TOPO. **Fe_3O_4nanoring structure** is also another type of morphology which is not favoured for the application of contrast agents for MRI.[162] Iron oxide nanorings with a magnetization out-of-plane register r_2 values of 74 and 55 $mM^{-1}\cdot s^{-1}$ for 200 and 100 nm nanorings respectively.[304]

The growth of **flower-like γ-Fe_2O_3nanoparticles** by the polyol method has brought an improvement on the relaxometric properties of the particles for MRI when evaluated for T2 contrast agents (Fig. 23). Thus, 10 nm particles clustered in small aggregates of around 30 nm and coated by citric acid, exhibit a r_2 constant of 365 $mM^{-1}\cdot s^{-1}$, 1.8 times higher than single core nanoparticles made by the same method.[144] This improvement is due to the cooperative behaviour of the magnetic moment which increases the intensity of the local magnetic. It has been observed from theoretical studies that the spin-spin relaxation occurs in the motional average regime (MAR) for clusters up to 120 nm and the r_2 increases with the particle size. However, if the particles are highly aggregated or are too big, the magnetic particles generate a strong magnetic field, the nearby protons are completely dephased (static dephase regime, SDR)[305] and do not contribute to the MRI signal. For larger clusters with similar core size it has been observed greater r_2 values up to 405 $mM^{-1}\cdot s^{-1}$ for 50 nm clusters and 508 $mM^{-1}\cdot s^{-1}$ in the case of clusters of around 86 nm.[252] Larger particles (15 nm) with a cluster size of 39 nm show r_2 values up to 418 $mM^{-1}\cdot s^{-1}$.[227].

During the last years, the number of studies based on the possibilities of iron oxide as T1 contrast agents has increased [306]. Magnetic iron oxide T1- contrast agents, lead to bright contrast, as it was proposed for gadolinium complexes[307] or MnO nanoparticles,[308] but is proposed as a safer alternative to gadolinium-based T1 contrast agents [306]. For example, ultrathin iron oxide nanowhiskers (20×2 nm) growth by the hydrolysis of iron(III) oleate and oleylamine at 150 °C and capped by tween-80, show interesting properties as T1 contrast agents due to its high r_1 (6.3 $mM^{-1}\cdot s^{-1}$) and low r_2 (11.15 $mM^{-1}\cdot s^{-1}$). The reason for such behaviour lies on its nearly paramagnetic behaviour due to its ultra-small diameter [245].

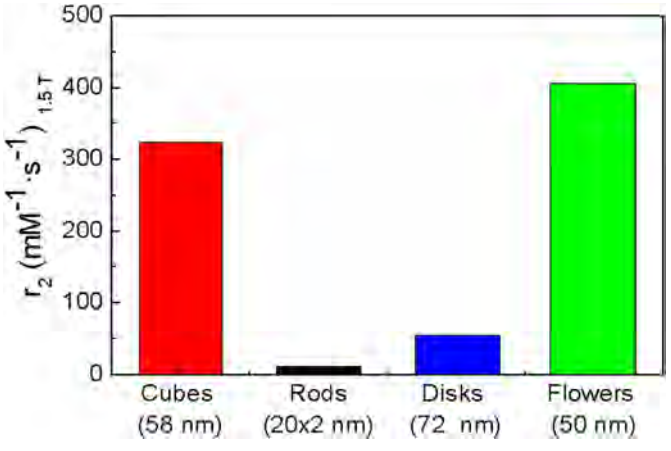

Fig. 23. r_2 relaxivity values at 1.4 or 1.5 T fields (~60 MHz) for magnetic nanoparticles of different shapes.

In summary, there are two morphologies showing great performance for T2-contrast agents, i.e. elongated nanostructures and flower-like nanoparticles (Fig. 23). In the first case, the large magnetic shape anisotropy together with the high surface-to-volume ratio seems to be the origin of the MRI enhancement. In the case of the nanoflowers, the superferrimagnetism arising from the clustered morphology seems to be responsible for it. Cluster size and morphology, which sets the crystal facets exposed to nearby water molecules, have been shown to be critical parameters for the performance of such magnetic particles as MRI T2 contrast agents. A new alternative based on the exploitation of the near-paramagnetic properties of elongated and low crystalline magnetic iron oxide nanoparticles opens a new scope for magnetic iron oxide nanoparticles and their used as T1-contrast agents.

5.3. Drug delivery

Magnetic nanoparticles can deliver active compounds to targeted organ/tissue or cells, active or passively. The active targeting depends on the attachment of ligands to the nanoparticles surface, which bind specifically to certain receptors on the targeted cells. [309,310] On the other hand, passive targeting depends on the enhanced permeability and retention effect (EPR effect), explaining their diffusion and accumulation in sites with compromised vascular system.[311] The use of anisometric nanoparticles for drug delivery relies on their high surface-to-volume ratio in combination with enhanced magnetic response and also the possibility of cargo in the case of the hollowed structures. On top of that, drug delivery can be combined with magnetic heating to control the drug release and with MRI to follow the treatment and biodistribution/degradation of the particles.

Iron oxide nanocubes (19-22 nm) have been used as drug carriers [312] with a thermoresponsive polymer shell (Poly(N-isopropylacrylamide)), via RAFT (reversible addition-fragmentation chain transfer) polymerization (Fig. 24 A-B), loading an anticancer drug, Doxorubicin (Dox), which could be released due to the heat generated by the nanocubes under an alternating magnetic field. The drug loading was around 45 % with respect to the initial Dox amount. For the release it was found that only 8% of the drug loaded was released over 24 hours at 37 °C, and more than 90 % was released in less than 5 hours when the temperature was raised until 50 °C, clearly demonstrating that the release was heat triggered (Fig. 24 C). In the same study, triggered drug release was remotely controlled by an alternating magnetic field (220 kHz and 250 Oe) with an iron concentration of 3.8 mg/mL, where about 25% of the drug was released over 4 hours. During the magnetic field exposure the temperature of the solution reached 80 °C in the first 15 minutes.

Moreover, 18 nm iron oxide nanocubes were loaded in the shell of polyelectrolyte microcapsules of 4.6 μm diameter with Cascade Blue-labelled dextran (Fig. 24 D-E) and the release was performed by applying an AMF (300 kHz, 300 Oe) [313]. Upon 90 minutes of exposure time the final temperature was about 90 °C using a concentration of 4.8 $g\cdot L^{-1}$. Some capsules were damaged due to the heat and got partially broken resulting in the release of free magnetic nanoparticles from the capsule wall, as well as the release of Cascade Blue-labelled dextran (Fig. 24 F). For a controlled release of the cargo, an iron concentration of 2.7 mg/mL allowed a suitable temperature increase for opening the walls of the capsules, with a final temperature above 80 °C. However, the field treatment did not release all the cargo molecules, which could be due to the structure of the polyelectrolyte capsules. Some cargo molecules can stay attached to the charged polyelectrolytes of the matrix, even after disruption of the wall.

Please cite this article as: A.G. Roca, L. Gutiérrez, H. Gavilán, et al., Design strategies for shape-controlled magnetic iron oxide nanoparticles, Adv. Drug Deliv. Rev., https://doi.org/10.1016/j.addr.2018.12.008

Table 9
Summary of the different relaxivity rates of iron oxide nanoparticles with different morphologies and under different fields.

Morphology	Author/Year/reference	Size (nm)	Field (T)	r_1 ($mM^{-1}\cdot s^{-1}$)	r_2 ($mM^{-1}\cdot s^{-1}$)	r_2/r_1
Cubic	Zhou/2015[301]	7	0.5	25	76	3
		15	0.5	19	80	4.2
		21	0.5	27	298	11
	Materia/2015[73]	23 single	1.0	24.2	398	16.4
		23 (200nm beads)	0.5	2.25	161	72
	Lee/2011 [302]	58	1.5	----	324	----
Elongated	Mohapatra/2015[135]	30x4	3	----	312	----
		70x12	3	----	608	----
	Orza/2017[303]	25x5	3	----	670	----
		50x5	3	----	905	----
	Macher/2014[245]	20x2	1.4	6.3	11.15	1.8
Flowers	Lartigue/2012[144]	10(30 nm cluster)	0.2	----	365	----
	Kostopoulo/2014[252]	8-10 (50 nm cluster)	1.4	----	405	----
		8-10 (86 nm cluster)	1.4	----	508	----
	Thomas/2016[227]	15 (39 nm cluster)	3	----	418	----
Hollows	An/2008[162]	11 (void of 5 nm)	1.5	0.16	1.25	7.8
Disk/rings	Liu/2015[225]	72	1.5	0.59	55.1	93
		162	1.5	0.44	73.8	167

Iron oxide nanoflowers with a diameter of 1 μm coated by a carbon shell and tunable porosity, [314] were tested for loading acetaminophen, an antipyretic and analgesic drug (Fig. 24 G). The porous and heavily functionalized carbon shell with carboxyl and hydroxyl groups provides a pathway for molecules to diffuse or bind together by collective hydrogen bonding. The drug loading is affected by the mesoporous structure, surface property and morphology, being increased with the increase of the specific surface area and pore volume of the material. In the case of these nanoflowers with a pore diameter of 65 nm the acetaminophen loading was around 30% (saturation) in 2 hours, with a loading degree of 26% in 1 hour. With regard to the release, the rate of the process was studied in PBS (Phosphate-buffered saline) at 37°C, exhibiting faster release rate those samples with larger average pore size (Fig. 24 H). The initial burst release of Fe_3O_4 NFs reached 74% in 2 hours and 80% after 4 h.

Hollow microspheres of rattle-type magnetic carbon (Fe_3O_4@C) were synthesized (Fig. 25 A) and investigated as drug carriers [315]. The final size of these microcapsules loaded with Doxorrubicin was estimated to be 235 nm and tunable C shell thickness (Fig. 25 B). The release of the drug occurs by diffusion and almost all the drug was released within 12 hours (82 %). The shell thickness (12 nm, 28 nm, and 40 nm) had influence on this release, the thinner carbon shell releases faster, i.e. 82% (12 nm), 74% (28 nm) and 69% (40 nm) respectively to the shell thickness (Fig. 25 C).

Porous hollow nanoparticles of Fe_3O_4, with an average size of 16 nm, prepared by controlled oxidation of amorphous core/shell Fe nanoparticles by the oxygen-transfer reagent trimethylamine N-oxide (Me_3NO) were used as a cisplatin delivery vehicle (Fig. 25 D-E). [316] The release by diffusion through the pores could be easily controlled by adjusting the pore sizes and medium pH, since the acidic medium results in wider pore opening and faster release of cisplatin (Fig. 25 F). The shell has a thickness of about 3 nm and a hollow interior about 10 nm in diameter, with pores of around 2-4 nm. The pH-sensitive pore opening can accelerate the cisplatin release in the acidic endosomes/lysosomes once the nanoparticles are internalized. For example, at pH 7.4 the nanoparticles show a gradual release with $t_{1/2} = 16$ h (the time needed for the release of 50% of the dose) while at pH 5 the cisplatin release is accelerated with $t_{1/2} = 4$ h. Likewise, **hollow iron oxide nanoparticles** were used to encapsulate Doxorrubicin which has also a pH-dependent drug release behaviour. [269] The nanoparticles synthesis renders particles with an average hydrodynamic diameter of about 120 nm (with the doxorubicin encapsulated) and with a charge of +16 mV. [316] Doxorrubicin release rate was measured at room temperature with two different pH values (pH 7.4 and 5). After 24 h incubation at pH 7.4 only 30% of the doxorubicin was released, while the release rate at pH 5 was much faster, where over 80% of doxorubicin was released.

Magnetic hollow spheres of Fe_3O_4nanosheets (2-4 μm) were prepared by precursor-templated conversion method, with surface modified with poly(ethylene glycol) (PEG) (Fig. 25 G-H). [317] Ibuprofen was used for drug loading and the release behavior was investigated in a simulated body fluid (SBF) over a time period of 136 h. The drug was progressively released by desorption and diffusion. At pH 7.4 about 37% of the loaded drug was released for the first 24 h and 67% for 72 h, and then the drug release rate decreased and reached a value 74% for 136 h (Fig. 25 I).

5.4. Other biomedical applications

Magnetic hyperthermia, Magnetic Resonance Imagining and Drug delivery, described above, are by far the most studied biomedical applications being developed using magnetic nanoparticles. Nevertheless, these materials are constantly showing their great potential to revolutionize classical medical treatments and therefore the number of new biomedical applications using magnetic iron oxide nanoparticles has been increasing exponentially over time. However, in many cases, given the novelty of such applications, the impact of the nanoparticles shape on their performance has not been fully elucidated yet. A few relevant applications are briefly described below.

5.4.1. Magnetic biosensor systems

Magnetic biosensor systems are based on magnetic nanoparticles functionalized with molecules able to recognize specific molecular targets. Sensing can be based on modifications of different properties of the materials in presence of the target, such properties are the water proton relaxation rates, the relaxation of the particles magnetic moment or the effect of their magnetic properties in devices sensitive to the magnetic fields.[318] For these tests, each particle acts as a probe giving a different signal. Given that the alteration of the magnetic nanoparticles shape strongly affect their magnetic properties, very distinct magnetic properties can be obtained for a set of particles with different sizes and shapes. If the particles are then functionalized with different recognition molecules, the simultaneous detection of different biological molecules is allowed. For example, magnetite **nanospheres, nanohexagons, cubes** and **rods** were tested as part of a sensor based on the signal corresponding to the second derivative of magnetization around a zero field.[319] These differences opened the way to the use of anisometric magnetic nanoparticles in multiparametric immunoassays given their characteristic magnetic signature.

Please cite this article as: A.G. Roca, L. Gutiérrez, H. Gavilán, et al., Design strategies for shape-controlled magnetic iron oxide nanoparticles, Adv. Drug Deliv. Rev., https://doi.org/10.1016/j.addr.2018.12.008

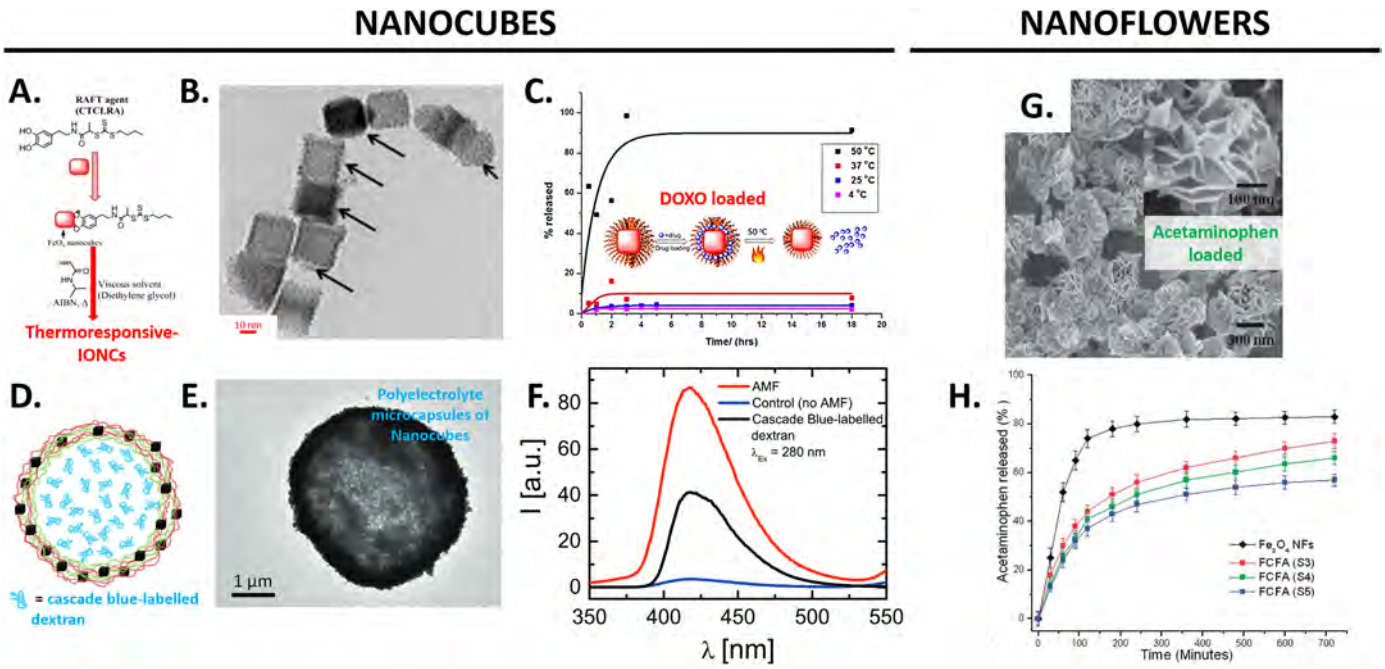

Fig. 24. Different systems of iron oxide magnetic nanocubes and nanoflowers used for drug delivery purposes: nanohybrids of iron oxide nanocubes with a thermoresponsive polymer shell that can act as drug carriers for doxorubicin (doxo). (A) Scheme showing the synthetic approach, (B) Nanocubes singly coated by a thin polymer layer (arrows), (C) Drug release from thermoresponsive cubic IONPs in a water bath at various temperatures. Reprinted with permission from ref [312]. © 2015 American Chemical Society. Iron oxide nanocube's modified microcapsules as a platform for magnetically triggered molecular release of Cascade Blue-labelled dextran (D-E). Fluorescence emission spectra (at $\lambda_{exc} = 280$ nm excitation) (F) of: free Cascade Blue-labelled dextran (black line), the supernatant of a capsule solution which had been treated for 90 minutes under an AMF (300 kHz and 24 kAm^{-1}) (red line), and the supernatant of a control sample of capsules which had been kept at room temperature for 90 minutes and thus had not been exposed to an AMF (blue line). Reprinted with permission from ref [313]. © 2015 Royal Society of Chemistry. Fe_3O_4 nanoflowers (G) used in the drug delivery test (H) with acetaminophen along with composites with increasing porosity (S3-S5). Reprinted with permission from ref [314]. © 2013 Royal Society of Chemistry.

5.4.2. Magnetic particle imaging (MPI)

Magnetic particle imaging (MPI) is an imaging modality based on the direct mapping of iron oxide nanoparticles. Most of the MPI tracers studied until now are based on spherical particles, although there are some recent works using nanoparticles with different shape. For example, 15 nm **cubes** have been compared to 19 nm spherical magnetite particles (prepared to have similar volumes) and the results were that the spherical particles outperformed the cubic ones.[320] These results, that also occurred in doped particles of the two morphologies, could be explained by the increase in anisotropy of the material, that results in detrimental performance in the MPI signal. In addition, **flower-like** multi-core structures with particle diameters between 40 and 120 nm and core sizes in the range between 16 and 56 nm were evaluated as MPI tracers.[321] Given the complex and heterogeneous structures of the materials prepared, a wide variety of magnetic behaviours were observed for this group of nanoflowers. As a result, these differences allowed tunning their performance in MPI depending on the drive field.

5.4.3. Cell separation

Cell separation comprise a group of technologies that enable to identify a specific type of cell from a heterogeneous mixture of them.[322] This technology plays a fundamental role both in the diagnosis and treatment of diseases. Magnetic cell sorting relies on the interaction between molecules attached to the magnetic particles that interact with the cell surface. Then the nanoparticles must respond to a magnetic force in order to be guided to specific locations. One recent example of anisometric nanoparticles for magnetic separation has been just developed based on the use of **nanooctapods** provided their enhanced magnetic susceptibility, small coercivity and good magnetophoretic mobility.[323]

6. Conclusions and future remarks

The improvement of the performance of magnetic iron oxide nanoparticles in the different applications requires the design of more complex synthetic nanostructures, uniform in size and with morphologies different from the spherical one, leading to enhanced properties, i.e. high magnetic anisotropy, larger specific area, and new ones like vortex magnetic domains structures or magnetomechanical properties. Those properties are very advantageous not only in theranostic applications (MRI and magnetic hyperthermia) but also in others like environmental remediation, Li-ion batteries, spintronics and microwave absorption.

This review summarizes the colloidal synthetic routes that lead to magnetic nanoparticles with morphologies different from the spherical one and analyses the key parameters on each route that control particle size and shape. Although the final size and shape of the nanocrystals can be interpreted in terms of classical nucleation and growth theory, it is worth to note that there are several factors that govern the growth and subtle changes could lead to a change in size and morphology. There is no unique route to obtain a specific morphology, so the final choice should depend on the target size, capping molecules and dispersant. Moreover, factors like time, energy consumption, environmental issues, cost and scalability should be considered when translating these processes to the industry. Thermal decomposition and solvothermal approaches can lead to almost all the morphologies presented in the review. Thermal decomposition has the advantages of producing highly monodisperse nanoparticles with high crystallinity. However, it needs the use of organic solvents that are not environmentally friendly, and for the application in biomedicine, a further step for water transference and colloidal stabilization is needed. On the other side, solvothermal methods are able to produce nanoparticles stable in water, with protocols less sophisticated than the thermal decomposition, and using solvents more environmentally friendly. Nevertheless,

Please cite this article as: A.G. Roca, L. Gutiérrez, H. Gavilán, et al., Design strategies for shape-controlled magnetic iron oxide nanoparticles, Adv. Drug Deliv. Rev., https://doi.org/10.1016/j.addr.2018.12.008

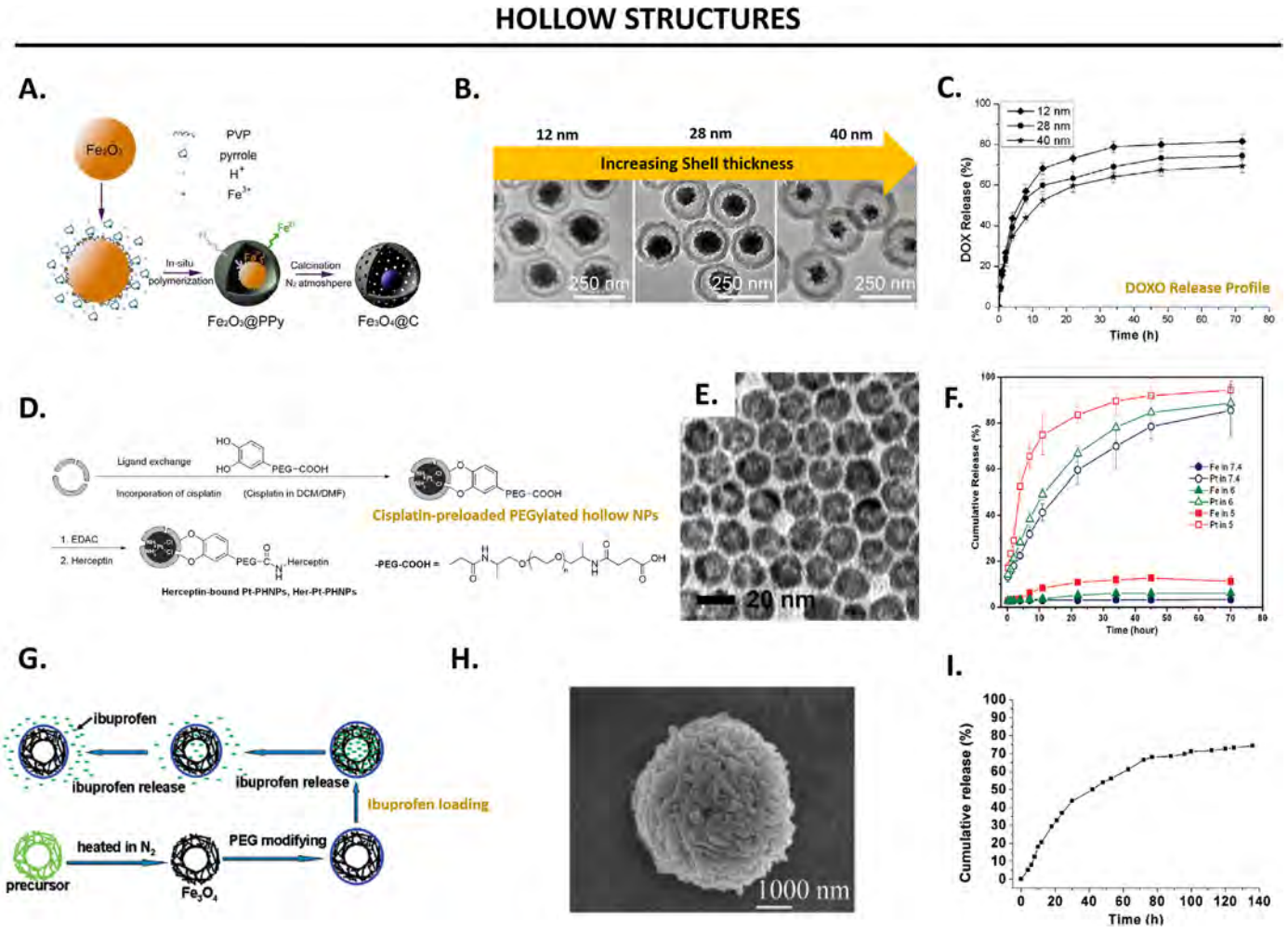

Fig. 25. Different systems of iron oxide hollow particles and used for drug delivery purposes: porous hollow nanoparticles for cisplatin storage and release. Magnetic carbon (Fe_3O_4@C) hollow microspheres were synthesized for sustained-release of doxorubicin. (A) Schematic synthetic approach, (B) TEM images of the synthesized hollow microspheres prepared with increasing shell thickness, optimizing the pyrrole concentration (0.1, 0.75 and 2 ml) and (C) Drug-release kinetic curves obtained from three products with different shell thicknesses (12, 28, and 40 nm). Reprinted with permission from ref [315]. © 2017 Elsevier. Hierarchically nanostructured hollow spheres assembled by magnetic iron oxide nanosheets for the favourable release of ibuprofen. (D) Schematic illustration the synthetic approach and the loading, (E) TEM image of the 16 nm porous hollow nanoparticles and (F) pH-dependent release of cisplatin from Pt-PHNPs (19.6% Pt/Fe). The Pt-PHNPs were incubated in PBS at pH = 7.4 or at pH = 6.0 or 5.0) at 37 °C. Reprinted with permission from ref [316]. © 2009 American Chemical Society. (G) Scheme for the preparation of the hollow structures and the ibuprofen loading, (H) SEM image of the final particles where the constituent nanosheets are visible. (I) Ibuprofen release profile from ibuprofen-PEG-coated Fe_3O_4 hollow spheres in simulated body fluid. Reprinted with permission from ref [317]. © 2008 American Chemical Society.

the synthesis is not easily scalable, requires long reaction times and in many cases, a final step for the reduction of the resulting nanoparticles to magnetite.

Structural and magnetic properties of the anisometric nanoparticles depend on the choice of the synthetic route. For example, in the case of elongated nanoparticles, porous structures can be achieved by using shape-templating routes and further reduction to magnetite. In contrast, elongated nanoparticles grown by solvothermal method are generally highly crystalline. Regarding the magnetic properties, it is remarkable the finding of magnetic vortex spin configurations in nanodisks leading to negligible interparticle interactions, which could be very advantageous for biomedical applications.

In addition to the effect of the shape on the particles physicochemical properties, other relevant parameters related to their use in biomedical applications, such as their toxicity, cell uptake, biodistribution or degradation, have to be evaluated. However, given the complexity of the biological environment, it is very difficult to isolate the nanoparticles shape from other relevant factors that may have an impact of the materials properties such as the particles size, polidispersity, stability, surface coating, protein corona formation or endotoxin presence. The lack of standardization on the analysis of some of these properties makes it difficult to compare results from different research groups. Therefore, we believe that the research community working on magnetic nanoparticles for biomedical applications should make a big effort towards the development of standard protocols that would facilitate the comparison of data.

Most of the research on magnetic nanoparticles for biomedicine until the last decade has been carried out with spherical particles, focusing on particle and aggregate size, the synthetic route chosen and the coating. Since the last decade, the number of literature regarding the synthesis and applications in biomedicine of non-spherical particles has boosted, demonstrating the interest respect to their spherical equivalents. For example, the use of magnetic nanocubes and nanodisks in magnetic hyperthermia leads to an increment in the SAR values, also showing a great performance in *in vitro* studies. Interestingly, the potential of these particles can be increased if magnetic hyperthermia is combined with photothermal therapy or if the nanocubes are integrated into a hybrid heterostructure with gold particles. In the case of the nanodisks and elongated nanoparticles, the benefits come not only from the high SAR values, but also for the possibility to induce physical

Please cite this article as: A.G. Roca, L. Gutiérrez, H. Gavilán, et al., Design strategies for shape-controlled magnetic iron oxide nanoparticles, Adv. Drug Deliv. Rev., https://doi.org/10.1016/j.addr.2018.12.008

rotation or vibration when subject to an alternating magnetic field of few Hz inducing a mechanical effect on the cell membranes leading to apoptosis.

The synthesis of anisometric magnetic iron oxide nanoparticles also brings benefits for MRI. On one hand, due to the high specific area, elongated nanoparticles are a promising geometry leading to higher r_2 values. Magnetic nanoflowers, due to its spatial clustered configuration, which enables the superferrimagnetism, have also exhibited a great potentiality for MRI. On the other hand, magnetic particles with poor magnetic properties such as nanowhiskers have shown excellent performance as T1-contrast agents due to their low r_2/r_1 values.

Although there are a vast number of synthetic routes leading to anisometric magnetic iron oxide nanoparticles showing a great performance in biomedicine, there is room for improvement to control how these materials are produced in a more robust, reproducible and scalable way in order to fulfil the requirements of the FDA and other regulatory agencies before they reach the clinical practice. Moreover, an accurate and standardized systematic cytotoxicity assessment is needed to understand the interaction of cells with nano-objects with special geometries.

Acknowledgements

This work was supported by the European Commission Framework Program 7 (NanoMag project, No. 604448). We acknowledge the Spanish Ministry of Economy and Competitiveness through MAT2016-77391-R and MAT2017-88148-R grants, and Consejo Superior de Investigaciones Científicas through PIE-201760E007 project. L.G. acknowledges financial support from the MINECO Ramón y Cajal program (RYC-2014-15512). M. E.F.B. acknowledges the Brazilian agency CNPq for her grant within the Science without Borders Program (232947/2014-7). A.G.R. thanks the Generalitat de Catalunya through 2017-SGR-292 project. The ICN2 is funded by the CERCA programme / Generalitat de Catalunya. The ICN2 is supported by the Severo Ochoa program from Spanish MINECO (Grant No. SEV-2017-0706). We acknowledge Miguel Ruiz for the design of most of the figures displayed in this review.

References

[1] D.V. Talapin, J.-S. Lee, M.V. Kovalenko, E.V. Shevchenko, Prospects of colloidal nanocrystals for electronic and optoelectronic applications, Chem. Rev. 110 (2010) 389–458.
[2] J. Yang, M.K. Choi, D.-H. Kim, T. Hyeon, Designed assembly and integration of colloidal nanocrystals for device applications, Adv. Mater. 28 (2016) 1176–1207.
[3] D. Kim, J. Kim, Y. Il Park, N. Lee, T. Hyeon, Recent development of inorganic nanoparticles for biomedical imaging, ACS Cent. Sci. 4 (2018) 324–336.
[4] D.H. Ortgies, F.J. Teran, U. Rocha, L. de la Cueva, G. Salas, D. Cabrera, A.S. Vanetsev, M. Rähn, V. Sammelselg, Y.V. Orlovskii, D. Jaque, Optomagnetic nanoplatforms for in situ controlled hyperthermia, Adv. Funct. Mater. 28 (2018), 1704434. .
[5] X. Yang, M. Yang, B. Pang, M. Vara, Y. Xia, Gold nanomaterials at work in biomedicine, Chem. Rev. 115 (2015) 10410–10488.
[6] S. Schauermann, N. Nilius, S. Shaikhutdinov, H.-J. Freund, Nanoparticles for heterogeneous catalysis: new mechanistic insights, Acc. Chem. Res. 46 (2013) 1673–1681.
[7] I. Venditti, Gold nanoparticles in photonic crystals applications: a review, Materials (Basel). 10 (2017) 97.
[8] L. Liu, A. Corma, Metal catalysts for heterogeneous catalysis: from single atoms to nanoclusters and nanoparticles, Chem. Rev. 118 (2018) 4981–5079.
[9] M. Haase, H. Schäfer, Upconverting nanoparticles, Angew. Chemie Int. Ed. 50 (2011) 5808–5829.
[10] B. Pelaz, C. Alexiou, R.A. Alvarez-Puebla, F. Alves, A.M. Andrews, S. Ashraf, L.P. Balogh, L. Ballerini, A. Bestetti, C. Brendel, S. Bosi, M. Carril, W.C.W. Chan, C. Chen, X. Chen, X. Chen, Z. Cheng, D. Cui, J. Du, C. Dullin, A. Escudero, N. Feliu, M. Gao, M. George, Y. Gogotsi, A. Grünweller, Z. Gu, N.J. Halas, N. Hampp, R.K. Hartmann, M.C. Hersam, P. Hunziker, J. Jian, X. Jiang, P. Jungebluth, P. Kadhiresan, K. Kataoka, A. Khademhosseini, J. Kopeček, N.A. Kotov, H.F. Krug, D.S. Lee, C.M. Lehr, K.W. Leong, X.J. Liang, M. Ling Lim, L.M. Liz-Marzán, X. Ma, P. Macchiarini, H. Meng, H. Möhwald, P. Mulvaney, A.E. Nel, S. Nie, P. Nordlander, T. Okano, J. Oliveira, T.H. Park, R.M. Penner, M. Prato, V. Puntes, V.M. Rotello, A. Samarakoon, R.E. Schaak, Y. Shen, S. Sjöqvist, A.G. Skirtach, M.G. Soliman, M.M. Stevens, H.W. Sung, B.Z. Tang, R. Tietze, B.N. Udugama, J.S. VanEpps, T. Weil, P.S. Weiss, I. Willner, Y. Wu, L. Yang, Z. Yue, Q. Zhang, Q. Zhang, X.E. Zhang, Y. Zhao, X. Zhou, W.J. Parak, Diverse applications of nanomedicine, ACS Nano. 11 (2017) 2313–2381.
[11] J. Lee, J. Yang, S.G. Kwon, T. Hyeon, Nonclassical nucleation and growth of inorganic nanoparticles, Nat. Rev. Mater. 1 (2016), 16034. .
[12] J. van Embden, A.S.R. Chesman, J.J. Jasieniak, The heat-up synthesis of colloidal nanocrystals, Chem. Mater. 27 (2015) 2246–2285.
[13] N.G. Bastús, F. Merkoçi, J. Piella, V. Puntes, Synthesis of highly monodisperse citrate-stabilized silver nanoparticles of up to 200 nm: kinetic control and catalytic properties, Chem. Mater. 26 (2014) 2836–2846.
[14] J. Ulama, M. Zackrisson Oskolkova, J. Bergenholtz, Monodisperse PEGylated spheres: an aqueous colloidal model system, J. Phys. Chem. B. 118 (2014) 2582–2588.
[15] J. Yang, T. Ling, W.-T. Wu, H. Liu, M.-R. Gao, C. Ling, L. Li, X.-W. Du, A top–down strategy towards monodisperse colloidal lead sulphide quantum dots, Nat. Commun. 4 (2013) 1695.
[16] A. Kuijk, A. van Blaaderen, A. Imhof, Synthesis of monodisperse, rodlike silica colloids with tunable aspect ratio, J. Am. Chem. Soc. 133 (2011) 2346–2349.
[17] M. Estrader, A. Lopez-Ortega, I.V. Golosovsky, S. Estrade, A.G. Roca, G. Salazar-Alvarez, L. Lopez-Conesa, D. Tobia, E. Winkler, J.D. Ardisson, W.A.A. Macedo, A. Morphis, M. Vasilakaki, K.N. Trohidou, A. Gukasov, I. Mirebeau, O.L. Makarova, R. D. Zysler, F. Peiro, M.D. Baro, L. Bergstrom, J. Nogues, Origin of the large dispersion of magnetic properties in nanostructured oxides: FexO/Fe3O4 nanoparticles as a case study, Nanoscale. 7 (2015) 3002–3015.
[18] E. Wetterskog, C.-W. Tai, J. Grins, L. Bergström, G. Salazar-Alvarez, Anomalous magnetic properties of nanoparticles arising from defect structures: topotaxial oxidation of Fe(1-x)O|Fe(3-δ)O4 core|shell nanocubes to single-phase particles, ACS Nano. 7 (2013) 7132–7144.
[19] F. Ludwig, O. Kazakova, L.F. Barquin, A. Fornara, L. Trahms, U. Steinhoff, P. Svedlindh, E. Wetterskog, Q.A. Pankhurst, P. Southern, M.P. Morales, M.F. Hansen, C. Frandsen, E. Olsson, S. Gustafsson, N. Gehrke, K. Ludtke-Buzug, C. Gruttner, C. Jonasson, C. Johansson, Magnetic, structural, and particle size analysis of single- and multi-core magnetic nanoparticles, IEEE Trans. Magn. 50 (2014) 1–4.
[20] B. Faure, E. Wetterskog, K. Gunnarsson, E. Josten, R.P. Hermann, T. Brückel, J.W. Andreasen, F. Meneau, M. Meyer, A. Lyubartsev, L. Bergström, G. Salazar-Alvarez, P. Svedlindh, 2D to 3D crossover of the magnetic properties in ordered arrays of iron oxide nanocrystals, Nanoscale. 5 (2013) 953–960.
[21] S. Disch, E. Wetterskog, R.P. Hermann, D. Korolkov, P. Busch, P. Boesecke, O. Lyon, U. Vainio, G. Salazar-Alvarez, L. Bergström, T. Brückel, Structural diversity in iron oxide nanoparticle assemblies as directed by particle morphology and orientation, Nanoscale. 5 (2013) 3969.
[22] N.T.K. Thanh, N. Maclean, S. Mahiddine, Mechanisms of nucleation and growth of nanoparticles in solution, Chem. Rev. 114 (2014) 7610–7630.
[23] R. Massart, Preparation of aqueous magnetic liquids in alkaline and acidic media, IEEE Trans. Magn. 17 (1981) 1247–1248.
[24] I.-M. Grabs, C. Bradtmöller, D. Menzel, G. Garnweitner, Formation mechanisms of iron oxide nanoparticles in different nonaqueous media, Cryst. Growth Des. 12 (2012) 1469–1475.
[25] V. Privman, D.V. Goia, J. Park, E. Matijević, Mechanism of formation of monodispersed colloids by aggregation of nanosize precursors, J. Colloid Interface Sci. 213 (1999) 36–45.
[26] M.A. Watzky, R.G. Finke, Nanocluster Size-Control and "Magic Number" Investigations. Experimental Tests of the "Living-Metal Polymer" Concept and of Mechanism-Based Size-Control Predictions Leading to the Syntheses of Iridium(0) Nanoclusters Centering about Four Sequential Magic Numbers†, Chem. Mater. 9 (1997) 3083–3095.
[27] B.H. Kim, J. Yang, D. Lee, B.K. Choi, T. Hyeon, J. Park, Liquid-phase transmission electron microscopy for studying colloidal inorganic nanoparticles, Adv. Mater. 30 (2018), 1703316. .
[28] S.G. Kwon, Y. Piao, J. Park, S. Angappane, Y. Jo, N.-M. Hwang, J.-G. Park, T. Hyeon, Kinetics of monodisperse iron oxide nanocrystal formation by "heating-up" process, J. Am. Chem. Soc. 129 (2007) 12571–12584.
[29] R.L. Penn, J.F. Banfield, Imperfect oriented attachment: dislocation generation in defect-free nanocrystals, Science. 281 (1998) 969–971.
[30] Y.W. Jun, J.S. Choi, J. Cheon, Shape control of semiconductor and metal oxide nanocrystals through nonhydrolytic colloidal routes, Angew. Chemie - Int. Ed. 45 (2006) 3414–3439.
[31] S. Ener, E. Anagnostopoulou, I. Dirba, L.-M. Lacroix, F. Ott, T. Blon, J.-Y. Piquemal, K. P. Skokov, O. Gutfleisch, G. Viau, Consolidation of cobalt nanorods: A new route for rare-earth free nanostructured permanent magnets, Acta Mater. 145 (2018) 290–297.
[32] N.D. Burrows, A.M. Vartanian, N.S. Abadeer, E.M. Grzincic, L.M. Jacob, W. Lin, J. Li, J. M. Dennison, J.G. Hinman, C.J. Murphy, Anisotropic nanoparticles and anisotropic surface chemistry, J. Phys. Chem. Lett. 7 (2016) 632–641.
[33] H. Nishi, T. Nagano, T. Kameyama, S. Kuwabata, T. Torimoto, Well-controlled synthesis of wurtzite-type Cu 2 ZnSnS 4 nanoparticles using multiple sulfur sources via a two-step heating process, CrystEngComm. 17 (2015) 174–182.
[34] N.G. Bastús, E. Gonzalez, J. Esteve, J. Piella, J. Patarroyo, F. Merkoçi, V. Puntes, Exploring new synthetic strategies for the production of advanced complex inorganic nanocrystals, Zeitschrift Für Phys. Chemie. 229 (2015).
[35] P. Hugounenq, M. Levy, D. Alloyeau, L. Lartigue, E. Dubois, V. Cabuil, C. Ricolleau, S. Roux, C. Wilhelm, F. Gazeau, R. Bazzi, Iron oxide monocrystalline nanoflowers for highly efficient magnetic hyperthermia, J. Phys. Chem. C. 116 (2012) 15702–15712.
[36] T.K. Sau, A.L. Rogach, Nonspherical noble metal nanoparticles: colloid-chemical synthesis and morphology control, Adv. Mater. 22 (2010) 1781–1804.
[37] M.V. Kovalenko, L. Manna, A. Cabot, Z. Hens, D.V. Talapin, C.R. Kagan, V.I. Klimov, A. L. Rogach, P. Reiss, D.J. Milliron, P. Guyot-Sionnnest, G. Konstantatos, W.J. Parak, T.

Please cite this article as: A.G. Roca, L. Gutiérrez, H. Gavilán, et al., Design strategies for shape-controlled magnetic iron oxide nanoparticles, Adv. Drug Deliv. Rev., https://doi.org/10.1016/j.addr.2018.12.008

Hyeon, B.A. Korgel, C.B. Murray, W. Heiss, Prospects of nanoscience with nanocrystals, ACS Nano. 9 (2015) 1012–1057.
[38] W. Qi, Nanoscopic thermodynamics, Acc. Chem. Res. 49 (2016) 1587–1595.
[39] Y. Wang, J. He, C. Liu, W.H. Chong, H. Chen, Thermodynamics versus kinetics in nanosynthesis, Angew. Chemie Int. Ed. 54 (2015) 2022–2051.
[40] L. Qiao, Z. Fu, J. Li, J. Ghosen, M. Zeng, J. Stebbins, P.N. Prasad, M.T. Swihart, Standardizing size- and shape-controlled synthesis of monodisperse magnetite (Fe 3 O 4) nanocrystals by identifying and exploiting effects of organic impurities, ACS Nano. 11 (2017) 6370–6381.
[41] Y. Xia, X. Xia, H.-C. Peng, Shape-controlled synthesis of colloidal metal nanocrystals: thermodynamic versus kinetic products, J. Am. Chem. Soc. 137 (2015) 7947–7966.
[42] Z.A. Peng, X. Peng, Nearly monodisperse and shape-controlled cdse nanocrystals via alternative routes: nucleation and growth, J. Am. Chem. Soc. 124 (2002) 3343–3353.
[43] J. Chen, B. Lim, E.P. Lee, Y. Xia, Shape-controlled synthesis of platinum nanocrystals for catalytic and electrocatalytic applications, Nano Today. 4 (2009) 81–95.
[44] C. Yang, J. Wu, Y. Hou, Fe_3O_4 nanostructures: synthesis, growth mechanism, properties and applications, Chem. Commun. 47 (2011) 5130.
[45] M. Ocaña, R. Rodriguez-Clemente, C.J. Serna, Uniform colloidal particles in solution: Formation mechanisms, Adv. Mater. 7 (1995) 212–216.
[46] M.P. Morales, T. Gonzalez-Carreno, C.J. Serna, The formation of & alpha-Fe_2O_3 monodispersed particles in solution, J. Mater. Res. 7 (1992) 2538–2545.
[47] M.A. Verges, A. Mifsud, C.J. Serna, Formation of rod-like zinc oxide microcrystals in homogeneous solutions, J. Chem. Soc. Faraday Trans. 86 (1990) 959.
[48] F. Wang, V.N. Richards, S.P. Shields, W.E. Buhro, Kinetics and Mechanisms of aggregative nanocrystal growth, Chem. Mater. 26 (2014) 5–21.
[49] C.J. Murphy, T.K. Sau, A.M. Gole, C.J. Orendorff, J. Gao, L. Gou, S.E. Hunyadi, T. Li, Anisotropic metal nanoparticles: synthesis, assembly, and optical applications, J. Phys. Chem. B. 109 (2005) 13857–13870.
[50] E.C. Dreaden, A.M. Alkilany, X. Huang, C.J. Murphy, M.A. El-Sayed, The golden age: gold nanoparticles for biomedicine, Chem. Soc. Rev. 41 (2012) 2740–2779.
[51] Y. Xia, W. Li, C.M. Cobley, J. Chen, X. Xia, Q. Zhang, M. Yang, E.C. Cho, P.K. Brown, Gold nanocages: from synthesis to theranostic applications, Acc. Chem. Res. 44 (2011) 914–924.
[52] S. Pud, A. Kisner, M. Heggen, D. Belaineh, R. Temirov, U. Simon, A. Offenhäusser, Y. Mourzina, S. Vitusevich, Features of transport in ultrathin gold nanowire structures, Small. 9 (2013) 846–852.
[53] Y. Yin, A.P. Alivisatos, Colloidal nanocrystal synthesis and the organic–inorganic interface, Nature. 437 (2005) 664–670.
[54] L.-M. Lacroix, C. Gatel, R. Arenal, C. Garcia, S. Lachaize, T. Blon, B. Warot-Fonrose, E. Snoeck, B. Chaudret, G. Viau, Tuning complex shapes in platinum nanoparticles: from cubic dendrites to fivefold stars, Angew. Chemie Int. Ed. 51 (2012) 4690–4694.
[55] K.M. Bratlie, H. Lee, K. Komvopoulos, P. Yang, G.A. Somorjai, Platinum nanoparticle shape effects on benzene hydrogenation selectivity, Nano Lett. 7 (2007) 3097–3101.
[56] E. Anagnostopoulou, B. Grindi, L.-M. Lacroix, F. Ott, I. Panagiotopoulos, G. Viau, Dense arrays of cobalt nanorods as rare-earth free permanent magnets, Nanoscale. 8 (2016) 4020–4029.
[57] Nguyen T.K. Thanh, Magnetic Nanoparticles: From Fabrication to Clinical Applications, CRC Press, 2012.
[58] C. Kinnear, T.L. Moore, L. Rodriguez-Lorenzo, B. Rothen-Rutishauser, A. Petri-Fink, Form follows function: nanoparticle shape and its implications for nanomedicine, Chem. Rev. 117 (2017) 11476–11521.
[59] A. Ali, H. Zafar, M. Zia, I. ul Haq, A.R. Phull, J.S. Ali, A. Hussain, Synthesis, characterization, applications, and challenges of iron oxide nanoparticles, Nanotechnol. Sci. Appl. Volume 9 (2016) 49–67.
[60] M. Colombo, S. Carregal-Romero, M.F. Casula, L. Gutiérrez, M.P. Morales, I.B. Böhm, J.T. Heverhagen, D. Prosperi, W.J. Parak, Biological applications of magnetic nanoparticles, Chem. Soc. Rev. 41 (2012) 4306.
[61] M.R. Ghazanfari, M. Kashefi, S.F. Shams, M.R. Jaafari, Perspective of Fe_3O_4 nanoparticles role in biomedical applications, Biochem. Res. Int. 2016 (2016).
[62] M. Mohapatra, S. Anand, Synthesis and applications of nano-structured iron oxides / hydroxides – a review, Int. J. Eng. Sci. Technol. 2 (2010) 127–146.
[63] A.G. Roca, R. Costo, A.F. Rebolledo, S. Veintemillas-Verdaguer, P. Tartaj, T. González-Carreño, M.P. Morales, C.J. Serna, Progress in the preparation of magnetic nanoparticles for applications in biomedicine, J. Phys. D. Appl. Phys. 42 (2009), 224002. .
[64] P. Tartaj, M.P. Morales, S. Veintemillas-Verdaguer, T. Gonzalez-Carreño, C.J. Serna, The preparation of magnetic nanoparticles for applications in biomedicine, J. Phys. D. Appl. Phys. 36 (2003) R182–R197.
[65] D. Lisjak, A. Mertelj, Anisotropic magnetic nanoparticles: A review of their properties, syntheses and potential applications, Prog. Mater. Sci. 95 (2018) 286–328.
[66] J. Liu, Z. Wu, Q. Tian, W. Wu, X. Xiao, Shape-controlled iron oxide nanocrystals: synthesis, magnetic properties and energy conversion applications, CrystEngComm. 18 (2014) 6303–6326.
[67] G.I. Frolov, Film carriers for super-high-density magnetic storage, Tech. Phys. 46 (2001) 1537–1544.
[68] M.P. Sharrock, Recent advances in metal particulate recording media: Toward the ultimate particle, IEEE Trans. Magn. 36 (2000) 2420–2425.
[69] R. Horimizu, H. Inoue, I. Matsuyama, M. Katsumoto, Oxidation kinetics of acicular iron particles for magnetic recording media, J. Magn. Magn. Mater. 114 (1992) 202–206.
[70] X. Yao, K. Sabyrov, T. Klein, R. Lee Penn, T.S. Wiedmann, Evaluation of magnetic heating of asymmetric magnetite particles, J. Magn. Magn. Mater. 381 (2015) 21–27.
[71] D. Cheng, X. Li, G. Zhang, H. Shi, Morphological effect of oscillating magnetic nanoparticles in killing tumor cells, Nanoscale Res. Lett. 9 (2014) 195.
[72] A.O. Fung, V. Kapadia, E. Pierstorff, D. Ho, Y. Chen, Induction of cell death by magnetic actuation of nickel nanowires internalized by fibroblasts, J. Phys. Chem. C. 112 (2008) 15085–15088.
[73] M.E. Materia, P. Guardia, A. Sathya, M. Pernia Leal, R. Marotta, R. Di Corato, T. Pellegrino, Mesoscale assemblies of iron oxide nanocubes as heat mediators and image contrast agents, Langmuir. 31 (2015) 808–816.
[74] A. Espinosa, R. Di Corato, J. Kolosnjaj-Tabi, P. Flaud, T. Pellegrino, C. Wilhelm, Duality of iron oxide nanoparticles in cancer therapy: amplification of heating efficiency by magnetic hyperthermia and photothermal bimodal treatment, ACS Nano. 10 (2016) 2436–2446.
[75] C.S.B. Dias, T.D.M. Hanchuk, H. Wender, W.T. Shigeyosi, J. Kobarg, A.L. Rossi, M.N. Tanaka, M.B. Cardoso, F. Garcia, Shape tailored magnetic nanorings for intracellular hyperthermia cancer therapy, Sci. Rep. 7 (2017), 14843. .
[76] R.M. Cornell, U. Schwertmann, The Iron Oxides, 2003.
[77] J. Majzlan, K.-D. Grevel, A. Navrotsky, Thermodynamics of Fe oxides: Part II. Enthalpies of formation and relative stability of goethite (α-FeOOH), lepidocrocite (γ-FeOOH), and maghemite (γ-Fe 2 O 3), Am. Mineral. 88 (2003) 855–859.
[78] A. Navrotsky, L. Mazeina, J. Majzlan, Size-driven structural and thermodynamic complexity in iron oxides, Science (80-.) 319 (2008) 1635–1638.
[79] M.P. Morales, C. Pecharroman, T.G. Carreño, C.J. Serna, Structural characteristics of uniform γ-Fe2O3 particles with different axial (length/width) ratios, J. Solid State Chem. 108 (1994) 158–163.
[80] P.B. Braun, A superstructure in spinels, Nature. 170 (1952) 1123.
[81] K.V.P.M. Shafi, A. Ulman, A. Dyal, X.Z. Yan, N.L. Yang, C. Estournes, L. Fournes, A. Wattiaux, H. White, M. Rafailovich, Magnetic Enhancement of γ-Fe2O3 Nanoparticles by Sonochemical Coating, Chem. Mater. 14 (2002) 1778.
[82] W. Wu, Z. Wu, T. Yu, C. Jiang, W.-S. Kim, Recent progress on magnetic iron oxide nanoparticles: synthesis, surface functional strategies and biomedical applications, Sci. Technol. Adv. Mater. 16 (2015), 023501. .
[83] R. Massart, E. Dubois, V. Cabuil, E. Hasmonay, Preparation and properties of monodisperse magnetic fluids, J. Magn. Magn. Mater. 149 (1995) 1–5.
[84] R. Massart, Preparation of aqueous magnetic liquids in alkaline and acidic media, IEEE Trans. Magn. 17 (1981) 1247–1248.
[85] J.-H.J.-G.J. Park, K. An, Y. Hwang, J.-H.J.-G.J. Park, H.-J. Noh, J.-Y. Kim, J.-H.J.-G.J. Park, N.-M. Hwang, T. Hyeon, Ultra-large-scale syntheses of monodisperse nanocrystals, Nat. Mater. 3 (2004) 891–895.
[86] F.X. Redl, C.T. Black, G.C. Papaefthymiou, R.L. Sandstrom, M. Yin, H. Zeng, C.B. Murray, S.P. O'Brien, Magnetic, electronic, and structural characterization of nonstoichiometric iron oxides at the nanoscale, J. Am. Chem. Soc. 126 (2004) 14583–14599.
[87] S. Sun, H. Zeng, Size-controlled synthesis of magnetite nanoparticles, J. Am. Chem. Soc. 124 (2002) 8204–8205.
[88] T. Hyeon, S.S. Lee, J. Park, Y. Chung, H. Bin Na, Synthesis of highly crystalline and monodisperse maghemite nanocrystallites without a size-selection process, J. Am. Chem. Soc. 123 (2001) 12798–12801.
[89] A. Pineau, N. Kanari, I. Gaballah, Kinetics of reduction of iron oxides by H2, Thermochim. Acta. 447 (2006) 89–100.
[90] H. Gavilán, O. Posth, L.K. Bogart, U. Steinhoff, L. Gutiérrez, M.P. Morales, How shape and internal structure affect the magnetic properties of anisometric magnetite nanoparticles, Acta Mater. 125 (2017) 416–424.
[91] S. Geng, H. Yang, X. Ren, Y. Liu, S. He, J. Zhou, N. Su, Y. Li, C. Xu, X. Zhang, Z. Cheng, Anisotropic magnetite nanorods for enhanced magnetic hyperthermia, Chem. - An Asian J. 11 (2016) 2996–3000.
[92] M.A. Blesa, M. Mijalchik, M. Villegas, G. Rigotti, Transformation of akaganeite into magnetite in aqueous hydrazine suspensions, React. Solids. 2 (1986) 85–94.
[93] M. Kiyama, Conditions for the Formation of Fe_3O_4 by the Air Oxidation of $Fe(OH)_2$ Suspensions, Bull. Chem. Soc. Jpn. 47 (1974) 1646–1650.
[94] R.S. Sapieszko, E. Matijević, Preparation of well-defined colloidal particles by thermal decomposition of metal chelates. I. Iron oxides, J. Colloid Interface Sci. 74 (1980) 405–422.
[95] H.D. Pedersen, D. Postma, R. Jakobsen, O. Larsen, Fast transformation of iron oxyhydroxides by the catalytic action of aqueous Fe(II), Geochim. Cosmochim. Acta. 69 (2005) 3967–3977.
[96] R.M. Cornell, U. Schwertmann, John Wiley & Sons, The iron oxides : structure, properties, reactions, occurrences, and uses, Wiley-VCH, 2003.
[97] J. Choi, J. Cha, J.-K. Lee, Synthesis of various magnetite nanoparticles through simple phase transformation and their shape-dependent magnetic properties, RSC Adv. 3 (2013) 8365.
[98] C.J. Serna, M.P. Morales, Maghemite (γ-Fe2O3): A Versatile Magnetic Colloidal Material, Surf. Colloid Sci, Springer US, Boston, MA 2004, pp. 27–81.
[99] M. Andrés Vergés, R. Costo, A.G. Roca, J.F. Marco, G.F. Goya, C.J. Serna, M.P. Morales, Uniform and water stable magnetite nanoparticles with diameters around the monodomain–multidomain limit, J. Phys. D. Appl. Phys. 41 (2008), 134003. .
[100] M. Kosmulski, pH-dependent surface charging and points of zero charge II. Update, J. Colloid Interface Sci. 275 (2004) 214–224.
[101] M. Kosmulski, The pH-dependent surface charging and points of zero charge. V. Update, J. Colloid Interface Sci. 353 (2011) 1–15.
[102] D. Kim, N. Lee, M. Park, B.H. Kim, K. An, T. Hyeon, Synthesis of uniform ferrimagnetic magnetite nanocubes, J. Am. Chem. Soc. 131 (2009) 454–455.
[103] S. Mann, R.B. Frankel, R.P. Blakemor, Structure, morphology and crystal growth of bacterial magnetite, Nature. 310 (1984) 405–407.
[104] C. Moya, X. Batlle, A. Labarta, The effect of oleic acid on the synthesis of Fe3−xO4 nanoparticles over a wide size range, Phys. Chem. Chem. Phys. 17 (2015) 27373–27379.

Please cite this article as: A.G. Roca, L. Gutiérrez, H. Gavilán, et al., Design strategies for shape-controlled magnetic iron oxide nanoparticles, Adv. Drug Deliv. Rev., https://doi.org/10.1016/j.addr.2018.12.008

[105] P. Guardia, N. Pérez, A. Labarta, X. Batlle, Controlled synthesis of iron oxide nanoparticles over a wide size range, Langmuir. 26 (2010) 5843–5847.
[106] H. Yang, T. Ogawa, D. Hasegawa, M. Takahashi, Synthesis and magnetic properties of monodisperse magnetite nanocubes, J. Appl. Phys. 103 (2008), 07D526. .
[107] M.V. Kovalenko, M.I. Bodnarchuk, R.T. Lechner, G. Hesser, F. Schäffler, W. Heiss, Fatty acid salts as stabilizers in size- and shape-controlled nanocrystal synthesis: the case of inverse spinel iron oxide, J. Am. Chem. Soc. 129 (2007) 6352–6353.
[108] G. Gao, X. Liu, R. Shi, K. Zhou, Y. Shi, R. Ma, E. Takayama-Muromachi, G. Qiu, Shape-controlled synthesis and magnetic properties of monodisperse Fe_3O_4 nanocubes, Cryst. Growth Des. 10 (2010) 2888–2894.
[109] B. Park, B.H. Kim, T. Yu, Synthesis of spherical and cubic magnetic iron oxide nanocrystals at low temperature in air, J. Colloid Interface Sci. 518 (2018) 27–33.
[110] D. Faivre, D. Schüler, Magnetotactic bacteria and magnetosomes, Chem. Rev. 108 (2008) 4875–4898.
[111] R.E. Dunin-Borkowski, M.R. McCartney, R.B. Frankel, D.A. Bazylinski, M. Pósfai, P.R. Buseck, Magnetic Microstructure of Magnetotactic Bacteria by Electron Holography, Science1. 282 (1998) 1868–1870.
[112] P. Guardia, A. Labarta, X. Batlle, Tuning the size, the shape, and the magnetic properties of iron oxide nanoparticles, J. Phys. Chem. C. 115 (2011) 390–396.
[113] Z.L. Wang, Transmission electron microscopy of shape-controlled nanocrystals and their assemblies, J. Phys. Chem. B. 104 (2000) 1153–1175.
[114] G. Salazar-Alvarez, J. Qin, V. Šepelák, I. Bergmann, M. Vasilakaki, K.N. Trohidou, J.D. Ardisson, W.A.A. Macedo, M. Mikhaylova, M. Muhammed, M.D. Baró, J. Nogués, Cubic versus spherical magnetic nanoparticles: the role of surface anisotropy, J. Am. Chem. Soc. 130 (2008) 13234–13239.
[115] E. Wetterskog, M. Agthe, A. Mayence, J. Grins, D. Wang, S. Rana, A. Ahniyaz, G. Salazar-Alvarez, L. Bergström, Precise control over shape and size of iron oxide nanocrystals suitable for assembly into ordered particle arrays, Sci. Technol. Adv. Mater. 15 (2014), 055010. .
[116] Z. Xu, C. Shen, Y. Tian, X. Shi, H.-J. Gao, Organic phase synthesis of monodisperse iron oxide nanocrystals using iron chloride as precursor, Nanoscale. 2 (2010) 1027.
[117] W.E.M. Elsayed, F.S. Al-Hazmi, L.S. Memesh, L.M. Bronstein, A novel approach for rapid green synthesis of nearly mono-disperse iron oxide magnetic nanocubes with remarkable surface magnetic anisotropy density for enhancing hyperthermia performance, Colloids Surfaces A Physicochem. Eng. Asp. 529 (2017) 239–245.
[118] L. Zhang, J. Wu, H. Liao, Y. Hou, S. Gao, Octahedral Fe_3O_4 nanoparticles and their assembled structures, Chem. Commun. (2009) 4378.
[119] A. Shavel, B. Rodri, J. Pacifico, M. Spasova, M. Farle, L.M. Liz-marza, B. Rodrı, Shape Control in Iron Oxide Nanocrystal Synthesis , Induced by Trioctylammonium Ions Shape Control in Iron Oxide Nanocrystal Synthesis , Induced by Trioctylammonium Ions, 2009 5843–5849.
[120] A. Shavel, L.M. Liz-Marzán, Shape control of iron oxide nanoparticles, Phys. Chem. Chem. Phys. 11 (2009) 3762–3763.
[121] J. Cheon, N.-J. Kang, S.-M. Lee, J.-H. Lee, J.-H. Yoon, S.J. Oh, Shape evolution of single-crystalline iron oxide nanocrystals, J. Am. Chem. Soc. 126 (2004) 1950–1951.
[122] A. Mitra, J. Mohapatra, S.S. Meena, C.V. Tomy, M. Aslam, Verwey transition in ultra-small-sized octahedral fe_3o_4 nanoparticles, J. Phys. Chem. C. 118 (2014) 19356–19362.
[123] M. Ozaki, S. Kratohvil, E. Matijević, Formation of monodispersed spindle-type hematite particles, J. Colloid Interface Sci. 102 (1984) 146–151.
[124] H. Wiogo, M. Lim, P. Munroe, R. Amal, Understanding the formation of iron oxide nanoparticles with acicular structure from iron(III) chloride and hydrazine monohydrate, Cryst. Growth Des. 11 (2011) 1689–1696.
[125] S. Palchoudhury, W. An, Y. Xu, Y. Qin, Z. Zhang, N. Chopra, R.A. Holler, C.H. Turner, Y. Bao, Synthesis and growth mechanism of iron oxide nanowhiskers, Nano Lett. 11 (2011) 1141–1146.
[126] A.F. Rebolledo, O. Bomatí-Miguel, J.F. Marco, P. Tartaj, A facile synthetic route for the preparation of superparamagnetic iron oxide nanorods and nanorices with tunable surface functionality, Adv. Mater. 20 (2008) 1760–1765.
[127] B. Tang, G. Wang, L. Zhuo, J. Ge, L. Cui, Facile Route to α-FeOOH and α-Fe_2O_3 nanorods and magnetic property of α-Fe_2O_3 nanorods, Inorg. Chem. 45 (2006) 5196–5200.
[128] S. Xuan, F. Liang, K. Shu, Novel method to fabricate magnetic hollow silica particles with anisotropic structure, J. Magn. Magn. Mater. 321 (2009) 1029–1033.
[129] O. Bomati-Miguel, A.F. Rebolledo, P. Tartaj, Controlled formation of porous magnetic nanorods via a liquid/liquid solvothermal method, Chem. Commun. (Camb). (2008) 4168–4170.
[130] M. Ocaña, M.P. Morales, C.J. Serna, Homogeneous precipitation of uniform α-Fe_2O_3 Particles from iron salts solutions in the presence of urea, J. Colloid Interface Sci. 212 (1999) 317–323.
[131] S.-J. Park, S. Kim, S. Lee, Z.G. Khim, K. Char, T. Hyeon, Synthesis and magnetic studies of uniform iron nanorods and nanospheres, J. Am. Chem. Soc. 122 (2000) 8581–8582.
[132] R. Das, J. Alonso, Z. Nemati Porshokouh, V. Kalappattil, D. Torres, M.-H. Phan, E. Garaio, J.Á. García, J.L. Sanchez Llamazares, H. Srikanth, Tunable high aspect ratio iron oxide nanorods for enhanced hyperthermia, J. Phys. Chem. C. 120 (2016) 10086–10093.
[133] K.E. Gonsalves, H. Li, P. Santiago, No Title, J. Mater. Sci. 36 (2001) 2461–2471.
[134] Y. Piao, J. Kim, H. Bin Na, D. Kim, J.S. Baek, M.K. Ko, J.H. Lee, M. Shokouhimehr, T. Hyeon, Wrap-bake-peel process for nanostructural transformation from beta-FeOOH nanorods to biocompatible iron oxide nanocapsules, Nat. Mater. 7 (2008) 242–247.
[135] J. Mohapatra, A. Mitra, H. Tyagi, D. Bahadur, M. Aslam, Iron oxide nanorods as high-performance magnetic resonance imaging contrast agents, Nanoscale. 7 (2015) 9174–9184.
[136] S. Lentijo Mozo, E. Zuddas, A. Casu, A. Falqui, Synthesizing Iron Oxide Nanostructures: The Polyethylenenemine (PEI) Role, Crystals. 7 (2017) 22.
[137] E. Matijević, P. Scheiner, Ferric hydrous oxide sols, J. Colloid Interface Sci. 63 (1978) 509–524.
[138] S. Zhang, W. Wu, X. Xiao, J. Zhou, F. Ren, C. Jiang, Preparation and characterization of spindle-like Fe_3O_4 mesoporous nanoparticles, Nanoscale Res. Lett. 6 (2011) 89.
[139] S. Sacanna, L. Rossi, B.W.M. Kuipers, A.P. Philipse, Fluorescent monodisperse silica ellipsoids for optical rotational diffusion studies, Langmuir. 22 (2006) 1822–1827.
[140] Y. Yang, X. Liu, Y. Lv, T.S. Herng, X. Xu, W. Xia, T. Zhang, J. Fang, W. Xiao, J. Ding, Orientation mediated enhancement on magnetic hyperthermia of Fe3 O4 nanodisc, Adv. Funct. Mater. 25 (2015) 812–820.
[141] L. Chen, X. Yang, J. Chen, J. Liu, H. Wu, H. Zhan, C. Liang, M. Wu, Continuous shape- and spectroscopy-tuning of hematite nanocrystals, Inorg. Chem. 49 (2010) 8411–8420.
[142] Y. Huang, D. Ding, M. Zhu, W. Meng, Y. Huang, F. Geng, J. Li, J. Lin, C. Tang, Z. Lei, Z. Zhang, C. Zhi, Facile synthesis of α-Fe 2 O 3 nanodisk with superior photocatalytic performance and mechanism insight, Sci. Technol. Adv. Mater. 16 (2015), 014801. .
[143] J. Lu, X. Jiao, D. Chen, W. Li, Solvothermal synthesis and characterization of Fe3O4 and γ-Fe_2O_3 nanoplates, J. Phys. Chem. C. 113 (2009) 4012–4017.
[144] L. Lartigue, P. Hugounenq, D. Alloyeau, S.P. Clarke, M. Lévy, J.-C. Bacri, R. Bazzi, D.F. Brougham, C. Wilhelm, F. Gazeau, Cooperative organization in iron oxide multi-core nanoparticles potentiates their efficiency as heating mediators and MRI contrast agents, ACS Nano. 6 (2012) 10935–10949.
[145] S. Palchoudhury, Y. Xu, A. Rushdi, R.A. Holler, Y. Bao, Controlled synthesis of iron oxide nanoplates and nanoflowers, Chem. Commun. 48 (2012), 10499. .
[146] S. Yu, G.M. Chow, Synthesis of monodisperse iron oxide and iron/iron oxide core/shell nanoparticles via iron-oleylamine complex, J. Nanosci. Nanotechnol. 6 (2006) 2135–2140.
[147] W. Li, S.S. Lee, J. Wu, C.H. Hinton, J.D. Fortner, Shape and size controlled synthesis of uniform iron oxide nanocrystals through new non-hydrolytic routes, Nanotechnology. 27 (2016), 324002. .
[148] H. Gavilán, M. Brollo, L. Gutiérrez, S. Veintemillas-Verdaguer, M.P. Morales, Controlling the size and shape of uniform magnetic iron oxide nanoparticles for biomedical applications, in: N.T. Thanh (Ed.), Clin. Appl. Magn. Nanoparticles, CRC Press 2018, p. 1.
[149] H. Gavilán, A. Kowalski, D. Heinke, A. Sugunan, J. Sommertune, M. Varón, L.K. Bogart, O. Posth, L. Zeng, D. González-Alonso, C. Balceris, J. Fock, E. Wetterskog, C. Frandsen, N. Gehrke, C. Grüttner, A. Fornara, F. Ludwig, S. Veintemillas-Verdaguer, C. Johansson, M.P. Morales, Colloidal flower-shaped iron oxide nanoparticles: synthesis strategies and coatings, Part. Part. Syst. Charact. 34 (2017), 1700094. .
[150] D. Caruntu, G. Caruntu, C.J. O'Connor, Magnetic properties of variable-sized Fe_3O_4 nanoparticles synthesized from non-aqueous homogeneous solutions of polyols, J. Phys. D. Appl. Phys. 40 (2007) 5801–5809.
[151] D. Caruntu, G. Caruntu, Y. Chen, G. Goloverda O'Connor, V.L. Kolesnichenko, Synthesis of Variable-Sized Nanocrystals of Fe3O4 with High Surface Reactivity, Chem. Mater. 16 (2004) 5527–5534.
[152] J. Liu, Z. Sun, Y. Deng, Y. Zou, C. Li, X. Guo, L. Xiong, Y. Gao, F. Li, D. Zhao, Highly water-dispersible biocompatible magnetite particles with low cytotoxicity stabilized by citrate groups, Angew. Chemie Int. Ed. 48 (2009) 5875–5879.
[153] J. Liang, H. Ma, W. Luo, S. Wang, Synthesis of magnetite submicrospheres with tunable size and superparamagnetism by a facile polyol process, Mater. Chem. Phys. 139 (2013) 383–388.
[154] Q. Sun, Z. Ren, R. Wang, W. Chen, C. Chen, Magnetite hollow spheres: solution synthesis, phase formation and magnetic property, J. Nanoparticle Res. 13 (2011) 213–220.
[155] C. Cheng, F. Xu, H. Gu, Facile synthesis and morphology evolution of magnetic iron oxide nanoparticles in different polyol processes, New J. Chem. 35 (2011) 1072.
[156] Q.Q. Xiong, J.P. Tu, Y. Lu, J. Chen, Y.X. Yu, Y.Q. Qiao, X.L. Wang, C.D. Gu, Synthesis of Hierarchical Hollow-Structured Single-Crystalline Magnetite (Fe 3 O 4) Microspheres: The Highly Powerful Storage versus Lithium as an Anode for Lithium Ion Batteries, J. Phys. Chem. C. 116 (2012) 6495–6502.
[157] W. Luo, H. Ma, F. Mou, M. Zhu, J. Yan, J. Guan, Steric-repulsion-based magnetically responsive photonic crystals, Adv. Mater. 26 (2014) 1058–1064.
[158] H. Wang, Y.-B. Sun, Q.-W. Chen, Y.-F. Yu, K. Cheng, Synthesis of carbon-encapsulated superparamagnetic colloidal nanoparticles with magnetic-responsive photonic crystal property, Dalt. Trans. 39 (2010) 9565.
[159] R. Di Corato, P. Piacenza, M. Musarò, R. Buonsanti, P.D. Cozzoli, M. Zambianchi, G. Barbarella, R. Cingolani, L. Manna, T. Pellegrino, Magnetic-fluorescent colloidal nanobeads: preparation and exploitation in cell separation experiments, Macromol. Biosci. 9 (2009) 952–958.
[160] G. Hemery, A.C. Keyes, E. Garaio, I. Rodrigo, J.A. Garcia, F. Plazaola, E. Garanger, O. Sandre, Tuning sizes, morphologies, and magnetic properties of monocore versus multicore iron oxide nanoparticles through the controlled addition of water in the polyol synthesis, Inorg. Chem. 56 (2017) 8232–8243.
[161] F. Vita, H. Gavilán, F. Rossi, C. de Julián Fernández, A. Secchi, A. Arduini, F. Albertini, M.P. Morales, Tuning morphology and magnetism of magnetite nanoparticles by calix[8]arene-induced oriented aggregation, CrystEngComm. 18 (2016) 8591–8598.
[162] K. An, S.G. Kwon, M. Park, H. Bin Na, S.-I. Baik, J.H. Yu, D. Kim, J.S. Son, Y.W. Kim, I.C. Song, W.K. Moon, H.M. Park, T. Hyeon, Synthesis of uniform hollow oxide nanoparticles through nanoscale acid etching, Nano Lett. 8 (2008) 4252–4258.
[163] A. Cabot, V.F. Puntes, E. Shevchenko, Y. Yin, L. Balcells, M.A. Marcus, S.M. Hughes, A. P. Alivisatos, Vacancy coalescence during oxidation of iron nanoparticles, J. Am. Chem. Soc. 129 (2007) 10358–10360.

Please cite this article as: A.G. Roca, L. Gutiérrez, H. Gavilán, et al., Design strategies for shape-controlled magnetic iron oxide nanoparticles, Adv. Drug Deliv. Rev., https://doi.org/10.1016/j.addr.2018.12.008

[164] S. Peng, S. Sun, Synthesis and characterization of monodisperse hollow Fe_3O_4 nanoparticles, Angew. Chemie - Int. Ed. 46 (2007) 4155–4158.
[165] L. Balcells, C. Martínez-Boubeta, J. Cisneros-Fernández, K. Simeonidis, B. Bozzo, J. Oró-Sole, N. Bagués, J. Arbiol, N. Mestres, B. Martínez, One-step route to iron oxide hollow nanocuboids by cluster condensation: implementation in water remediation technology, ACS Appl. Mater. Interfaces. 8 (2016) 28599–28606.
[166] K. Ota, S. Mitsushima, N. Hattori, N. Kamiya, Corrosion of Fe with Sodium compounds with molten sodium hydroxide, Bull. Chem. Soc. Jpn. 75 (2002) 1855–1859.
[167] N. Ohtori, T. Furukawa, F. Ueno, n situ Raman spectroscopic observation of corrosion reaction of Fe with Na_2O_2 up to 833 K, Electrochemistry. 73 (2005) 675–679.
[168] M.H. Oh, T. Yu, S.-H. Yu, B. Lim, K.-T. Ko, M.-G. Willinger, D.-H. Seo, B.H. Kim, M.G. Cho, J.-H. Park, K. Kang, Y.-E. Sung, N. Pinna, T. Hyeon, Galvanic replacement reactions in metal oxide nanocrystals, Science 340 (2013) 964–968.
[169] C.-J. Jia, L.-D. Sun, Z.-G. Yan, L.-P. You, F. Luo, X.-D. Han, Y.-C. Pang, Z. Zhang, C.-H. Yan, Single-crystalline iron oxide nanotubes, Angew. Chemie Int. Ed. 44 (2005) 4328–4333.
[170] C.-J. Jia, L.-D.S. Sun, F. Luo, X.-D. Han, L.J. Heyderman, Z.-G. Yan, C.-H. Yan, K. Zheng, Z. Zhang, M. Takano, N. Hayashi, M. Eltschka, M. Kläui, U. Rüdiger, T. Kasama, L. Cervera-Gontard, R.E. Dunin-Borkowski, G. Tzvetkov, J. Raabe, Large-scale synthesis of single-crystalline iron oxide magnetic nanorings, J. Am. Chem. Soc. 130 (2008) 16968–16977.
[171] L.L. Wang, J. Bao, L.L. Wang, F. Zhang, Y. Li, One-pot synthesis and bioapplication of amine-functionalized magnetite nanoparticles and hollow nanospheres, Chem. - A Eur. J. 12 (2006) 6341–6347.
[172] D. Kim, J. Park, K. An, N.-K. Yang, J.-G. Park, T. Hyeon, Synthesis of hollow iron nanoframes, J. Am. Chem. Soc. 129 (2007) 5812–5813.
[173] A. López-Ortega, A.G. Roca, P. Torruella, M. Petrecca, S. Estradé, F. Peiró, V. Puntes, J. Nogués, Galvanic replacement onto complex metal-oxide nanoparticles: impact of water or other oxidizers in the formation of either fully dense onion-like or multicomponent hollow MnO x /FeO x structures, Chem. Mater. 28 (2016) 8025–8031.
[174] A.H. Latham, M.J. Wilson, P. Schiffer, M.E. Williams, TEM-induced structural evolution in amorphous Fe oxide nanoparticles, J. Am. Chem. Soc. 128 (2006) 12632–12633.
[175] D.A.J. Herman, S. Cheong, M.J. Banholzer, R.D. Tilley, How hollow structures form from crystalline iron–iron oxide core–shell nanoparticles in the electron beam, Chem. Commun. 49 (2013) 6203.
[176] J.H. Park, G. Von Maltzahn, L. Zhang, M.P. Schwartz, E. Ruoslahti, S.N. Bhatia, M.J. Sailor, Magnetic iron oxide nanoworms for tumor targeting and imaging, Adv. Mater. 20 (2008) 1630–1635.
[177] S. Palchoudhury, Y. Xu, J. Goodwin, Y. Bao, Synthesis of iron oxide nanoworms, J. Appl. Phys. 109 (2011) 21–23.
[178] L.M. Bronstein, J.E. Atkinson, A.G. Malyutin, F. Kidwai, B.D. Stein, D.G. Morgan, J.M. Perry, J.A. Karty, Nanoparticles by decomposition of long chain iron carboxylates: from spheres to stars and cubes, Langmuir. 27 (2011) 3044–3050.
[179] P.D. Cozzoli, E. Snoeck, M.A. Garcia, C. Giannini, A. Guagliardi, A. Cervellino, F. Gozzo, A. Hernando, K. Achterhold, N. Ciobanu, F.G. Parak, R. Cingolani, L. Manna, Colloidal synthesis and characterization of tetrapod-shaped magnetic nanocrystals, Nano Lett. 6 (2006) 1966–1972.
[180] X. Li, Z. Si, Y. Lei, J. Tang, S. Wang, S. Su, S. Song, L. Zhao, H. Zhang, Direct hydrothermal synthesis of single-crystalline triangular Fe_3O_4 nanoprisms, CrystEngComm. 12 (2010) 2060.
[181] Y. Zeng, R. Hao, B. Xing, Y. Hou, Z. Xu, One-pot synthesis of Fe_3O_4 nanoprisms with controlled electrochemical properties, Chem. Commun. 46 (2010) 3920.
[182] Y. Zeng, R. Hao, B. Xing, Y. Hou, Z. Xu, One-pot synthesis of Fe3O4 nanoprisms with controlled electrochemical properties, Chem. Commun. 46 (2010) 3920.
[183] K. Hola, Z. Markova, G. Zoppellaro, J. Tucek, R. Zboril, Tailored functionalization of iron oxide nanoparticles for MRI, drug delivery, magnetic separation and immobilization of biosubstances, Biotechnol. Adv. 33 (2015) 1162–1176.
[184] I. Hilger, W.A. Kaiser, Iron oxide-based nanostructures for MRI and magnetic hyperthermia, Nanomedicine. 7 (2012) 1443–1459.
[185] Y. Xu, J. Sherwood, Y. Qin, R.A. Holler, Y. Bao, A general approach to the synthesis and detailed characterization of magnetic ferrite nanocubes, Nanoscale. 7 (2015) 12641–12649.
[186] A. Sathya, P. Guardia, R. Brescia, N. Silvestri, G. Pugliese, S. Nitti, L. Manna, T. Pellegrino, $Co_x Fe_{3-x} O_4$ Nanocubes for Theranostic Applications: Effect of Cobalt Content and Particle Size, Chem. Mater. 28 (2016) 1769–1780.
[187] M.F. Casula, E. Conca, I. Bakaimi, A. Sathya, M.E. Materia, A. Casu, A. Falqui, E. Sogne, T. Pellegrino, A.G. Kanaras, Manganese doped-iron oxide nanoparticle clusters and their potential as agents for magnetic resonance imaging and hyperthermia, Phys. Chem. Chem. Phys. 18 (2016) 16848–16855.
[188] S. Yang, J.-T. Jiang, C.-Y. Xu, Y. Wang, Y.-Y. Xu, L. Cao, L. Zhen, Synthesis of Zn(II)-Doped Magnetite Leaf-Like Nanorings for Efficient Electromagnetic Wave Absorption, Sci. Rep. 7 (2017), 45480. .
[189] Z. Wu, S. Yang, W. Wu, Shape control of inorganic nanoparticles from solution, Nanoscale. 8 (2016) 1237–1259.
[190] J.H. Lee, J.E. Ju, B. Il Kim, P.J. Pak, E.-K. Choi, H.-S. Lee, N. Chung, Rod-shaped iron oxide nanoparticles are more toxic than sphere-shaped nanoparticles to murine macrophage cells, Environ. Toxicol. Chem. 33 (2014) 2759–2766.
[191] Y. Jun, J.-H. Lee, J. Choi, J. Cheon, Symmetry-controlled colloidal nanocrystals: nonhydrolytic chemical synthesis and shape determining parameters, J. Phys. Chem. B. 109 (2005) 14795–14806.
[192] S.G. Kwon, T. Hyeon, Colloidal chemical synthesis and formation kinetics of uniformly sized nanocrystals of metals, oxides, and chalcogenides, Acc. Chem. Res. 41 (2008) 1696–1709.
[193] E.R. Leite, C. Ribeiro, Crystallization and Growth of Colloidal Nanocrystals, Springer New York, New York, NY, 2012.
[194] T. Sugimoto, Formation of monodispersed nano- and micro-particles controlled in size, shape, and internal structure, Chem. Eng. Technol. 26 (2003) 313–321.
[195] C. Burda, X. Chen, R. Narayanan, M.A. El-Sayed, Chemistry and properties of nanocrystals of different shapes, Chem. Rev. 105 (2005) 1025–1102.
[196] J. Park, J. Joo, S.G. Kwon, Y. Jang, T. Hyeon, Synthesis of monodisperse spherical nanocrystals, Angew. Chemie Int. Ed. 46 (2007) 4630–4660.
[197] V.K. LaMer, R.H. Dinegar, Theory, production and mechanism of formation of monodispersed hydrosols, J. Am. Chem. Soc. 72 (1950) 4847–4854.
[198] M. Chen, J.P. Liu, S. Sun, One-step synthesis of fept nanoparticles with tunable size, J. Am. Chem. Soc. 126 (2004) 8394–8395.
[199] T. Sugimoto, E. Matijević, Formation of uniform spherical magnetite particles by crystallization from ferrous hydroxide gels, J. Colloid Interface Sci. 74 (1980) 227–243.
[200] E. Ringe, R.P. Van Duyne, L.D. Marks, Wulff construction for alloy nanoparticles, Nano Lett. 11 (2011) 3399–3403.
[201] P. Hartman, W.G. Perdok, On the relations between structure and morphology of crystals. I, Acta Crystallogr. 8 (1955) 49–52.
[202] P. Hartman, W.G. Perdok, On the relations between structure and morphology of crystals. II, Acta Crystallogr. 8 (1955) 521–524.
[203] P. Hartman, W.G. Perdok, On the relations between structure and morphology of crystals. III, Acta Crystallogr. 8 (1955) 525–529.
[204] X. Peng, L. Manna, W. Yang, J. Wickham, E. Scher, A. Kadavanich, A.P. Alivisatos, Shape control of CdSe nanocrystals, Nature. 404 (2000) 59–61.
[205] L. Manna, E.C. Scher, A.P. Alivisatos, Synthesis of soluble and processable rod-, arrow-, teardrop-, and tetrapod-shaped CdSe nanocrystals, J. Am. Chem. Soc. 122 (2000) 12700–12706.
[206] Z.A. Peng, X. Peng, Mechanisms of the Shape Evolution of CdSe Nanocrystals, J. Am. Chem. Soc. 123 (2001) 1389–1395.
[207] P. Guardia, J. Pérez-Juste, A. Labarta, X. Batlle, L.M. Liz-Marzán, Heating rate influence on the synthesis of iron oxide nanoparticles : the case of decanoic acid, Chem. Commun. 46 (2010) 6108–6110.
[208] D. Niculaes, A. Lak, G.C. Anyfantis, S. Marras, O. Laslett, S.K. Avugadda, M. Cassani, D. Serantes, O. Hovorka, R. Chantrell, T. Pellegrino, Asymmetric assembling of iron oxide nanocubes for improving magnetic hyperthermia performance, ACS Nano. 11 (2017) 12121–12133.
[209] Z. Xu, C. Shen, Y. Hou, H. Gao, S. Sun, Oleylamine as Both Reducing Agent and Stabilizer in a Facile Synthesis of Magnetite Nanoparticles, Oleylamine as Both Reducing Agent and Stabilizer in a Facile Synthesis of Magnetite Nanoparticles, Communications 21 (2009) 1778–1780.
[210] Y. Hou, Z. Xu, S. Sun, Controlled synthesis and chemical conversions of FeO nanoparticles, Angew. Chemie - Int. Ed. 46 (2007) 6329–6332.
[211] H. Sun, B. Chen, X. Jiao, Z. Jiang, Z. Qin, D. Chen, Solvothermal Synthesis of Tunable Electroactive Magnetite Nanorods by Controlling the Side Reaction, J. Phys. Chem. C. 116 (2012) 5476–5481.
[212] K. An, T. Hyeon, Synthesis and biomedical applications of hollow nanostructures, Nano Today. 4 (2009) 359–373.
[213] A. Cabot, A.P. Alivisatos, V.F. Puntes, L. Balcells, Ò. Iglesias, A. Labarta, Magnetic domains and surface effects in hollow maghemite nanoparticles, Phys. Rev. B. 79 (2009), 094419. .
[214] A. Pardo, R. Pujales, M. Blanco, E.M. Villar-Alvarez, S. Barbosa, P. Taboada, V. Mosquera, Analysis of the influence of synthetic paramaters on the structure and physico-chemical properties of non-spherical iron oxide nanocrystals and their biological stability and compatibility, Dalt. Trans. 45 (2016) 797–810.
[215] H. Yang, D. Hasegawa, M. Takahashi, T. Ogawa, Facile synthesis, phase transfer, and magnetic properties of monodisperse magnetite nanocubes, IEEE Trans. Magn. 44 (2008) 3895–3898.
[216] A. López-Ortega, E. Lottini, G. Bertoni, C. de Julián Fernández, C. Sangregorio, Topotaxial phase transformation in cobalt doped iron oxide core/shell hard magnetic nanoparticles, Chem. Mater. 29 (2017) 1279–1289.
[217] M. Figlarz, Topotaxy, nucleation and growth, Solid State Ionics. 43 (1990) 143–170.
[218] B. Devouard, M. Posfai, X. Hua, D.A. Bazylinski, R.B. Frankel, P.R. Buseck, Magnetite from magnetotactic bacteria; size distributions and twinning, Am. Mineral. 83 (1998) 1387–1398.
[219] G. Mirabello, J.J.M. Lenders, N.A.J.M. Sommerdijk, Bioinspired synthesis of magnetite nanoparticles, Chem. Soc. Rev. 45 (2016) 5085–5106.
[220] Y. Amemiya, A. Arakaki, S.S. Staniland, T. Tanaka, T. Matsunaga, Controlled formation of magnetite crystal by partial oxidation of ferrous hydroxide in the presence of recombinant magnetotactic bacterial protein Mms6, Biomaterials. 28 (2007) 5381–5389.
[221] A. Arakaki, F. Masuda, Y. Amemiya, T. Tanaka, T. Matsunaga, Control of the morphology and size of magnetite particles with peptides mimicking the Mms6 protein from magnetotactic bacteria, J. Colloid Interface Sci. 343 (2010) 65–70.
[222] I. Milosevic, H. Jouni, C. David, F. Warmont, D. Bonnin, L. Motte, Facile microwave process in water for the fabrication of magnetic nanorods, J. Phys. Chem. C. 115 (2011) 18999–19004.
[223] P.R. Swann, N.J. Tighe, High voltage microscopy of the reduction of hematite to magnetite, Metall. Trans. B. 8 (1977) 479–487.
[224] Y. Yang, M. Li, Y. Wu, T. Wang, E. Shi, G. Choo, J. Ding, B. Zong, Z. Yang, J. Xue, Nanoscaled self-alignment of Fe 3 O 4 nanodiscs in ultrathin rGO films with engineered conductivity for electromagnetic interference shielding, Nanoscale. 8 (2016) 15989–15998.
[225] X.-L. Liu, Y. Yang, J.-P. Wu, Y.-F. Zhang, H.-M. Fan, J. Ding, Novel magnetic vortex nanorings/nanodiscs: Synthesis and theranostic applications, Chinese Phys. B. 24 (2015), 127505. .

Please cite this article as: A.G. Roca, L. Gutiérrez, H. Gavilán, et al., Design strategies for shape-controlled magnetic iron oxide nanoparticles, Adv. Drug Deliv. Rev., https://doi.org/10.1016/j.addr.2018.12.008

[226] B. Lv, Y. Xu, D. Wu, Y. Sun, Single-crystal α-Fe 2 O 3 hexagonal nanorings: stepwise influence of different anionic ligands (F − and SCN − anions), Chem. Commun. 47 (2011) 967–969.
[227] G. Thomas, F. Demoisson, R. Chassagnon, E. Popova, N. Millot, One-step continuous synthesis of functionalized magnetite nanoflowers, Nanotechnology. 27 (2016), 135604. .
[228] R. Ramesh, M. Rajalakshmi, C. Muthamizhchelvan, S. Ponnusamy, Synthesis of Fe 3O 4 nanoflowers by one pot surfactant assisted hydrothermal method and its properties, Mater. Lett. 70 (2012) 73–75.
[229] L.S. Zhong, J.S. Hu, H.P. Liang, A.M. Cao, W.G. Song, L.J. Wan, Self-assembled 3D flowerlike iron oxide nanostructures and their application in water treatment, Adv. Mater. 18 (2006) 2426–2431.
[230] P. Guardia, R. Di Corato, L. Lartigue, C. Wilhelm, A. Espinosa, M. Garcia-Hernandez, F. Gazeau, L. Manna, T. Pellegrino, Water-soluble iron oxide nanocubes with high values of specific absorption rate for cancer cell hyperthermia treatment, ACS Nano. 6 (2012) 3080–3091.
[231] C. Blanco-Andujar, A. Walter, G. Cotin, C. Bordeianu, D. Mertz, D. Felder-Flesch, S. Begin-Colin, Design of iron oxide-based nanoparticles for MRI and magnetic hyperthermia, Nanomedicine. 11 (2016) 1889–1910.
[232] A. Ruiz, P.C. Morais, R. Bentes de Azevedo, Z.G.M. Lacava, A. Villanueva, M.P. Morales, Magnetic nanoparticles coated with dimercaptosuccinic acid: development, characterization, and application in biomedicine, J. Nanoparticle Res. 16 (2014) 2589.
[233] T. Pellegrino, L. Manna, S. Kudera, T. Liedl, D. Koktysh, A.L. Rogach, S. Keller, J. Rädler, G. Natile, W.J. Parak, Hydrophobic Nanocrystals Coated with an Amphiphilic Polymer Shell: A General Route to Water Soluble Nanocrystals, 2004.
[234] M. Barrow, A. Taylor, P. Murray, M.J. Rosseinsky, D.J. Adams, Design considerations for the synthesis of polymer coated iron oxide nanoparticles for stem cell labelling and tracking using MRI, Chem. Soc. Rev. 44 (2015) 6733–6748.
[235] D.M. Monti, D. Guarnieri, G. Napolitano, R. Piccoli, P. Netti, S. Fusco, A. Arciello, Biocompatibility, uptake and endocytosis pathways of polystyrene nanoparticles in primary human renal epithelial cells, J. Biotechnol. 193 (2015) 3–10.
[236] A. Banerjee, J. Qi, R. Gogoi, J. Wong, S. Mitragotri, Role of nanoparticle size, shape and surface chemistry in oral drug delivery, J. Control. Release. 238 (2016) 176–185.
[237] C. Martinez-Boubeta, K. Simeonidis, A. Makridis, M. Angelakeris, O. Iglesias, P. Guardia, A. Cabot, L. Yedra, S. Estrade, F. Peiro, Z. Saghi, P.A. Midgley, I. Conde-Leboran, D. Serantes, D. Baldomir, Learning from Nature to Improve the Heat Generation of Iron-Oxide Nanoparticles for Magnetic Hyperthermia Applications, Sci. Rep. 3 (2013).
[238] E. Alphandéry, Y. Ding, A.T. Ngo, Z.L. Wang, L.F. Wu, M.P. Pileni, Assemblies of Aligned Magnetotactic Bacteria and Extracted Magnetosomes: What Is the Main Factor Responsible for the Magnetic Anisotropy? ACS Nano. 3 (2009) 1539–1547.
[239] F. Vereda, J. de Vicente, R. Hidalgo-Alvarez, Oxidation of ferrous hydroxides with nitrate: A versatile method for the preparation of magnetic colloidal particles, J. Colloid Interface Sci. 392 (2013) 50–56.
[240] K. Nishio, M. Ikeda, N. Gokon, S. Tsubouchi, H. Narimatsu, Y. Mochizuki, S. Sakamoto, A. Sandhu, M. Abe, H. Handa, Preparation of size-controlled (30-100 nm) magnetite nanoparticles for biomedical applications, J. Magn. Magn. Mater. 310 (2007) 2408–2410.
[241] S. Chandra, R. Das, V. Kalappattil, T. Eggers, C. Harnagea, R. Nechache, M.-H. Phan, F. Rosei, H. Srikanth, Epitaxial magnetite nanorods with enhanced room temperature magnetic anisotropy, Nanoscale. 9 (2017) 7858–7867.
[242] F. Walz, The Verwey transition - a topical review, J. Phys. Condens. Matter. 14 (2002) R285–R340.
[243] G.F. Goya, T.S. Berquó, F.C. Fonseca, M.P. Morales, Static and dynamic magnetic properties of spherical magnetite nanoparticles, J. Appl. Phys. 94 (2003) 3520–3528.
[244] J.-C. Si, Y. Xing, M.-L. Peng, C. Zhang, N. Buske, C. Chen, Y.-L. Cui, Solvothermal synthesis of tunable iron oxide nanorods and their transfer from organic phase to water phase, CrystEngComm. 16 (2014) 512–516.
[245] T. Macher, J. Totenhagen, J. Sherwood, Y. Qin, D. Gurler, M.S. Bolding, Y. Bao, Ultrathin iron oxide nanowhiskers as positive contrast agents for magnetic resonance imaging, Adv. Funct. Mater. 25 (2015) 490–494.
[246] Y.J. Chen, P. Gao, C.L. Zhu, R.X. Wang, L.J. Wang, M.S. Cao, X.Y. Fang, Synthesis, magnetic and electromagnetic wave absorption properties of porous Fe_3O_4/Fe/SiO2 core/shell nanorods, J. Appl. Phys. 106 (2009), 054303. .
[247] W.W. Wang, J.L. Yao, Synthesis and magnetic property of silica/iron oxides nanorods, Mater. Lett. 64 (2010) 840–842.
[248] O. Özdemir, Low-temperature properties of a single crystal of magnetite oriented along principal magnetic axes, Earth Planet. Sci. Lett. 165 (1999) 229–239.
[249] B.D. Cullity, Introduction to Magnetic Materials, John Wiley & Sons, Inc, 2009.
[250] Y. Yang, X.L. Liu, J.B. Yi, Y. Yang, H.M. Fan, J. Ding, Stable vortex magnetite nanorings colloid: Micromagnetic simulation and experimental demonstration, J. Appl. Phys. 111 (2012) 1–9.
[251] S. Dutz, Are magnetic multicore nanoparticles promising candidates for biomedical applications? IEEE Trans. Magn. 52 (2016) 1–3.
[252] A. Kostopoulou, S.K.P. Velu, K. Thangavel, F. Orsini, K. Brintakis, S. Psycharakis, A. Ranella, L. Bordonali, A. Lappas, A. Lascialfari, Colloidal assemblies of oriented maghemite nanocrystals and their NMR relaxometric properties, Dalt. Trans. 43 (2014) 8395–8404.
[253] A.P. Roberts, Y. Cui, K.L. Verosub, Wasp-waisted hysteresis loops: Mineral magnetic characteristics and discrimination of components in mixed magnetic systems, J. Geophys. Res. Solid Earth. 100 (1995) 17909–17924.
[254] R. Crichton, Inorganic Biochemistry of Iron Metabolism, John Wiley & Sons, Ltd, Chichester, UK, 2001.
[255] J.M. Rojas, H. Gavilán, V. del Dedo, E. Lorente-Sorolla, L. Sanz-Ortega, G.B. da Silva, R. Costo, S. Perez-Yagüe, M. Talelli, M. Marciello, M.P. Morales, D.F. Barber, L. Gutiérrez, Time-course assessment of the aggregation and metabolization of magnetic nanoparticles, Acta Biomater. 58 (2017) 181–195.
[256] A. Ruiz, L. Gutiérrez, P.R. Cáceres-Vélez, D. Santos, S.B. Chaves, M.L. Fascineli, M.P. Garcia, R.B. Azevedo, M.P. Morales, Biotransformation of magnetic nanoparticles as a function of coating in a rat model, Nanoscale. 7 (2015) 16321–16329.
[257] J. Wang Yi-Xiang, Superparamagnetic iron oxide based MRI contrast agents: Current status of clinical application, Quant. Imaging Med. Surg. 1 (2011) 35–40.
[258] V. Valdiglesias, N. Fernández-Bertólez, G. Kiliç, C. Costa, S. Costa, S. Fraga, M.J. Bessa, E. Pásaro, J.P. Teixeira, B. Laffon, Are iron oxide nanoparticles safe? Current knowledge and future perspectives, J. Trace Elem. Med. Biol. 38 (2016) 53–63.
[259] L. Lartigue, D. Alloyeau, J. Kolosnjaj-Tabi, Y. Javed, P. Guardia, A. Riedinger, C. Péchoux, T. Pellegrino, C. Wilhelm, F. Gazeau, Biodegradation of iron oxide nanocubes: high-resolution in situ monitoring, ACS Nano. 7 (2013) 3939–3952.
[260] K.H. Bae, M. Park, M.J. Do, N. Lee, J.H. Ryu, G.W. Kim, C. Kim, T.G. Park, T. Hyeon, Chitosan oligosaccharide-stabilized ferrimagnetic iron oxide nanocubes for magnetically modulated cancer hyperthermia, ACS Nano. 6 (2012) 5266–5273.
[261] V.K. Sharma, A. Alipour, Z. Soran-Erdem, Z.G. Aykut, H.V. Demir, Highly monodisperse low-magnetization magnetite nanocubes as simultaneous T 1 – T 2 MRI contrast agents, Nanoscale. 7 (2015) 10519–10526.
[262] F. Ghaemi-Oskouie, Y. Shi, The role of uric acid as an endogenous danger signal in immunity and inflammation, Curr. Rheumatol. Rep. 13 (2011) 160–166.
[263] F.J. Lázaro, A.R. Abadía, M.S. Romero, L. Gutiérrez, J. Lázaro, M.P. Morales, Magnetic characterisation of rat muscle tissues after subcutaneous iron dextran injection, Biochim. Biophys. Acta - Mol. Basis Dis. 1740 (2005) 434–445.
[264] M. Safi, S. Clowez, A. Galimard, J.-F. Berret, In vitro toxicity and uptake of magnetic nanorods, J. Phys. Conf. Ser. 304 (2011), 012033. .
[265] Z.-G. Yue, W. Wei, Z.-X. You, Q.-Z. Yang, H. Yue, Z.-G. Su, G.-H. Ma, Iron oxide nanotubes for magnetically guided delivery and ph-activated release of insoluble anticancer drugs, Adv. Funct. Mater. 21 (2011) 3446–3453.
[266] K. Simeonidis, M.P. Morales, M. Marciello, M. Angelakeris, P. de la Presa, A. Lazaro-Carrillo, A. Tabero, A. Villanueva, O. Chubykalo-Fesenko, D. Serantes, In-situ particles reorientation during magnetic hyperthermia application: Shape matters twice, Sci. Rep. 6 (2016), 38382. .
[267] G. Hemery, C. Genevois, F. Couillaud, S. Lacomme, E. Gontier, E. Ibarboure, S. Lecommandoux, E. Garanger, O. Sandre, Monocore vs. multicore magnetic iron oxide nanoparticles: uptake by glioblastoma cells and efficiency for magnetic hyperthermia, Mol. Syst. Des. Eng. 2 (2017) 629–639.
[268] M. Marín-Barba, H. Gavilán, L. Gutiérrez, E. Lozano-Velasco, I. Rodríguez-Ramiro, G. N. Wheeler, C.J. Morris, M.P. Morales, A. Ruiz, Unravelling the mechanisms that determine the uptake and metabolism of magnetic single and multicore nanoparticles in a Xenopus laevis model, Nanoscale. 10 (2018) 690–704.
[269] R. Xing, A.A. Bhirde, S. Wang, X. Sun, G. Liu, Y. Hou, X. Chen, Hollow iron oxide nanoparticles as multidrug resistant drug delivery and imaging vehicles, Nano Res. 6 (2013) 1–9.
[270] P.P. Wyss, S. Lamichhane, M. Rauber, R. Thomann, K.W. Krämer, V.P. Shastri, Tripod USPIONs with high aspect ratio show enhanced T2 relaxation and cytocompatibility, Nanomedicine. 11 (2016) 1017–1030.
[271] X. Zhou, Y. Shi, L. Ren, S. Bao, Y. Han, S. Wu, H. Zhang, L. Zhong, Q. Zhang, Controllable synthesis, magnetic and biocompatible properties of Fe3O4 and α-Fe2O3 nanocrystals, J. Solid State Chem. 196 (2012) 138–144.
[272] K. Luyts, D. Napierska, B. Nemery, P.H.M. Hoet, How physico-chemical characteristics of nanoparticles cause their toxicity: complex and unresolved interrelations, Environ. Sci. Process. Impacts. 15 (2013) 23–38.
[273] R. Di Corato, A. Espinosa, L. Lartigue, M. Tharaud, S. Chat, T. Pellegrino, C. Ménager, F. Gazeau, C. Wilhelm, Magnetic hyperthermia efficiency in the cellular environment fordifferent nanoparticle designs, Biomaterials. 35 (2014) 6400–6411.
[274] Z. Zhao, Z. Zhou, J. Bao, Z. Wang, J. Hu, X. Chi, K. Ni, R. Wang, X. Chen, Z. Chen, J. Gao, Octapod iron oxide nanoparticles as high-performance T2 contrast agents for magnetic resonance imaging, Nat. Commun. 4 (2013) 2266.
[275] Y. Javed, L. Lartigue, P. Hugounenq, Q.L. Vuong, Y. Gossuin, R. Bazzi, C. Wilhelm, C. Ricolleau, F. Gazeau, D. Alloyeau, Biodegradation mechanisms of iron oxide monocrystalline nanoflowers and tunable shield effect of gold coating, Small. 10 (2014) 3325–3337.
[276] N. Feliu, D. Docter, M. Heine, P. del Pino, S. Ashraf, J. Kolosnjaj-Tabi, P. Macchiarini, P. Nielsen, D. Alloyeau, F. Gazeau, R.H. Stauber, W.J. Parak, In vivo degeneration and the fate of inorganic nanoparticles, Chem. Soc. Rev. 45 (2016) 2440–2457.
[277] S.J. Dixon, K.M. Lemberg, M.R. Lamprecht, R. Skouta, E.M. Zaitsev, C.E. Gleason, D.N. Patel, A.J. Bauer, A.M. Cantley, W.S. Yang, B. Morrison, B.R. Stockwell, Ferroptosis: an iron-dependent form of nonapoptotic cell death, Cell. 149 (2012) 1060–1072.
[278] T. Hirschhorn, B.R. Stockwell, The development of the concept of ferroptosis, Free Radic, Biol. Med. (2018)https://doi.org/10.1016/j.freeradbiomed.2018.09.043 (in press).
[279] Z. Shen, J. Song, B.C. Yung, Z. Zhou, A. Wu, X. Chen, Emerging strategies of cancer therapy based on ferroptosis, Adv. Mater. 30 (2018) 1704007.
[280] R. Hergt, S. Dutz, R. Müller, M. Zeisberger, Magnetic particle hyperthermia: nanoparticle magnetism and materials development for cancer therapy, J. Phys. Condens. Matter. 18 (2006) S2919–S2934.
[281] R. Hergt, S. Dutz, Magnetic particle hyperthermia—biophysical limitations of a visionary tumour therapy, J. Magn. Magn. Mater. 311 (2007) 187–192.
[282] R. Hergt, R. Hiergeist, M. Zeisberger, D. Schüler, U. Heyen, I. Hilger, W.A. Kaiser, Magnetic properties of bacterial magnetosomes as potential diagnostic and therapeutic tools, J. Magn. Magn. Mater. 293 (2005) 80–86.

Please cite this article as: A.G. Roca, L. Gutiérrez, H. Gavilán, et al., Design strategies for shape-controlled magnetic iron oxide nanoparticles, Adv. Drug Deliv. Rev., https://doi.org/10.1016/j.addr.2018.12.008

[283] E.A. Périgo, G. Hemery, O. Sandre, D. Ortega, E. Garaio, F. Plazaola, F.J. Teran, Fundamentals and advances in magnetic hyperthermia, Appl. Phys. Rev. 2 (2015) 041302.

[284] G. Vallejo-Fernandez, O. Whear, A.G. Roca, S. Hussain, J. Timmis, V. Patel, K. O'Grady, Mechanisms of hyperthermia in magnetic nanoparticles, J. Phys. D. Appl. Phys. 46 (2013), 312001. .

[285] P. Guardia, A. Riedinger, S. Nitti, G. Pugliese, S. Marras, A. Genovese, M.E. Materia, C. Lefevre, L. Manna, T. Pellegrino, One pot synthesis of monodisperse water soluble iron oxide nanocrystals with high values of the specific absorption rate, J. Mater. Chem. B. 2 (2014) 4426.

[286] J.G. Ovejero, D. Cabrera, J. Carrey, T. Valdivielso, G. Salas, F.J. Teran, Effects of inter- and intra-aggregate magnetic dipolar interactions on the magnetic heating efficiency of iron oxide nanoparticles, Phys. Chem. Chem. Phys. 18 (2016) 10954–10963.

[287] D. Serantes, K. Simeonidis, M. Angelakeris, O. Chubykalo-Fesenko, M. Marciello, M. P. Morales, D. Baldomir, C. Martinez-Boubeta, Multiplying magnetic hyperthermia response by nanoparticle assembling, J. Phys. Chem. C. 118 (2014) 5927–5934.

[288] Z. Nemati, R. Das, J. Alonso, E. Clements, M.H. Phan, H. Srikanth, Iron oxide nanospheres and nanocubes for magnetic hyperthermia therapy: a comparative study, J. Electron. Mater. 46 (2017) 3764–3769.

[289] J. Tang, M. Myers, K.A. Bosnick, L.E. Brus, Magnetite Fe 3 O 4 nanocrystals: spectroscopic observation of aqueous oxidation kinetics, J. Phys. Chem. B. 107 (2003) 7501–7506.

[290] J. Mohapatra, A. Mitra, M. Aslam, D. Bahadur, Octahedral-Shaped Fe_3O_4 nanoparticles with enhanced specific absorption rate and R_2 relaxivity, IEEE Trans. Magn. 51 (2015) 1–3.

[291] Y. Lv, Y. Yang, J. Fang, H. Zhang, E. Peng, X. Liu, W. Xiao, J. Ding, Size dependent magnetic hyperthermia of octahedral Fe_3O_4anoparticles, RSC Adv. 5 (2015) 76764–76771.

[292] M. Ma, Y. Zhang, Z. Guo, N. Gu, Facile synthesis of ultrathin magnetic iron oxide nanoplates by Schikorr reaction, Nanoscale Res. Lett. 8 (2013) 16.

[293] A. Wachowiak, Direct observation of internal spin structure of magnetic vortex cores, Science (80-.) 298 (2002) 577–580.

[294] D.-H. Kim, E.A. Rozhkova, I.V. Ulasov, S.D. Bader, T. Rajh, M.S. Lesniak, V. Novosad, Biofunctionalized magnetic-vortex microdiscs for targeted cancer-cell destruction, Nat. Mater. 9 (2010) 165–171.

[295] S. Tong, C.A. Quinto, L. Zhang, P. Mohindra, G. Bao, Size-dependent heating of magnetic iron oxide nanoparticles, ACS Nano. 11 (2017) 6808–6816.

[296] Z. Nemati, S.M. Salili, J. Alonso, A. Ataie, R. Das, M.H. Phan, H. Srikanth, Superparamagnetic iron oxide nanodiscs for hyperthermia therapy: Does size matter? J. Alloys Compd. 714 (2017) 709–714.

[297] P. Bender, J. Fock, C. Frandsen, M.F. Hansen, C. Balceris, F. Ludwig, O. Posth, E. Wetterskog, L.K. Bogart, P. Southern, W. Szczerba, L. Zeng, K. Witte, C. Grüttner, F. Westphal, D. Honecker, D. González-Alonso, L. Fernández Barquín, C. Johansson, Relating magnetic properties and high hyperthermia performance of iron oxide nanoflowers, J. Phys. Chem. C. 122 (2018) 3068–3077.

[298] Use of magnetosomes of biological origin, by magnetic hyperthermia for the treatment of tumors, in: E. Alphandéry (Ed.), Front. Anti-Cancer Drug Discov, Bentham science publishers 2015, pp. 218–248.

[299] R. Weissleder, M. Nahrendorf, M.J. Pittet, Imaging macrophages with nanoparticles, Nat. Mater. 13 (2014) 125–138.

[300] V. Hatje, K.W. Bruland, A.R. Flegal, Increases in anthropogenic gadolinium anomalies and rare earth element concentrations in san francisco bay over a 20 year record, Environ. Sci. Technol. 50 (2016) 4159–4168.

[301] Z. Zhou, X. Zhu, D. Wu, Q. Chen, D. Huang, C. Sun, J. Xin, K. Ni, J. Gao, Anisotropic shaped iron oxide nanostructures: Controlled synthesis and proton relaxation shortening effects, Chem. Mater. 27 (2015) 3505–3515.

[302] N. Lee, H. Kim, S.H. Choi, M. Park, D. Kim, H.-C. Kim, Y. Choi, S. Lin, B.H. Kim, H.S. Jung, H. Kim, K.S. Park, W.K. Moon, T. Hyeon, Magnetosome-like ferrimagnetic iron oxide nanocubes for highly sensitive MRI of single cells and transplanted pancreatic islets, Proc. Natl. Acad. Sci. 108 (2011) 2662–2667.

[303] A. Orza, H. Wu, Y. Xu, Q. Lu, H. Mao, One-step facile synthesis of highly magnetic and surface functionalized iron oxide nanorods for biomarker-targeted applications, ACS Appl. Mater. Interfaces. 9 (2017) 20719–20727.

[304] H.M. Fan, M. Olivo, B. Shuter, J.B. Yi, R. Bhuvaneswari, H.R. Tan, G.C. Xing, C.T. Ng, L. Liu, S.S. Lucky, B.H. Bay, J. Ding, Quantum dot capped magnetite nanorings as high performance nanoprobe for multiphoton fluorescence and magnetic resonance imaging, J. Am. Chem. Soc. 132 (2010) 14803–14811.

[305] E. Pöselt, H. Kloust, U. Tromsdorf, M. Janschel, C. Hahn, C. Ma??lo, H. Weller, Relaxivity optimization of a pegylated iron-oxide-based negative magnetic resonance contrast agent for T 2-weighted spin-echo imaging, ACS Nano. 6 (2012) 1619–1624.

[306] Y. Bao, J.A. Sherwood, Z. Sun, Magnetic iron oxide nanoparticles as T 1 contrast agents for magnetic resonance imaging, J. Mater. Chem. C. 6 (2018) 1280–1290.

[307] H. Bin Na, T. Hyeon, Nanostructured T1 MRI contrast agents, J. Mater. Chem. 19 (2009) 6267.

[308] F.-Y. Chen, Z.-J. Gu, H.-P. Wan, X.-Z. Xu, Q. Tang, Manganese nanosystem for new generation of MRI contrast agent, Rev. Nanosci. Nanotechnol. 4 (2015) 81–91.

[309] R. Langer, Drug delivery and targeting, Nature. 392 (1998) 5–10.

[310] W. Schütt, C. Grüttner, U. Häfeli, M. Zborowski, J. Teller, H. Putzar, C. Schümichen, Applications of magnetic targeting in diagnosis and therapy–possibilities and limitations: a mini-review, Hybridoma. 16 (1997) 109–117.

[311] Y. Matsumura, H. Maeda, A new concept for macromolecular therapeutics in cancer chemotherapy: mechanism of tumoritropic accumulation of proteins and the antitumor agent smancs, Cancer Res. 46 (1986) 6387–6392.

[312] H. Kakwere, M.P. Leal, M.E. Materia, A. Curcio, P. Guardia, D. Niculaes, R. Marotta, A. Falqui, T. Pellegrino, Functionalization of strongly interacting magnetic nanocubes with (thermo)responsive coating and their application in hyperthermia and heat-triggered drug delivery, ACS Appl. Mater. Interfaces. 7 (2015) 10132–10145.

[313] S. Carregal-Romero, P. Guardia, X. Yu, R. Hartmann, T. Pellegrino, W.J. Parak, Magnetically triggered release of molecular cargo from iron oxide nanoparticle loaded microcapsules, Nanoscale. 7 (2015) 570–576.

[314] C. Zhang, Z. Mo, G. Teng, B. Wang, R. Guo, P. Zhang, Superparamagnetic functional C@Fe3O4 nanoflowers: development and application in acetaminophen delivery, J. Mater. Chem. B. 1 (2013) 5908.

[315] L. Cheng, W. Ruan, B. Zou, Y. Liu, Y. Wang, Chemical template-assisted synthesis of monodisperse rattle-type Fe 3 O 4 @C hollow microspheres as drug carrier, Acta Biomater. 58 (2017) 432–441.

[316] K. Cheng, S. Peng, C. Xu, S. Sun, Porous hollow Fe_3O_4 nanoparticles for targeted delivery and controlled release of cisplatin, J. Am. Chem. Soc. 131 (2009) 10637–10644.

[317] S.-W. Cao, Y.-J. Zhu, M.-Y. Ma, L. Li, L. Zhang, Hierarchically nanostructured magnetic hollow spheres of Fe3O4 and γ-Fe2O3: preparation and potential application in drug delivery, J. Phys. Chem. C. 112 (2008) 1851–1856.

[318] I. Koh, L. Josephson, I. Koh, L. Josephson, Magnetic nanoparticle sensors, Sensors. 9 (2009) 8130–8145.

[319] C. de Montferrand, L. Hu, I. Milosevic, V. Russier, D. Bonnin, L. Motte, A. Brioude, Y. Lalatonne, Iron oxide nanoparticles with sizes, shapes and compositions resulting in different magnetization signatures as potential labels for multiparametric detection, Acta Biomater. 9 (2013) 6150–6157.

[320] L.M. Bauer, S.F. Situ, M.A. Griswold, A.C.S. Samia, High-performance iron oxide nanoparticles for magnetic particle imaging – guided hyperthermia (hMPI), Nanoscale. 8 (2016) 12162–12169.

[321] L. Pan, B.C. Park, M. Ledwig, L. Abelmann, Y.K. Kim, Magnetic particle spectrometry of Fe_3O_4 multi-granule nanoclusters, IEEE Trans. Magn. 53 (2017) 1–4.

[322] M. Zborowski, J.J. Chalmers, Rare cell separation and analysis by magnetic sorting, Anal. Chem. 83 (2011) 8050–8056.

[323] M. Testa-Anta, S. Liébana-Viñas, B. Rivas-Murias, B. Rodríguez González, M. Farle, V. Salgueiriño, Shaping iron oxide nanocrystals for magnetic separation applications, Nanoscale. 10 (2018) 20462–20467.

Please cite this article as: A.G. Roca, L. Gutiérrez, H. Gavilán, et al., Design strategies for shape-controlled magnetic iron oxide nanoparticles, Adv. Drug Deliv. Rev., https://doi.org/10.1016/j.addr.2018.12.008